

Characterizing a Novel Enzyme Involved in Cardiolipin Remodelling

by

Ashkan Hashemi

A thesis

presented to the University of Waterloo

in fulfillment of the

requirement for the degree of

Doctor of Philosophy

in

Kinesiology

Waterloo, Ontario, Canada, 2023

©Ashkan Hashemi 2023

Examining Committee Membership

The following served on the Examining Committee for this thesis. The decision of the Examining Committee is by majority vote.

External Examiner	Vernon Dolinsky Professor Department of Pharmacology and Therapeutics University of Manitoba
Supervisor	Robin E. Duncan, Ph.D. Associate Professor Department of Kinesiology, Faculty of Health University of Waterloo
Internal Member	Ken D. Stark, Ph.D. Canada Research Chair in Nutritional Lipidomics Professor Department of Kinesiology, Faculty of Health University of Waterloo
Internal-external Member	Dale Martin, Ph.D. Assistant Professor Department of Biology, Faculty of Science University of Waterloo
Other Member(s)	Michaela Devries-Aboud, Ph.D. Associate Professor Department of Kinesiology, Faculty of Health University of Waterloo

Author's Declaration

This thesis consists of material all of which I authored or co-authored: see Statement of Contributions included in this thesis. This is a true copy of the thesis, including any required final revisions, as accepted by my examiners.

I understand that this thesis may be made electronically available to the public.

Statement of Contributions

Chapter 3 of this thesis contains material that has been previously published in the International Journal of Sciences. The contributions of the authors are listed below:

PLAAT1 Exhibits Phosphatidylcholine: Monolysocardiolipin Transacylase Activity

International Journal of Sciences

2022 June; 23(12): 6714. doi: 10.3390/ijms23126714

Bradley RM*¹, Hashemi, A*¹, Aristizabal-Henao JJ¹, Stark KD¹, & Duncan RE¹

¹From the Department of Kinesiology, Faculty of Applied Health Sciences, University of Waterloo, 200 University Avenue West, Waterloo, Ontario, Canada N2L 3G1

Statement of contributions:

RMB and AH reviewed the literature, created all tables and figures, and drafted the manuscript.

RED was involved in the conception and design of the manuscript, and critically revised all elements. All authors read and approved the final manuscript.

In addition, work from this thesis was performed in collaboration with the following individuals, whom I thank for their contributions in the completion of this thesis:

Genotyping experiments

- Joey Hung, MSc, University of Waterloo
- Alex Cocco, BSc, University of Waterloo

Enzymology experiments

- Dr. Ryan Bradley, University of Waterloo
- Dr. Robin Duncan, University of Waterloo

CLAMS and Treadmill experiments

- Michelle Tomczewski, MSc, University of Waterloo
- Dr. Maria Fernanda Fernandes, University of Waterloo

Gas chromatography experiments

- Simon Liu, BSc, University of Waterloo
- John Chan, MSc, University of Waterloo
- Dr. Ken Stark, University of Waterloo

Abstract

Background: Cardiolipin (CL) is a specialized dimeric phospholipid comprising approximately 25% of total phospholipids in the inner mitochondrial membrane in eukaryotes, where it functions in energy metabolism, autophagy and apoptosis, and other important cellular processes. CL produced de-novo in the Kennedy pathway is considered nascent due to its non-specific acyl chain profile and is then remodeled to mature CL in the Lands pathway. CL plays several important roles within the mitochondria, including interacting with the electron transport complexes, maintaining the cristae architecture, mediating the apoptotic process, as well as acting in the initiation of mitophagy. Due to these reasons, the appropriate synthesis and remodelling of CL has implications for healthy physiological function. We have discovered a potential novel enzyme involved in CL metabolism, and the purpose of this thesis was to characterize the function of this enzyme in these processes.

Major Aims and Approach: The major aims of this thesis were: 1) To investigate the *in vitro* effects of this enzyme on CL synthesis and 2) To characterize the role of this enzyme in normal physiology using mice deficient in this gene.

Results: For our first aim, we discovered that overexpressing this enzyme in HEK-293 cells caused alterations in CL levels *in vitro*, while the partially purified enzyme displayed an ability to directly remodel monolysocardilipin using phosphatidylcholine as an acyl donor *in vitro*, which indicates a new and previously unreported function for this enzyme. My second aim had three objectives. The first was to assess alterations in CL content in tissues of mice deficient in this enzyme, versus *Wt* controls, and we discovered that gene ablated mice displayed tissue-specific alterations in CL content, and this was present in both male and female mice deficient in this enzyme.

The second objective was to determine if there are differences in growth, food intake, and gross morphology between wildtype and gene ablated mice. Male gene-deficient mice exhibited differences in food intake, organ weights, and life span. These differences were not observed in female mice, though they followed similar trends despite not reaching statistical significance.

The final objective of this thesis was to assess metabolic measures and exercise tolerance. Deficiency in this enzyme caused differences in oxygen consumption, carbon dioxide production, and energy expenditure in both sexes. Male gene-ablated mice also exhibited differences in rearing activity, and exercise tolerance. The differences in rearing activity and exercise tolerance were however not observed in female gene deficient mice.

Conclusions: The findings of this thesis indicate a novel role for this enzyme in CL metabolism, including an ability to remodel CL *in vitro*. Characterization of gene-deficient mice also indicated significant phenotypic differences, especially in male mice, while gas chromatography analysis demonstrated major tissue-specific changes in CL content. These results provide insight into the function of this enzyme.

Acknowledgments

First and foremost, thank you to Dr. Robin Duncan for taking me on as a PhD student, and also for giving me an opportunity 11 years ago and allowing me to volunteer in her lab. I would have never thought that 2 degrees and a decade later I would be the senior PhD student in that same lab. That initial opportunity has been transformative in my life. The kindness and genuine desire that you have for your students to succeed shouldn't be overlooked.

Thank you to the members of my thesis committee, Dr. Ken Stark and Dr. Michaela Devries-About for your guidance through this process and conversations throughout the years. Your feedback has been invaluable.

Thank you to Ryan Bradley for being a great friend and mentor whenever I've needed it. I appreciate you trusting me to continue your work, and for always setting the bar for work ethic and for what's possible to achieve. I'm sure we're both cringing at how long this degree has taken me.

Thank you to my lab mates and department friends throughout the years, I hope to stay in touch with all of you. To Emma J for sticking this out with me from the start, you're my day 1 and I appreciate you. To Jan and Dan for being great friends when I first started and didn't know anyone. To John Chan for being simultaneously a pain and also a great friend – senpai is proud of you. To Michelle for always being helpful and extremely competent. To Joey for the outrageous memes and great insight. To Klaudia for the wonderful talks while you were here. To Simon for your help on my final experiments – you know how much these results meant to me. To Megan Lo, Adi, and Mark – I'll miss you all and I couldn't have asked for a better group of friends to spend the final years of my PhD with. To Emma Tung for being my study buddy during my proposal and for all the 2 AM study talks. To Paige for all the 4th floor laughs. To the OG undergrads: MJ, Gabby, and Megan Weins – you 3 are wonderful humans and your time here was too short but I know you're all off doing amazing things. Thank you to Fernanda for your honesty, many laughs and conversations, and help trouble shooting. You're one of a kind and I'll surely miss you. To all of the friends I've made through working at CIF over years, thank you for always being a mental break and making athletics the best part time job. There are too many of you to name here.

Thank you to Felicity, for teaching me how to write, being the reason I stayed in research, and great friend for almost 14 years. You've been the most influential person in my adult life, and I'm always grateful for you. Thank you for everything.

Thank you to Michaela for being the best support that I could have asked for as I completed my thesis. You kept me sane and meeting you is why I'll never be mad at taking so long with this degree.

Thank you to my parents for enabling me to take this journey, always letting me choose my own path, and supporting me along the way. Your sacrifice in moving here, and allowing my individuality is what I cherish most.

Dedication

I dedicate this thesis to my parents, Mahtab and Hedayat.

Table of Contents

EXAMINING COMMITTEE MEMBERSHIP	II
AUTHOR'S DECLARATION	III
STATEMENT OF CONTRIBUTIONS.....	IV
ABSTRACT.....	V
ACKNOWLEDGMENTS	VII
DEDICATION.....	VIII
LIST OF FIGURES:.....	XI
LIST OF TABLES:.....	XIII
LIST OF ABBREVIATIONS.....	XIV
CHAPTER 1: INTRODUCTION.....	1
CHAPTER 2: BIOCHEMICAL FOUNDATIONS.....	4
<i>FUNCTIONS OF CARDIOLIPIN.....</i>	4
<i>KENNEDY PATHWAY OF CL SYNTHESIS.....</i>	7
<i>CARDIOLIPIN REMODELLING ENZYMES.....</i>	9
<i>Tafazzin.....</i>	9
<i>ALCAT1.....</i>	10
<i>Alpha Trifunctional Protein (αTFP).....</i>	11
<i>MLCL-AT1.....</i>	12
<i>OVERVIEW OF PHOSPHOLIPASE A/ACYLTRANSFERASE (PLAAT) ENZYMES.....</i>	13
<i>PLAAT1.....</i>	16
<i>PLAAT2.....</i>	18
<i>PLAAT3.....</i>	19
<i>PLAAT4.....</i>	20
<i>PLAAT5.....</i>	20
<i>N-ACYLETHANOLAMINES (NAEs).....</i>	21
<i>Arachidonylethanolamine (AEA).....</i>	22
<i>Palmitoylethanolamide (PEA).....</i>	23
<i>Oleoylethanolamide (OEA).....</i>	24
<i>Linoleoylethanolamide (LEA).....</i>	25
<i>Stearoylethanolamide (SEA).....</i>	25
<i>CURRENT UNDERSTANDING OF A ROLE FOR PLAAT1 IN CL REMODELLING.....</i>	27
<i>GAPS IN KNOWLEDGE:.....</i>	31
<i>SUMMARY OF STUDIES ON GENE ABLATION OF CL REMODELLING ENZYMES.....</i>	33
<i>Tafazzin Gene Ablation.....</i>	33
<i>ALCAT 1 Gene Ablation.....</i>	37
<i>Alpha Trifunctional Protein (αTFP) and MLCL-AT1 Gene Ablation.....</i>	39
CHAPTER 3: THESIS STUDY I – CHARACTERIZING THE O-TRANSACYLASE ACTIVITY OF PLAAT1 IN CARDIOLIPIN REMODELING USING AFFINITY-PURIFIED PROTEIN.....	41
<i>BACKGROUND AND RATIONALE:.....</i>	41
<i>OBJECTIVES AND HYPOTHESES.....</i>	42
<i>Adenoviral Overexpression System and Affinity Purification.....</i>	43
<i>In vitro PC:MLCL Transacylase Activity Assay.....</i>	44
<i>RESULTS:.....</i>	45
<i>DISCUSSION.....</i>	47

CHAPTER 4: THESIS STUDY II - CHARACTERIZATION OF CARDIOLIPIN CONTENT AND COMPOSITION IN PLAAT1-DEFICIENT HEART, BRAIN, AND SKELETAL MUSCLE	48
<i>INTRODUCTION AND STUDY RATIONALE</i>	48
<i>OBJECTIVES AND HYPOTHESES</i>	50
<i>STUDY DESIGN:.....</i>	51
<i>ANIMALS:</i>	51
<i>STATISTICAL ANALYSIS:.....</i>	53
<i>RESULTS</i>	54
<i>DISCUSSION</i>	82
CHAPTER 5: THESIS STUDY III - GROSS MORPHOLOGY AND SURVIVAL ANALYSIS OF PLAAT1^{-/-} MICE	85
<i>INTRODUCTION AND STUDY RATIONALE</i>	85
<i>OBJECTIVES AND HYPOTHESIS:.....</i>	86
<i>STUDY DESIGN:.....</i>	87
<i>Animals:.....</i>	87
<i>Statistical Analysis.....</i>	87
<i>RESULTS:</i>	89
<i>DISCUSSION:</i>	99
CHAPTER 6: THESIS STUDY IV - PHENOTYPIC CHARACTERIZATION OF PLAAT1^{-/-} MICE.....	103
<i>INTRODUCTION AND STUDY RATIONALE:.....</i>	103
<i>OBJECTIVES AND HYPOTHESIS:.....</i>	105
<i>STUDY DESIGN.....</i>	106
<i>Animals:.....</i>	106
<i>Indirect Calorimetry:.....</i>	106
<i>Treadmill Exercise Capacity and Exercise Recovery Test:.....</i>	107
<i>Statistical Analysis.....</i>	108
<i>RESULTS:</i>	109
<i>DISCUSSION</i>	120
CHAPTER 7: THESIS SUMMARY, INTEGRATED DISCUSSION, AND FUTURE PERSPECTIVES ...	123
<i>SUMMARY OF KEY FINDINGS.....</i>	123
<i>INTEGRATED DISCUSSION AND FUTURE PERSPECTIVES.....</i>	124
REFERENCES.....	135
APPENDICES	148
<i>APPENDIX A: 2-WAY ANOVA ANALYSIS FOR DETERMINING SEX DIFFERENCES IN TOTAL CARDIOLIPIN CONTENT.....</i>	148
<i>APPENDIX B: 2-WAY ANOVA ANALYSIS FOR DETERMINING SEX DIFFERENCES IN BRAIN CARDIOLIPIN COMPOSITION. .</i>	149
<i>APPENDIX C: 2-WAY ANOVA ANALYSIS FOR DETERMINING SEX DIFFERENCES IN HEART CARDIOLIPIN COMPOSITION. 150</i>	
<i>APPENDIX D: 2-WAY ANOVA ANALYSIS FOR DETERMINING SEX DIFFERENCES IN GASTROCNEMIUS CARDIOLIPIN COMPOSITION.....</i>	151
<i>APPENDIX E: FATTY ACYL COMPOSITION OF CL ISOLATED FROM BRAIN TISSUES OF PLAAT1^{-/-} AND WT MICE.</i>	152
<i>APPENDIX F: FATTY ACYL COMPOSITION OF CL ISOLATED FROM HEART TISSUES OF PLAAT1^{-/-} AND WT MICE.....</i>	153
<i>APPENDIX G: FATTY ACYL COMPOSITION OF CL ISOLATED FROM GASTROCNEMIUS TISSUES OF PLAAT1^{-/-} AND WT MICE.</i>	154

List of Figures:

Figure 1: O-transacylase activity of PLAAT enzymes.....	17
Figure 2: N-transacylase activity of PLAAT enzymes.....	18
Figure 3: PLAAT1 expression and subcellular localization.....	28
Figure 4: PLAAT1 expression in HEK-293 cells increases cardiolipin content.....	30
Figure 5: Lineweaver-Burk plots displaying the reciprocal PLAAT1 CL O-transacylase activity.....	46
Figure 6: PLAAT1 deficiency alters total CL concentrations in various mouse tissues.....	66
Figure 7: PLAAT1 deficiency alters the concentration of CL in brain and relative proportional abundance of major classes of fatty acyls in isolated CL.....	67
Figure 8: PLAAT1 deficiency displays lowered relative proportional composition of specific SFA species in CL isolated from the brain.....	68
Figure 9: PLAAT1 deficiency displays lowered relative proportional composition of specific MUFA species in CL isolated from the brain.....	69
Figure 10: PLAAT1 deficiency alters relative proportional composition of specific N-6 PUFA species in CL isolated from the brain.....	70
Figure 11: PLAAT1 deficiency alters relative proportional composition of specific N-3 PUFA species in CL isolated from the mouse brain.....	71
Figure 12: PLAAT1 deficiency alters the concentration of CL in cardiac tissue and relative proportional abundance of major classes of fatty acyls in isolated CL.....	72
Figure 13: PLAAT1 deficiency displays higher relative proportional composition of specific SFA species in CL isolated from the heart.....	73
Figure 14: PLAAT1 deficiency alters relative proportional composition of specific MUFA species in CL isolated from the heart.....	74
Figure 15: PLAAT1 deficiency alters relative proportional composition of specific N-6 PUFA species in CL isolated from the heart.....	75
Figure 16: PLAAT1 deficiency alters relative proportional composition of specific N-3 PUFA species in CL isolated from the heart.....	76

Figure 17: PLAAT1 deficiency alters the concentration of CL in gastrocnemius muscle and relative proportional abundance of major classes of fatty acyls in CL isolated from this tissue.....	77
Figure 18: PLAAT1 deficiency displays lowered relative proportional composition of specific SFA species in CL isolated from gastrocnemius muscle.....	78
Figure 19: PLAAT1 deficiency alters relative proportional composition of specific MUFA species in CL isolated from gastrocnemius muscle.....	79
Figure 20: PLAAT1 deficiency alters relative proportional composition of specific N-6 PUFA species in CL isolated from gastrocnemius muscle.....	80
Figure 21: PLAAT1 deficiency alters relative proportional composition of specific N-3 PUFA species in CL isolated from gastrocnemius muscle.....	81
Figure 22: Female and male body weights from 4 to 20 weeks of age.....	92
Figure 23: Organ and tissue weights in male and female mice.....	93
Figure 24: Daily measures of food intakes.....	94
Figure 25: Kaplan–Meier survival curves.....	97
Figure 26: Respiration Measures in Male Mice.....	114
Figure 27: Respiration Measures in Female Mice.....	115
Figure 28: Voluntary Activity Measures in Male mice.....	116
Figure 29: Voluntary activity measures in female mice.....	117
Figure 30: Treadmill exercise capacity and recovery testing of male mice.....	118
Figure 31: Treadmill exercise capacity and recovery testing of female mice.....	119

List of Tables:

Table 1. Kinetic parameters for PLAAT1 with different substrates.....	46
Table 2. Ratio of genotypes at the time of weaning.....	95
Table 3. Phenotypic ratio at the time of weaning.....	96
Table 4: Cause of death for male and female <i>Plaat1</i> ^{-/-} and <i>Wt</i> mice.....	98

List of Abbreviations

1, 2 – DAG: 1, 2-diacylglycerol
AA: Arachidonic acid
AdPLA: Adipose-specific phospholipase A2
AdPLA2: Phospholipase A2
AGPATs: Acylglycerophosphate acyltransferases
ALCAT1: Acyl-CoA:lysocardiolipin acyltransferase-1
AT: O-acyltransferase
BAK: Bcl-2 antagonist/killer
BAX: Bcl-2-associated X
BID: Bcl-2 homology domain 3 interacting-domain death agonist
BTHS: Barth Syndrome
CDP-DAG: Cytidine diphosphate diacylglycerol
CDP: Cytidine diphosphate
CDS: CDP-diacylglycerol synthase
CL: Cardiolipin
CLAMS: Comprehensive Laboratory Animal Monitoring System
Cyt c: Cytochrome c
Cytochrome c oxidase: Cytochrome c to complex IV
DGATs: Diacylglycerol acyltransferases
DHA: Docosahexaenoic acid
Drp1: Dynamin-related protein 1
DTT: Dithiothreitol
EDL: Extensor digitorum longus
ER: Endoplasmic reticulum
ETC: Electron transport chain
ETC: Electron transport chain
FAAH: Fatty acid amide hydrolase
FABP: Fatty acid binding protein
G3P: Glycerol-3-phosphate
GFP: Green fluorescent protein
GPATs: Glycerol-3-phosphate acyltransferases
GTPases: Guanosine triphosphate hydases
HFD: High fat diet
HRASLS: Harvey-Ras-like tumor suppressor
Hrev107: H-ras revertant #107
HUFA: Unsaturated fatty acids
IFU: Infectious units
IL: Interleukin
iMAC: Immobilized metal affinity chromatography
iNATs: Independent N-transacylases
iNOS: Intestinal nitric oxide synthase
LEA: Linoleoylethanolamide
LP: Lysophospholipid
LPA: Lysophosphatidic acid

LPAATs: Lysophosphatidic acid acyltransferases
LPC: Lysophosphatidylcholine
LPG: Lysophosphatidylglycerol
LPS: Lipopolysaccharide
LRAT: Lecithin:retinol acyltransferase
LVFS: Left ventricular fractional shortening
MAM: Mitochondria-associated ER membranes
Mfn: Mitofusin
MFN2: Mitofusion 2
mito-mRFP: Mitochondrial matrix protein tagged with red fluorescent protein
MLCL-AT1: Monolysocardiolipin Acyltransferase -1
MLCL: Monolysocardiolipin
MLCL: Monolysocardiolipin
MOI: Multiplicity of infection
MPTP: Mitochondrial Permeability Transition Pore
MUFA: Monounsaturated fatty acids
N-3: Omega-3
N-6: Omega-6
NAEs: N-acylethanolamides
NAFLD: Non-alcoholic fatty liver disease
NAPE-PLD: N-acyl phosphatidylethanolamine-specific phospholipase D
NAPEs: N-acylphosphatidylethanolamines
NAT: N-acyltransferase
NLRP3: NLR family pyrin domain containing 3
NPPE: N-palmitoyl-PE
OEA: Oleoylethanolamide
OMM: Mitochondrial membrane
PA: Phosphatidic acid
PAMP: Pathogen-associated molecular patterns
PAP: Phosphatidate phosphatase
PC: Phosphatidyl choline
PE: Phosphatidyl ethanolamine
PEA: Palmitoylethanolamide
PG: Phosphatidylglycerol
PKB: Protein Kinase B
PLA: Phospholipase A1/2
PLA_{1/2}: Phospholipases
PLAAT: The phospholipase A/acyltransferase
PLAAT1: Phospholipase A and acyltransferase 1
PLS-3: Phospholipid scramblase 3
PPAR: Peroxisome proliferator-activated receptors
PSS1: Phosphatidylserine synthase 1
PTPMT1: Protein tyrosine phosphatase mitochondrial 1
PUFA: Polyunsaturated fatty acid
RARRES3: Retinoic acid receptor responder 3
RER: Respiratory exchange ratio

RIG1: Retinoid-inducible gene 1
ROS: Reactive oxygen species
SCD-1: Stearoyl-CoA desaturase-1
SEA: Stearoylethanolamide
SFA: Saturated fatty acids
Smac/DIABLO: Second mitochondria-derived activator of Casp/direct inhibitor of apoptosis-binding protein
SSM: Subsarcolemmal mitochondria
TAG: Triacylglycerol
Taz-KO: Taz knockout
TAZKD: Taz knockdown
TEE: Total energy expenditure
TFP: Trifunctional protein
TG1: Transglutaminase
TIG3: Tazarotene-induced gene 3
TLC: Thin layer chromatography
TLCL: Tetra-linoleoyl cardiolipin
TLR4: Toll-like receptor 4
TNF- α : As tumor necrosis factor- α
TRPV1: Transient receptor potential vanilloid 1
UCP-2: Uncoupling protein-2
VCO₂: Carbon dioxide consumption
VO₂: Oxygen consumption
WAT: White adipose tissue
Wt: Wildtype
 α TFP: Alpha Tri-functional protein

Chapter 1: Introduction

Cardiolipin (CL) is a specialized dimeric phospholipid comprising ~25% of total phospholipids in the inner mitochondrial membrane in eukaryotes and is produced de-novo in the Kennedy pathway (1). CL constitutes about 20% of total phospholipids. Given its requirement for oxidative phosphorylation, the total amount of CL content varies between tissues in proportion to their oxygen demand (1). Compared to other phospholipids, CL has among the slowest turnover rates, with a half-life of 10.4 days compared to other phospholipids exhibiting an average half-life of 5.4 days (2).

CL plays several important roles in mitochondria. CL interacts with each of the electron transport complexes (3, 4), stabilizes respiratory supercomplexes (5), participates in mitochondrial fusion and fission (6), mediates crosstalk between mitochondria and lysosomes during the autophagic process (7), and is involved in protein transportation (8). Additionally, CL is required to maintain proper cristae architecture within the mitochondria (9), and the relocation of CL from the inner mitochondrial membrane to the mitochondrial surface has been shown to play a role in signal recognition for mitophagy (10).

CL is also an important factor in the regulation of cell death (11). Among phospholipids, CL's specific mitochondrial location and typical enrichment with unsaturated fatty acyl chains cause it to be the most susceptible among cellular PLs to oxidative damage by reactive oxygen species (ROS) (12). Oxidation or peroxidation of CL by ROS can cause mitochondrial dysfunction by impairing the electron transport chain at complex I and III, and can also to promote apoptosis (13). This has implications for health and disease, since CL peroxidation is associated with a variety of disease states (14).

CL produced *de-novo* in the Kennedy pathway is considered ‘immature’ or ‘nascent’ and a mature CL molecule is one that contains a fatty acyl chain profile that is distinct to, and functionally useful for the tissue in which it is located (15). This chemical specificity is achieved via remodeling through a process that utilizes phospholipase, acyltransferase, and transacylase enzymes (16-18). Remodeling of ‘immature’ CL begins with phospholipases (PLA1/2) cleaving non-specific acyl chains from the glycerol backbone, producing monolysocardiolipin (MLCL) or dilysocardiolipin (DLCL) (19). Re-acylation is achieved by an acyltransferase that uses fatty acyl-CoAs as donor substrates, or a transacylase that cleaves a fatty acyl chain from another phospholipid, producing a fully acylated or ‘mature’ CL, as well as a new lysophospholipid (20). These acyltransferases and transacylases are identified as CL ‘remodelling’ enzymes, and to date, four enzymes have been identified by other labs that can re-synthesize CL by acylating MLCL or DLCL (21). Understanding the role of remodelling enzymes in tissue-specific CL formation is critical for understanding how mitochondria function in normal and disease states, given that altered mitochondrial function and health is implicated in the pathology of a host of diseases including Alzheimer’s disease (22), Parkinson’s disease (23), cardiovascular disease (24), diabetes (25), immunological conditions (26), several types of cancer (27-29), aging (30, 31), ischemia (32, 33), hypertension (34, 35), and heart failure (36).

Prior work by our laboratory had indicated a role for a fifth enzyme, Phospholipase A/acyltransferase 1 (PLAAT1), in CL remodeling. Our research group recently published work demonstrating that PLAAT1 localizes to the endoplasmic reticulum (ER) and mitochondria-associated ER membranes (MAM), and that cells overexpressing PLAAT1 have higher levels of total CL (37). Prior, unpublished work by our lab has also found that crude cell lysates from cells overexpressing PLAAT1 have increased transacylase activity using MLCL as an acyl acceptor,

and phosphatidylcholine as an acyl donor, suggesting that it may *directly* catalyze the formation of CL as a novel function (38). In support of this, PLAAT1 has been reported to have O-transacylase activity *in vitro* (39), although to the best of our knowledge, no prior reports of PLAAT1 activities with CL or CL-related substrates have been reported. However, PLAAT1 also has N-transacylase activity, and therefore functions in the regulation of production of N-acylethanolamides (NAEs) (39). These bioactive compounds can regulate cellular metabolic processes that control levels of mitochondria and levels of enzymes involved in CL biosynthesis, which ultimately influences CL levels (40). Thus, it is possible that our observations of a promoting effect of PLAAT1 on cellular CL levels and CL synthesis capacity of crude lysate may have occurred *indirectly*, as a result of enhanced NAE-mediated signaling. Definitive evidence that PLAAT1 can *directly* remodel CL thus requires analysis using purified enzyme.

This thesis therefore first describes a series of biochemical studies to characterize the CL remodeling activity of affinity-purified PLAAT1. While our lab has previously tested effects of PLAAT1 overexpression on CL content and CL synthesis in cells, effects of PLAAT1 deficiency have not yet been studied. To address this, we generated *Plaat1* gene knockout mice. The CL content of tissues expressing high levels of *Plaat1* were analyzed, as well as CL content and composition. Finally, an initial phenotypic characterization and morphology of *Plaat1* knockout mice were performed, with an emphasis on evaluation of characteristics that could be related to mitochondrial function.

Chapter 2: Biochemical Foundations

Functions of Cardiolipin

CL influences various aspects of mitochondrial membrane dynamics and function, playing a critical role in maintaining the integrity and permeability of the inner mitochondrial membrane (41). CL's high content of unsaturated fatty acids makes the inner mitochondrial membrane impermeable to protons and other ions, creating the electrochemical gradient necessary for ATP synthesis (41, 42). CL is also involved in oxidative phosphorylation through direct interaction with the proteins and complexes of the electron transport chain (ETC), and thereby influences their function. CL binds to Cytochrome C, an essential protein in the ETC, facilitating its connection to the inner mitochondrial membrane (41), and this interaction is critical for the efficient transfer of electrons from cytochrome c to complex IV (cytochrome c oxidase), in the final complex of the ETC (41).

CL is also involved in mitochondrial fusion and fission, and helps to regulate these processes. Mitochondria possess a unique double-membrane structure that enables them to segregate various biochemical processes. Their particular morphology, encompassing their dimensions, shape, and branching, is closely connected to their function, and fusion and fission events help them maintain both morphology and function (43). During fusion, two mitochondria merge to create a larger structure, while fission leads to the division of a single mitochondrion into two (44). In the fusion process, CL binds with Mitofusin (Mfn), a protein integral to the outer mitochondrial membrane, to facilitate tethering neighboring mitochondria together, which forms the initial step in the fusing of distinct mitochondria (44). In contrast, during fission, CL interacts with the Dynamin-related protein 1 (Drp1), a GTPase that wraps around the mitochondrion and constricts it to facilitate the division into two mitochondria (45). Therefore,

changes in the amount or composition of CL may induce changes in mitochondrial fusion and fission, impacting the overall mitochondrial morphology.

Apoptosis, a programmed cell death mechanism crucial for sustaining homeostasis, is influenced by alterations in CL's content, positioning, and structure (46). CL is pivotal to the onset of apoptosis due to its association with cytochrome c (Cyt_c) and its migration to the outer mitochondrial membrane (OMM) (47). Within a thriving, non-apoptotic cell, mature unsaturated CL serves as a tether for Cyt_c, facilitating its role in the electron transport chain (48). However, during apoptosis, Cyt_c not only becomes the primary agent in caspase-activated cell death but also, upon its release from the mitochondria, binds to APAF-1 (49-51). This binding forms the apoptosome, instigating the caspase cascade that ultimately culminates in apoptosis (46). In the initial stages of apoptosis, oxidizing agents like H₂O₂ cause the peroxidation of CL (49-51). This peroxidation process changes the double-bond configuration of mature unsaturated CL, which consists of hydrophobic acyl chains, leading to its oxidized state and the resultant dissociation of Cyt_c from the IMM (49-51). Furthermore, the detachment of Cyt_c could result from the remodeling of CL from its unsaturated state to a saturated one, given that Cyt_c primarily binds to the unsaturated variant of CL (49-51). When Cyt_c becomes unbound from CL, it is then released into the cytosol, where it interacts with Apaf-1 and procaspase-9, resulting in the formation of the apoptosome (52). However, before cytochrome c is released from the mitochondria during the apoptotic process, CL undergoes a shift from the IMM to the OMM (49-51). Factors promoting apoptosis, or pathogen-associated molecular patterns (PAMPs) like bacterial lipopolysaccharide (LPS), have the potential to harm mitochondria, and prompt the migration of CL from the IMM to the cytoplasmic aspect of the OMM (49-51). In this transition phase, the concentration of CL in the outer mitochondrial membrane escalates, constituting 40%

of its overall quantity, with the remaining 60% located in the inner membrane (49). For CL to become accessible to the cytosol, it needs to traverse from the inner facet of the IMM to its outer side, pass through the intermembrane space, and then shift from the inner to the outer side of the OMM (49-51). This translocation is thought to be facilitated by phospholipid scramblase 3 (PLS-3) (49-51). Notably, inactivation of PLS-3 leads to enhanced resistance against apoptosis, underscoring the significance of CL movement in cellular signaling during this event (49-51). Upon its exposure to the OMM, CL is involved in the creation of cytochrome c/CL peroxidase complexes (49-51). Following CL peroxidation, the Mitochondrial Permeability Transition Pore (MPTP) is formed, aiding in the release of cytochrome c and other proapoptotic elements (49-51). This is facilitated by the CL present on the OMM, which promotes the recruitment of pro-casp-8 to the OMM (50). At this stage, pro-casp-8 becomes activated and subsequently cleaves Bcl-2 homology domain 3 interacting-domain death agonist (BID) (51). The resulting C-terminal fragment of BID, known as tBID, attaches to B cell lymphoma protein 2 (Bcl-2)-associated X (BAX) and Bcl-2 antagonist/killer (BAK). This binding triggers structural alterations, enabling the oligomerization of BAX/BAK and the subsequent development of MPTP in the OMM (50). Through the MPTP, Cytochrome c (cyt c) and the second mitochondria-derived activator of Casp/direct inhibitor of apoptosis-binding protein (Smac/DIABLO) are released, instigating the activation of casp-9 and finally in apoptotic cell death (50).

Autophagy, a cellular degradation process, is another area where CL plays a role. Externalized CL on the OMM has been shown to bind directly to LC3, a protein critical to autophagosome formation (10). This system is critical for the degradation of damaged organelles, and the recycling of their components within cells (53). Autophagy also aids in the

clearance of intracellular pathogens and the presentation of antigens to the adaptive immune system, thereby regulating immunity. In this regard, CL also contributes to inflammasome activation (54). Inflammasomes are intracellular multi-protein complexes that detect pathogenic microbes and stressors, triggering the production of pro-inflammatory cytokines IL-1 β and IL-18 (54). Oxidized CL serves as a ligand for the NLR family pyrin domain containing 3 (NLRP3) inflammasome, leading to its activation and eventual role in inflammation, and signifying a critical role for CL in immune responses as well as autophagy (54). In addition, CL is involved in immune responses in microbial infections and sepsis (55). During sepsis, CL can activate toll-like receptor 4 (TLR4), an immune system receptor, promoting an inflammatory response to the bacterial infection (55).

Kennedy Pathway of CL Synthesis

The Kennedy Pathway, first described by Eugene Kennedy in 1956, describes the *de novo* synthesis of phospholipids and triacylglycerol (TAG) (56). This pathway primarily operates in the ER, the MAM, and the mitochondria (57). Enzymes involved in the *de-novo* synthesis of glycerolipids, including phospholipids such as CL, include glycerol-3-phosphate acyltransferases (GPATs), and acylglycerophosphate acyltransferases (AGPATs)/lysophosphatidic acid acyltransferases (LPAATs) (57). This thesis is focused on the remodeling, rather than *de novo* synthesis of CL, and so this pathway is outlined only in brief, as follows:

- 1) A fatty acyl-CoA is esterified to a glycerol- 3-phosphate (G3P) molecule by a GPAT enzyme, producing a molecule of lysophosphatidic acid (LPA) (56).
- 2) LPA is esterified with another fatty acyl chain by an AGPAT/LPAAT enzyme, synthesizing phosphatidic acid (PA) (56).
- 3) The formation of PA is a branching point in the Kennedy Pathway:

- a. In the first branch, PA can be dephosphorylated by a phosphatidate phosphatase (PAP) enzyme to produce 1, 2-diacylglycerol (1, 2 – DAG), which can subsequently be used as a substrate by one of two diacylglycerol acyltransferases (DGATs) to produce a TAG (58). In the same branch, 1,2-DAG can alternatively be used as a substrate in either the cytidine diphosphate (CDP)-choline pathway to produce phosphatidyl choline (PC), or in the CDP-ethanolamine pathway to produce phosphatidyl ethanolamine (PE) (56). Phosphatidyl serine (PS) can also be synthesized by metabolizing either PC or PE with either phosphatidylserine synthase 1 (PSS1) (59) or phosphatidylserine synthase 2 (PSS2) (60).
 - b. In the second branch of the Kennedy Pathway, PA can be transformed into cytidine diphosphate diacylglycerol (CDP-DAG) by CDP-diacylglycerol synthase (CDS) (61).
- 4) Following step 3b, CDP-DAG can then be joined by an inositol molecule to synthesize phosphatidylinositol (PI), an important signaling molecule prevalent in the brain (62, 63).
 - 5) Alternatively, CDP- DAG can be converted into phosphatidylglycerol phosphate (PGP) by PGP synthase, which is dephosphorylated by a phosphatase to produce phosphatidylglycerol (PG) (64).
 - a. Phosphatidylglycerol constitutes less than 1% of membrane glycerophospholipids, but is important since it can be used as a precursor to the mitochondrial phospholipid CL, as part of the CDP-DG pathway (65).
 - 6) Once PGP is formed, it can then be de-phosphorylated into PG by protein tyrosine phosphatase mitochondrial 1 (PTPMT1) (66).
 - 7) Lastly, through the condensation of CDP-DAG and PG, CL synthase is able to produce CL (66).

Newly synthesized CL contains fatty acyl chains are added by GPAT and LPAAT enzymes, which lack significant substrate specificity. As a result, the fatty acyl composition of nascent CL tends to reflect the composition of other cellular membrane phospholipids, and must be remodeled in order to provide a chemical composition that reflects the requirements of the cell.

Cardiolipin Remodelling Enzymes

The process of transforming "immature" or "nascent" CL takes place in the Lands' pathway and initiates through the collective action of PLA1/2 activity, cleaving fatty acyl chains from one or both of the glycerol backbones (19). This action results in the formation of MLCL or DLCL (19). Mature, fully acylated CL is then re-acylated through the "remodelling" activity of either an acyl-CoA-dependent acyltransferase, which employs fatty acyl-CoAs as donor substrates, or transacylases, which facilitate the transfer of a fatty acyl chain from a phospholipid like PC to the lysocardiolipin molecule (20). Differences in the enzymes involved in remodeling, and the substrates utilized, results in significant tissue-specific differences in CL fatty acyl profiles (15). The predominant form of CL in mammals is tetra-linoleoyl cardiolipin (TLCL), consisting of 4 linoleic acyl side chains (C18:2, *n*-6), and composing 70-80% of total body CL (67). The preference for linoleic acyl side chains is especially prominent in the mitochondria of skeletal and cardiac muscles (68). In contrast, optimal acylation of CL is highly diverse in neuronal tissues (69). Four enzymes have been identified by other labs that can re-synthesize CL by acylating MLCL or DLCL. These enzymes are Tafazzin, Acyl-CoA:lysocardiolipin acyltransferase-1 (ALCAT1), Monolysocardiolipin Acyltransferase -1 (MLCL-AT1), and alpha Tri-functional protein (α TFP) (21).

Tafazzin

The predominant mitochondrial transacylase in many tissues is called Tafazzin (70). This enzyme functions specifically as a linoleoyl transacylase, using linoleate residues on phosphatidylcholine to remodel MLCL (71). Mutations in the *TAZ* gene cause dysfunctional CL remodelling and thus mitochondrial defects. In tissues that normally have high TLCL content, these defects result in the reduction of total TLCL, and accumulation of CL species with acyl-

group compositions that are unusual, typically with higher degrees of saturation (72). Changes in CL content are associated with mitochondrial changes including decreased activity of complexes III and IV of the electron transport chain (ETC), decreased ATP synthase activity, decreased oxidative phosphorylation in isolated skeletal muscle mitochondria, decreased super-complex formation, and abnormal mitochondrial structure (73, 74).

In humans, mutations in Tafazzin result in a genetic disorder called Barth Syndrome (BTBS). BTBS is an X-linked mitochondrial disease that is characterized by skeletal- and cardiomyopathies (which are attributed to diminished O₂ utilization by skeletal muscle), impaired growth, chronic fatigue, neutropenia, and varying degrees of cognitive impairment, such as specific learning difficulties (42, 75). At a molecular level, skeletal muscle mitochondria from BTBS patients exhibit mitochondrial respiratory chain disturbances (76). Furthermore, BTBS cells exhibit mitochondrial fragmentation (77), impaired mitochondrial function (78), increased ROS production (79), and BTBS lymphoblast mitochondria exhibit a variety of structural abnormalities such as decreased cristae surface area, and increased mitochondrial volume and fragmentation (80). Research has also found links between Tafazzin and other diseases. In mice, Tafazzin deficiency leads to changes in the morphology and function of the heart, leading to cardiomyopathy (1). Additionally, alterations in CL content or composition due to Tafazzin deficiency have been linked to other conditions, including neurodegenerative diseases and diabetes (81).

ALCAT1

ALCAT1 is another major enzyme that was discovered to have a role in CL remodelling, and was first identified and characterized in 2006 (13). ALCAT 1 is an acyl-CoA:lysocardiolipin acyltransferase that can use both MLCL and DLCL as the acyl acceptor (20). ALCAT1 is mainly

localized in the ER and MAM (13, 82). The MAM bridges the ER and mitochondria, and is a site where phospholipid synthesis takes place, and is a conduit for phospholipid shuttling between membranes (13). Furthermore, some of the ALCAT1 protein also localizes to the mitochondrial (13). In comparison to other CL remodelling enzymes, ALCAT1 lacks preference for linoleic acid as a substrate (16, 17). Excessive remodelling of CL by ALCAT1 leads to TLCL depletion, and its replacement with CL enriched in docosahexaenoic acid (DHA) and arachidonic acid (AA) (17). DHA and AA are highly unsaturated, and therefore CL enriched in these fatty acyl species is more sensitive to oxidation by ROS and apoptotic stimuli (14, 51). Because of this, ALCAT1 remodeling of CL is associated with a greater production of dysfunctional forms that are commonly found in obesity, diabetes, and cardiovascular disease (14). In fact, upregulated ALCAT1 activity has been associated with the increased oxidized CL species observed in heart failure (51).

ALCAT1 is localized at the MAM, where autophagosome biogenesis takes place (13, 83). Overexpression of ALCAT1 causes dilation of the MAM (13), suggesting a potential role of this enzyme in regulating autophagy (13). Inhibition of ALCAT1 has been suggested as a possible therapeutic strategy for some conditions, as it was found that inhibiting ALCAT1 can significantly attenuate the production of abnormal CL species, preserve mitochondrial function, reduce oxidative stress, and thus ameliorate the progression of heart failure (51).

Alpha Trifunctional Protein (α TFP)

Trifunctional protein (TFP) is found in the MAM, and was originally characterized as an enzyme involved in catalyzing three reactions (17), long chain enoyl coenzyme A hydratase reactions, long chain 3-hydroxyacyl-coenzyme A dehydrogenase reactions, and long chain 3-oxoacyl coenzyme A thiolase reactions (84). In addition, the alpha subunit of TFP (α TFP) was

later found to exhibit acyl-CoA acyltransferase activity in the acylation of MLCL to CL with linoleoyl-CoA, oleoyl-CoA and palmitoyl-CoA as substrates, when increased expression of α TFP in HeLa cells was found to increase incorporation of the radioactive form of these substrates into CL (84). Expression of α TFP in Barth Syndrome lymphoblasts caused an increase in linoleoyl-CoA acylation of MLCL to CL *in vitro*, and increased the activity of mitochondrial respiratory complex proteins, but surprisingly resulted in a reduction in total TLCL (84). Knock down of α TFP in lymphoblasts deficient in Tafazzin increased the accumulation of MLCL relative to healthy lymphoblasts with normal α TFP levels (84).

It has been suggested that a potential indirect association may exist between the function of α -TFP and the balance of CL. For instance, the lack of α -TFP can lead to hindered β -oxidation, potentially leading to a buildup of long-chain fatty acids (85). Considering the significant need for fatty acids in the formation of mitochondrial phospholipids, including CL, any disruption in fatty acid metabolism could potentially influence CL homeostasis. Furthermore, mitochondrial impairment caused by α -TFP deficiency could also impact the environment of the mitochondrial membrane and the integrity of CL, resulting in further changes (86). This highlights the difficulty of definitively assessing biological roles of enzymes with multiple functions.

MLCL-AT1

MLCL AT-1 is a protein that exhibits structural identity to the α TFP but lacks the first 227 amino acids of α TFP, and is suggested to have been derived from α TFP (84). This suggests that both of these proteins are derivatives of splicing the same gene (84). MLCL-AT1, is a CoA-dependent mitochondrial MLCL acyltransferase that preferentially esterifies linoleoyl-CoA,

followed by oleoyl-CoA, and finally palmitoyl-CoA onto MLCL (17). It has been shown that in healthy lymphoblasts, decreased Tafazzin expression results in increased MLCL-AT1 mRNA, protein, and enzyme activity as a potential compensatory measure, but this compensation does not result in recovery of total CL (87). However, in Barth lymphoblasts that are deficient in Tafazzin, MLCL-AT1 enzyme levels are also decreased (87). It has been hypothesized that the extensive mitochondrial damage in BTHS cells prevents them from utilizing MLCL AT-1 to compensate for decreases in Tafazzin (87). Treatment of Barth lymphoblasts with increased MLCL-AT1 expression increases CL levels, improves mitochondrial respiration, and decreases the production of superoxide by cells, but does not restore the molecular composition of CL to that of healthy lymphoblasts (87). At the subcellular level, MLCL-AT1 has been shown to localize to the inner leaflet of the inner mitochondrial membrane (17), and in rats, it is physiologically most active in heart mitochondria (88). MLCL-AT1 was the last CL remodelling enzyme to be characterized prior to work by our laboratory on PLAAT1.

Overview of Phospholipase A/Acyltransferase (PLAAT) Enzymes

The phospholipase A/acyltransferase (PLAAT) enzymes, also known as Harvey-Ras-like tumor suppressor (HRASLS) enzymes, are a homologous group of proteins, and a part of the *H-rev107* gene family. There are currently five PLAAT enzymes identified in humans (PLAAT1-5)(89), while only three of these enzymes (PLAAT1, 3, 5) are conserved in rodents (89).

PLAAT enzymes have been characterized as class II tumor suppressors (90), and specifically as inhibitors of H-Ras-derived tumorigenesis (hence their alternative HRASLS moniker) (89).

Class II tumor suppressors are a group of enzymes that are characterized by their ability to down-regulate cell growth, particularly cancer cell growth, while themselves not being mutated or

changed in the cancerous tissue (91). Briefly, PLAAT1 has been shown to suppress the growth of H-Ras-transformed NIH3T3 cells (92). High expression of PLAAT2 suppresses the colony formation of HCT116 (colon cancer) and HeLa (cervical cancer) cells (93). PLAAT3 has been characterized to reverse H-Ras-derived transformation of rat fibroblasts (94), and suppress H-Ras signaling (95). PLAAT4 inhibits Ras activation (96), and the lung metastasis of breast cancer cells (97). PLAAT5 has yet to be characterized with regards to tumor suppressing properties.

PLAAT enzymes are also known as lecithin:retinol acyltransferase (LRAT)-like proteins due to their similar sequence homology to the enzyme LRAT (20). This includes a conserved NCEHFV motif in the C-terminal region that is pertinent to acylation and de-acylation reactions (98). Mass spectrometry analysis has characterized that a thioester intermediate forms between cysteine 161 of LRAT and the acyl side-chain donated by PC (99), suggesting that PLAAT enzymes catalyze glycerophospholipid reactions. Indeed, PLAAT proteins have been identified as enzymes that participate in the remodelling of acyl chains for glycerophospholipids (20). All known PLAAT enzymes possess lipid enzyme activities. These activities include phospholipase A_{1/2} (PLA) and O-transacylase activities (89) with the catalytic site being formed by histidine 23, histidine 35, and cysteine 113 (89, 100).

In vitro, Ca²⁺ independent PLA_{1/2} activities require a pH of 8–9, dithiothreitol (DTT), and Nonidet P-40 at 37 °C for 30 minutes for optimal enzymatic conditions (101). The activity of PLAAT enzymes results in a fatty acyl chain being cleaved from a phospholipid, generating an enzyme-fatty acyl intermediate and releasing of a free lysophospholipid (89). During this process, if the catalytic cleft releases a fatty acyl group instead of transferring it to a new lysophospholipid, then this process will be defined as phospholipase activity rather than

transacylase activity (102). PLA₁ activity utilizes PC and PE as substrates and appears to be preferred over PLA₂ activity for PLAAT1, 2, 4, and 5 (15, 98, 101). PLAAT3 shows both PLA_{1/2} activities while using PC, PE and also PS, and PI as substrates (103).

The PLAAT family of proteins also demonstrate O-transacylase activity, described as the acyl-CoA-independent transacylation of a lysophospholipid using a fatty acyl chain donated from another phospholipid (89). Specifically, this reaction involves the transfer of an acyl group from a phospholipid to G3P or a lysophospholipid (LP) (89). All PLAAT enzymes have shown a capacity for O-acylation of lysophosphatidylcholine (lyso PC) at the sn-1 position (39, 104), but none have been for O-acylation activity with MLCL or DLCL as fatty acyl acceptors.

Lastly, *in vitro* analysis has shown that the PLAAT family of enzymes display N-transacylase activity for the production of N-acylphosphatidylethanolamines (NAPEs), catalyzing the transfer of an acyl chain from the *sn-1* or *sn-2* position of a glycerophospholipid to the amino group of PE to produce NAPEs (104). Most research characterizing the N-transacylase activity of PLAAT enzymes utilize PC as an acyl donor (15, 39, 104-106). NAPE synthesis is biologically important, since cleavage of NAE groups from NAPEs can result in generation of free NAE molecules that are potent in cellular signaling.

Three groups of enzymes catalyze N-transacylase reactions: Ca²⁺-dependent N-transacylases (Ca-NATs), Ca²⁺-independent N-transacylases (iNATs), and PLAAT enzymes, which are also Ca²⁺-independent, but are categorized as a separate group (107). These groups of enzymes all utilize glycerophospholipids as acyl donors (89). Since glycerophospholipids tend to have a saturated and unsaturated fatty acyl chain in the *sn-1* and *sn-2* position respectively, the NAE group produced by transacylation followed by NAPE cleavage, will be influenced by the

positional-preference of the N-transacylase enzyme (108). The species of NAPE produced in cells have the potential to impact cellular function, since NAPE are important precursors to the biologically active NAE signaling molecules, and different chemical species of NAE display very different activities (109). A summary of the biological action of major NAE species, as well as the potential implications of the modulation of NAE levels for CL synthesis regulation, is provided in the section below the PLAAT enzymes.

PLAAT1

PLAAT1, first named A-C1, is a 167-amino acid long protein discovered in 1999, and found to be 45% homologous with PLAAT3 (92). Shinohara and colleagues characterized the O-transacylase activity of PLAAT1, reporting that PLAAT1 catalyzes *in vitro* O-transacylations, utilizing PC as an acyl donor and lysophosphatidylcholine (LPC) as an acyl acceptor (Fig. 1) (39). PLAAT1 functions in a CoA – independent manner in order to remodel PC. The enzyme prefers esterolysis at the *sn-1* position of PC, and esterification at the *sn-1* position of LPC (39). In 2011, research by Shinohara and colleagues showed that purified human PLAAT1 has N-transacylase activity when utilizing PE as an acyl acceptor and radiolabelled PC as an acyl donor (Fig. 2) (39). In experiments where [¹⁴C] radiolabelled palmitate was used to metabolically label COS-7 cells, overexpression of PLAAT1 in COS-7 cells increased the formation of [¹⁴C]N-palmitoyl-PE (NPPE) by approximately 100-fold when compared to controls, suggesting that PLAAT1 can synthesize NAPE *in vivo* as well (39).

Previous reports indicated that *in vitro* enzyme activity of PLAAT1 displays N-transacylase, O-transacylase, as well as PLA1/2 phospholipase activity when using purified human PLAAT1 protein in a radiolabelled enzyme assay (39). Among these, PLAAT-1

displayed the highest affinity for 2-[14C]palmitoyl-lyso PC for lyso PC O-acylation, displayed more than 1.0 $\mu\text{mol}/\text{min}/\text{mg}$ of substrate, while PLA1/2 phospholipase activity, N-transacylase activity, and O-transacylase activity using 1-[14C]palmitoyl-lyso PC all displayed less than 0.2 $\mu\text{mol}/\text{min}/\text{mg}$ of substrate (39). However, the presence and preference of these enzyme activities have not yet been demonstrated *in vivo*. In humans, mice, and rats, PLAAT1 expression were highest in the testis and skeletal muscle, followed by the brain and heart (39). Humans show low expression of PLAAT1 in most other tissues (39). In mice and rats, PLAAT1 is also abundantly expressed in these same tissues, as well as showing some expression in the thymus (39).

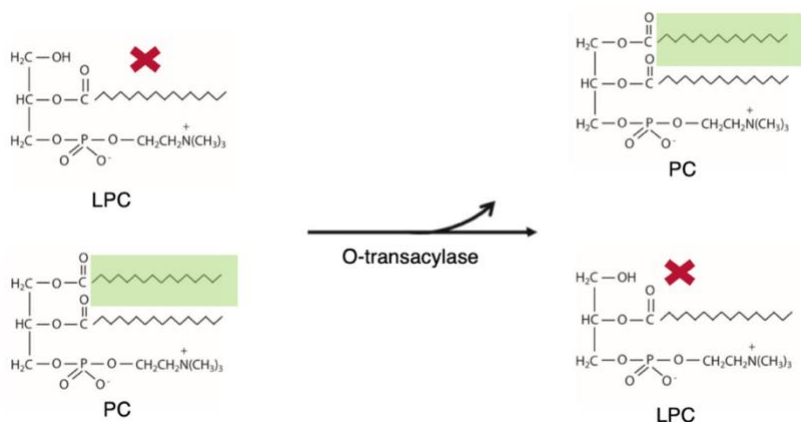


Figure 1: O-transacylase activity of PLAAT enzymes.

PLAAT enzymes can act as a LPC O-transacylase to create phospholipids with distinct acyl compositions. In this example, these enzymes extract a specific fatty acyl group from either the sn-1 or sn-2 position of PC and incorporate it into the sn-1 position of LPC, resulting in the production of PC.

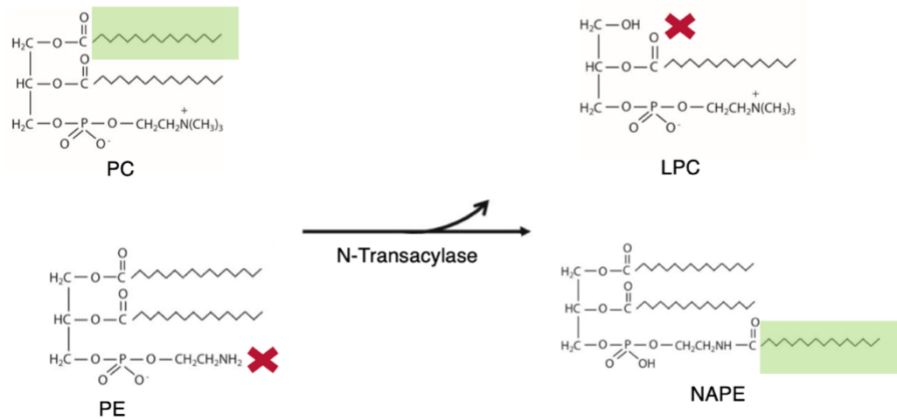


Figure 2: N-transacylase activity of PLAAT enzymes.

PLAAT enzymes can act as a PE N-transacylase to create NAPE. In this example, these enzymes extract a specific fatty acyl group from either the sn-1 or sn-2 position of PC and incorporate it into the amino group of PE, resulting in the production of NAPE.

PLAAT2

PLAAT2 was initially cloned from SW480 human colon cancer cells. It is positioned on chromosome 11 of the human genome and is absent from the genome of rodents (93). PLAAT2 is an 18 kDa protein that is made up of 162 amino acids and is situated in the perinuclear region, and the transcript of the *PLAAT2* gene is primarily found in gastrointestinal tissues (93).

PLAAT2 shares 47% and 69% sequence homology with PLAAT1 and PLAAT3 respectively (89).

The physiological role of PLAAT2 remains undetermined thus far. However, biochemical functions of this enzyme in phospholipid metabolism have been examined using both cell homogenates and purified enzyme (15). Overexpression of PLAAT2 in COS-7 cells, as well as in post-microsomal supernatants and microsomal pellets, were observed to enhance *in vitro* PLA1/2 activity, N- transacylase activity, as well as O-transacylase activity (15). PLAAT2

also displayed O- transacylase activity, forming [14C]PC from both 1-[14C]palmitoyl lyso PC and 2-[14C]palmitoyl lyso PC (15). Overall, *in vitro* PLAAT2 displays the highest level of enzyme function when being utilized as an O-transacylase activity while using and 2-[14C]palmitoyl lyso PC, followed by PLA1/2 activity, and finally N- transacylase activity (15)

PLAAT3

PLAAT3, alternatively known as adipose specific phospholipase A2 (AdPLA2) and H-ras revertant #107 (Hrev107), was the first enzyme to be characterized from the PLAAT family of enzymes and shares 46% sequence homology with PLAAT1 (94). PLAAT3 was initially identified through subtractive hybridization (a technique that enables PCR-based amplification of cDNA fragments) in rat fibroblasts (94), and it is found at greatest abundance in adipocytes (103).

The enzymatic characteristics of PLAAT3 were initially studied in 2007, revealing the *in vitro* N- transacylase activity of this enzyme (15). Further study suggested that PLA activity takes precedence over N- or O- transacylase activity for PLAAT3 *in vitro* (39, 104), specifically as an adipose-specific phospholipase A2 (AdPLA) (103). The enzyme's alternate name, AdPLA, reflects its primary expression in adipose tissue (110). PLAAT3 has been found to be the major enzyme in controlling the release of fatty acids in adipose tissue, as it regulates the levels of free AA, an omega-6 polyunsaturated fatty acid that participates in a variety of physiological functions (110). In mice deficient in the PLAAT3 enzyme, enhanced lipolysis levels were detected, leading to a lean phenotype, even when the mice were given a high-fat diet (110). These mice exhibited greater energy expenditure, better glucose tolerance, and increased insulin sensitivity compared to regular mice when both were given a high-fat (110).

PLAAT4

PLAAT4 was identified by three different groups, and hence it has been given three distinct names: tazarotene-induced gene 3 (TIG3) (111), retinoid-inducible gene 1 (RIG1) (112), and retinoic acid receptor responder 3 (RARRES3) (113), in addition to PLAAT4 (104). PLAAT4 displays 48% sequence homology with PLAAT1 and 51% sequence homology with PLAAT3, and is expressed in humans but not mice (96). Subcellularly, PLAAT4 is attached to both the ER and the Golgi apparatus (96). Like its family members, PLAAT4 also exhibits a suppressive effect on H-RAS-mediated signalling (89). However, the anti-tumor function of PLAAT4 is restricted to the Golgi apparatus, as this is the sole subcellular location where the enzyme triggers apoptosis in cancer cells (96).

Similar to other PLAAT enzymes, PLAAT4 participates in phospholipid metabolism, functioning as a Ca^{2+} independent PLA1/2 *in vitro* (15). Even though this enzyme doesn't exhibit *in vitro* N- transacylase activity *in vitro* (15), metabolic labeling experiments reveal that PLAAT4 over-expression elevates cellular levels of both NAPE and NAE (104). PLAAT4 is found in the suprabasal epidermis of the skin, where it activates transglutaminase (TG1), an enzyme involved in terminal differentiation, creating covalent bonds between proteins on the inner surface of the plasma membrane (114).

PLAAT5

PLAAT5 was identified in 2007 as a part of an effort to discover new Ca^{2+} -independent enzymes that participate in the production of NAPE (101). *In vitro*, PLAAT5 primarily exhibits N- transacylase activity over both PLA1/2 and O-acylation activities (89, 108). When PLAAT5 is overexpressed in cultured cells, it elevates the production of NAPE and NAE. However, it

doesn't display a preference for removing acyl groups from either the sn-1 or sn-2 positions of PC during N-acylation reactions (101). PLAAT5 shares 45% protein sequence homology with PLAAT1, but unlike other currently characterized PLAAT enzymes, its subcellular localization is predominantly in the cytosol, likely due to the absence of the characteristic C-terminal hydrophobic span present in PLAAT enzymes 1–4, and it is also not clear whether PLAAT5 possesses anti-tumorous characteristics like other enzymes within this family (101, 115). This enzyme is expressed at highest levels in the testes and is speculated to contribute to spermatogenesis (115), although the exact physiological function of this enzyme remains unclear.

N-acylethanolamines (NAEs)

All PLAAT enzymes, including PLAAT1, participate in the formation of NAPE that are precursors for NAEs (89). The production of NAEs is initiated in the cell membrane, where precursor phospholipids are located (108). Either the enzyme N- transacylase (NAT), or a PLAAT, moves an acyl group from a donor molecule, typically a phosphatidylcholine, to the primary amine group of PE (116). This process culminates in the generation of NAPEs, which can subsequently be altered into NAEs through the action of N-acyl phosphatidylethanolamine-specific phospholipase D (NAPE-PLD) (117). This enzyme cleaves between the phosphate group and the ethanolamine headgroup, resulting in the release of N-acylethanolamines (NAEs) (118).

NAEs are a family of bioactive lipids that are important signaling molecules in various biological systems, and are comprised of a fatty acyl chain that is attached to an ethanolamine group (119). NAEs are ubiquitous and have been identified in plants, mammals, and bacteria (118). The functions of NAEs vary greatly between different species and systems, and some of these functions include nociception, appetite regulation, thermogenesis regulation, as well as the

regulation of inflammatory responses (120-122). Additionally, the enzyme known as fatty acid amide hydrolase (FAAH) has the capability to decompose NAEs into their basic components of ethanolamine and fatty acid, thus managing the concentration of NAEs inside the cell (123, 124). The equilibrium between the liberation of NAEs by NAPE-PLD and their breakdown by FAAH plays a vital role in defining the level of NAEs (125). Once created, NAEs can engage with a variety of receptors to execute in signal transduction (118, 120-122). The following sections provide a brief overview of some of the more abundant species of NAE.

Arachidonylethanolamine (AEA)

AEA is a polyunsaturated fatty acyl amide, having an AA moiety linked to an ethanolamine (126). AEA has been identified as an endogenous ligand for CB1 receptors, which are primarily found in the central nervous system, and to a lesser extent for CB2 receptors, which are mainly expressed in the immune system (124, 127). While the interaction of AEA with CB1 receptors is well characterized, its role with CB2 receptors and other targets such as transient receptor potential vanilloid 1 (TRPV1) and peroxisome proliferator-activated receptors (PPARs) is less well understood but subject of research (128).

Degradation of AEA is largely handled by fatty acid amide hydrolase (FAAH), which hydrolyzes anandamide into free AA and ethanolamine (123, 124). The inhibition of FAAH, thereby preventing AEA breakdown, is considered a potential therapeutic strategy for several conditions, since a AEA is involved in a broad spectrum of physiological processes, including pain, appetite, and memory (124, 129-132). For instance, AEA can modulate nociception and has been suggested as an endogenous pain suppressor (133), and ablating the FAAH enzyme in mice results in a more than 10-fold elevation of AEA in many brain regions, resulting in an analgesic phenotype (124). In rodent models, acute administration of AEA has been shown to stimulate

appetite and impairs short-term memory (130, 132). Moreover, alterations in AEA signaling have been linked to a variety of pathological conditions. Elevated levels of AEA have been detected in patients with neuropsychiatric conditions such as schizophrenia and anxiety disorders (134), Conversely, reduced levels have been associated with major depression (135). The role of AEA in neuroinflammation and neurodegenerative diseases such as Alzheimer's and Parkinson's, is also currently under investigation (136).

Palmitoylethanolamide (PEA)

PEA is a naturally occurring NAE, constructed from palmitic acid and ethanolamine. It's most well-known mechanism involves interaction with PPAR- α , a receptor belonging to the family of nuclear receptor proteins that are critical for regulating gene expression and inflammation, maintaining energy balance, and regulating metabolic functions (133, 137, 138). Like OEA, PEA is an endocannabinoid – like compound, exerting it's effects independently of direct endocannabinoid activation (138), but may still influence the endocannabinoid system, through enhancing the actions of AEA through the 'entourage effect', attenuating the breakdown of AEA, thus enhancing signaling of CB1 and CB2 receptors (138, 139). In short, PEA may increase AEA levels by competing with it for hydrolysis by FAAH, resulting in less AEA being hydrolyzed, though this mechanism has only been observed *in vitro* (138, 139). Besides its known anti-inflammatory activity, PEA also produces analgesia, as it's been shown to attenuate several forms of laboratory induced nociception in mice (140, 141). This effect is hypothesized to act through binding the CB2-like receptors in the periphery, though the target receptor involved is still unclear (140, 141). Additionally, PEA has been studied for its anti-epileptic properties, though the mechanism of action for these effects has yet to be elucidated (142, 143). In an mouse model utilizing both, maximal electroshock seizures and chemically induced

convulsions, PEA was found to be an effective anti-convulsant for both forms of synthetically induced seizures (142). Similarly in a rat model of amygdaloid seizures, PEA was shown to be protective against tonic convulsions, while also prolonging the latency between convulsive episodes (143). One example of the previously defined ‘entourage effect’, is PEA’s apparent attenuation of MCF-7 breast cancer cell proliferation *in vitro* (144). Here, PEA is shown to enhance the effects of AEA by decreasing its degradation 3-6 fold through down-regulating FAAH expression and activity by 30-40% (144). By doing this, PEA enhances the AEA induced inhibition of NGF Trk receptors, which underlies the anti-proliferative effect of AEA on MCF-7 cells (144).

Oleoylethanolamide (OEA)

OEA is a biologically active NAE derived from the monounsaturated fatty acid oleic acid. It is produced in the small intestine, and is believed to play a role in managing feeding, body weight, and lipid metabolism (122). In contrast to AEA, an endocannabinoid, OEA is an endocannabinoid – like compound, functioning independently of cannabinoid receptors CB1 and CB2, suggesting that the effects exerted by this NAE are unlikely to be psychoactive (145). OEA is notably recognized for inducing an anorexigenic response, as it has been shown that administration of OEA in both rats and mice has a time- and dose-dependent effect on food intake, diminishing food consumption over a 24-h period (146). The satiety inducing effects of OEA are thought to be induced through PPAR- α , as it has been shown that the oral supplementation of OEA in healthy obese individuals over an 8-week period has been shown to increase PPAR α gene expression 2.41 fold (146). OEA is thought to bind to and activate PPAR- α in the small intestine, inhibiting the upregulation of intestinal nitric oxide synthase

(iNOS) (146), a family of enzymes whose inhibition have been shown to reduce energy intake (147).

Linoleoylethanolamide (LEA)

LEA structurally resembles OEA closely and is an endogenous ligand for the pain-associated TRPV1 (148). It stands alongside OEA as one of the strongest activators of PPAR- α (133). Activation of PPAR- α specifically has been shown to stimulate the turnover of fatty acids through the upregulating genes involved in fatty acid transport and fatty acid beta-oxidation, such as FAT/CD36, uncoupling protein-2 (UCP-2), and fatty acid binding protein (FABP)(146). Moreover, studies indicate that LEA can diminish the expression of inflammatory markers such as tumor necrosis factor- α (TNF- α), interleukin (IL)-1 β , and IL-6 triggered by lipopolysaccharide (LPS) (149). It also attenuates the rise of cyclooxygenase enzyme-2 and prostaglandin E2 due to LPS (149). When used on ear skin in a contact dermatitis animal test, LEA has been shown to alleviate symptoms caused by 2,4-dinitrofluorobenzene and reduced the pro-inflammatory cytokine production at the inflamed locations (149).

Stearoylethanolamide (SEA)

SEA is an NAE that is present in human, rat, and mouse brain in amounts comparable to those of AEA (150). From a chemical perspective, SEA is an amide that results from the combination of ethanolamine and stearic acid (C18:0) (118). Similar to other NAEs, SEA has the ability to engage with PPARs, specifically, PPAR γ (151). In an *in vitro* model using leukemia L1210 cells, SEA has been shown to inhibit IL-1 and IL-6 mRNA levels in a dose-dependent manner (152). In an insulin resistant rat model, SEA treatment induced normalization of TNF- α , and this effect was associated with the inhibition of nuclear NF- κ B translocation in rat peritoneal

macrophages (152). These findings seem to suggest that SEA may contribute to mitigation of inflammation, through attenuating the release of inflammation-promoting cytokines. Additional research also displays that both intraperitoneal and oral administration of SEA in mice behaves as an anorexigenic agent, reducing overall food intake (153). Researchers found that this anorexigenic response upon SEA administration was associated with marked decrease in hepatic stearoyl-CoA desaturase-1 (SCD-1) mRNA expression, the primary rate-limiting lipogenic enzyme that catalyzes the synthesis of MUFA, and is a molecular target for the treatment of obesity (153).

Current Understanding of a Role for PLAAT1 in CL Remodelling

Data from our laboratory, as well as information from published studies, has led us to hypothesize that PLAAT1 may play a role in CL metabolism, possibly through direct and/or indirect mechanisms. Indirectly, NAEs from PLAAT1-derived NAPEs may signal to enhance CL synthesis, either by affecting levels of mitochondria (40) or the expression of enzymes involved in CL synthesis (38). Directly, it is possible that PLAAT1 may catalyze the O-transacylation of MLCL (and/or DLCL) to synthesize CL in a remodeling reaction, similar to Tafazzin, MLCL-AT, α TFP, and ALCAT1. My thesis studies have focused first on testing whether PLAAT1 could play a direct enzymatic role in CL remodeling, and then next on understanding the physiological role of PLAAT1 *in vivo*. Notably, these latter studies do not disambiguate potential direct and indirect effects, but set a basis for future work on this topic. These concepts, and the current data supporting them, are summarized in the following sections.

Initial studies on a potential role for PLAAT1 in CL remodelling have been conducted by our research group, and data from some of these are published in the *International Journal of Molecular Sciences* in 2022 (37). This work formed the basis for my thesis studies related to a role for PLAAT1 in CL metabolism. The first two research objectives in this study were as follows:

1. To characterize the tissue expression profiles and subcellular localization of PLAAT1.
2. To investigate effects of PLAAT1 overexpression on cellular phospholipid levels.

For the first objective, our investigations found that PLAAT1 is universally expressed in all tissues examined, but that the brain and heart presented the highest expression levels of the enzyme's predominant murine transcript, transcript variant 1 (Figure 3A,B) (37). This variant of

Plaat1 was also present at varying levels in the other murine tissues, including liver, lung, kidney, gonadal white adipose tissue (WAT), skeletal muscle, spleen, pancreas, and testes (Figure 3) (37). We also found that PLAAT1 localizes to the endoplasmic reticulum, since it was predominately found in the microsomal fraction when cells were subjected to differential centrifugation, although it was also detected in the MAM (Figure 3C, D)(37).

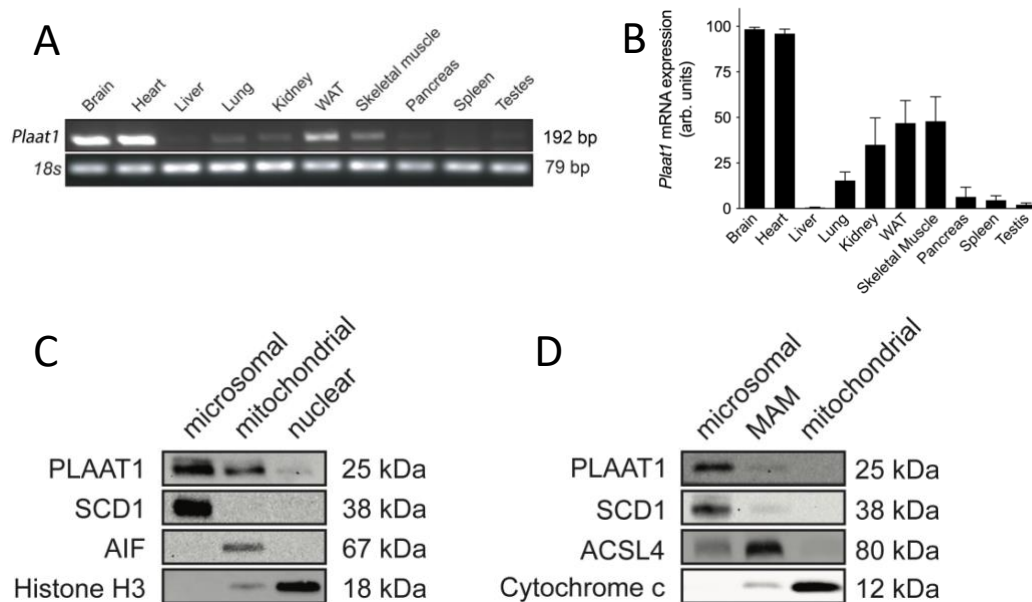


Figure 3: PLAAT1 expression and subcellular localization. *Plaatt1* gene expression was detected at highest levels in brain, heart, WAT, and skeletal muscle, but was also visualized (A) and found by density analysis of bands (B) to be present in other tissues at lower levels. Data are means \pm S.E.M., n = 3–6. Subcellular localization of PLAAT1 was investigated by immunoblotting microsomal, mitochondrial, and nuclear fractions produced by differential centrifugation of whole mouse brains for PLAAT1, or for markers of fractional purity including SCD1 as a marker of the ER, AIF as a mitochondria-specific marker, and histone H3 as a nuclear marker (C). Alternately, mouse brains were separated to derive ER (microsomal), MAM, and mitochondrial fractions for detection of PLAAT1 or markers of fractional purity (i.e., SCD1 (ER), ACSL4 (MAM), and cytochrome c (mitochondria)) (n = 3).

For our second objective, we expressed *Plaatt1* in HEK-293 cells (Figure 4A), and isolated major phospholipids for analysis by gas chromatography (Figure 4B,C) (37). Relative

to control cells, HEK-293 cells expressing *Plaat1* had 62% more total CL (Figure 4C), while total contents of PC, PE, PG, and PI were not significantly elevated (Figure 4B) (37). The increase in the overall amount of CL was tied to specific modifications in the fatty acyl profile of CL (37). While there was a marked increase in the CL content of SFAs, the overall CL content of MUFAs, n-3 PUFAs, and n-6 PUFAs, remained unchanged (Figure 4D–G) (37). Among individual SFA species, we found significantly higher contents in *Plaat1*-expressing cells compared to controls of myristic acid, palmitic acid, and stearic acid (Figure 4D) (37). Of the MUFAs analyzed, only erucic acid (22:1n-9) was higher in *Plaat1*-overexpressing cells (Figure 4E), while there were no significant differences in the CL content of any of the n-6 PUFA species analyzed (Figure 4F) (37). Among n-3 PUFA species, α -linolenic acid (18:3n-3), eicosatrienoic acid (20:3n-3), and eicosapentaenoic acid (20:5n-3) were all increased in CL from cells expressing *Plaat1* (Figure 4G) (37). Overall, the increased CL in *Plaat1*-overexpressing HEK-293 cells was associated primarily with a greater content of SFAs and, to a lesser extent, also n-3 PUFA species (37).

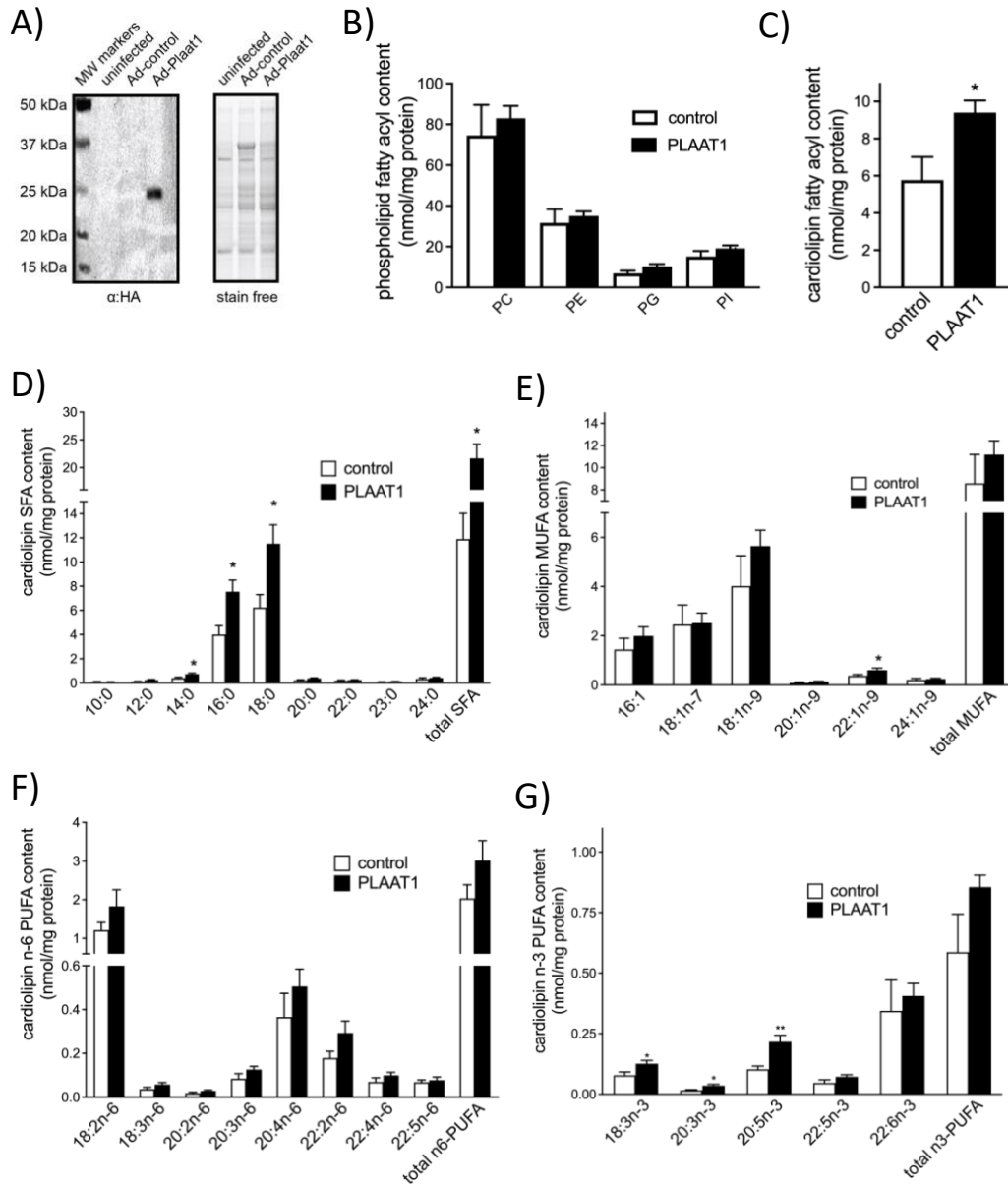


Figure 4: PLAAT1 expression in HEK-293 cells increases CL content. A representative immunoblot of HA-tagged PLAAT1 in HEK-293 cells is shown (left panel) with total protein loading imaged under UV light using a stain-free gel (right panel) (A). In HEK-293 cells expressing PLAAT1, or in control cells, the contents of major phospholipid species (B) and CL (C) were determined using gas chromatography. Analysis of the fatty acyl composition of CL is reported as individual and total SFAs (D), MUFAs (E), n-6 PUFAs (F), and n-3 PUFAs (G). Data are means \pm S.E.M. (n = 8–9). * $p < 0.05$, ** $p < 0.01$.

Gaps in knowledge:

These previous studies conducted in our laboratory provided considerable new information on PLAAT1, including evidence that this enzyme plays a role in CL regulation in cells. Nevertheless, they also raised several questions. All PLAAT family members share homology with LRAT, an acyl-CoA-independent transacylase, and prior studies have shown that all PLAAT family members have acyl-CoA-independent O- and N-transacylase activities. PLAAT1 overexpression in cells resulted in an increased capacity in crude lysates for CL synthesis using MLCL as an acyl donor, and PC as an acyl acceptor, suggesting the possibility that the O-transacylase activity of this enzyme may include direct actions in CL remodeling. However, in unpublished work from our lab, we have found that PLAAT1 overexpression in cells raises both acyl-CoA-dependent, and acyl-CoA independent CL synthesis, and also increases gene expression of enzymes involved in CL synthesis, such as cardiolipin synthase (CLS), providing compelling evidence that PLAAT1 also likely acts indirectly in the regulation of CL remodeling, potentially via signaling through NAE-regulated pathways.

The first question in this thesis was therefore whether PLAAT1 directly catalyzes a PC:MLCL O-transacylase reaction in CL remodeling. The remainder of the studies examined effects of loss of *Plaat1*, using our lab generated *Plaat11* knockout mice (*Plaat1^{-/-}*). In this regard, the physiological role of PLAAT1 at the level of the organism has only recently begun to be examined. Of note, there were no studies published when my thesis work began, and despite recent advances, questions also remain on the physiological role of PLAAT1 *in vivo*. In April 2021, Morishita and colleagues published the first study utilizing a *Plaat1^{-/-}* organism in *Nature* (154). This research group produced zebra fish with whole body *Plaat1* knockout, with the objective of comparing lens organelle degradation with wildtype (*Wt*) controls. In brief, they

found that PLAAT1 translocated from the cytosol to various damaged organelles in the zebra fish lens immediately before organelle degradation, suggesting a role for the enzyme in the autophagy process, and that *plaat1*-deficient zebrafish develop cataracts and refractive defects (154). Of particular interest to us, this group found an inverse relationship between fluorescence intensity levels of GFP tagged PLAAT1, and total content of cellular mitochondrial (based on co-imaging of a mitochondrial matrix protein tagged with red fluorescent protein (mito-mRFP)) (154).

More recently, in May 2023, the Ueda research group published the first research article utilizing *Plaat1*^{-/-} mice (155). They aimed to examine the effects of PLAAT1 deficiency on high fat diet (HFD)-induced obesity, hepatic lipid accumulation, and insulin resistance. The rationale for this work was built from previous research showing that *Plaat3*^{-/-} mice have a lean phenotype but hepatic fat accumulation under conditions of HFD feeding (110). The researchers discovered that during the administration of a HFD, the absence of PLAAT1 resulted in lower total weight gain versus wild-type mice, which was accompanied by lower liver weights, and reduced hepatic lipid accumulation (155). Moreover, although livers remained lean, PLAAT1 deficiency enhanced the HFD-induced liver dysfunction (155). Lipidomics analysis in the liver indicated an increase in various glycerophospholipids levels in *Plaat1*^{-/-} mice, whereas all lysophospholipids decreased, which the authors postulate is an indication of PLAAT1's role as a hepatic phospholipase A₁/A₂ (155), although an alternate interpretation could be that loss of PLAAT1 contributed to a reduction in the synthesis of various glycerolipids from their precursor lysophospholipids. Furthermore, this group found that the HFD in *Wt* mice resulted in increased mRNA levels of hepatic PLAAT1, leading the authors to suggest that PLAAT1 suppression can attenuate HFD-induced obesity as well as hepatic lipid accumulation (155).

For our work, comparisons between wildtype control mice and *Plaati*^{-/-} mice will allow for performance of an initial broad characterization of the phenotype caused by PLAAT1 deficiency. Mouse gene ablation models have been produced for other CL remodeling enzymes, and studies on these animals have yielded important advances, as compiled in the following section.

Summary of studies on gene ablation of CL remodelling enzymes

Tafazzin Gene Ablation

Tafazzin knockout mice have been generated by Douglas Strathdee (Glasgow University), and we currently have this model in our laboratory, but studies reporting the phenotype of these mice are limited. Prior to development of this model, a *Taz* knockdown mouse model was generated (TAZKD), which uses a doxycycline-inducible shRNA cassette transgene to reduce expression of *Taz* transcripts (156). This strategy is highly effective, reducing measurable *Taz* transcripts to almost undetectable levels (156). However, transcript levels are suppressed only while doxycycline is administered, and the *Taz* gene remains unaltered during this treatment (156). There are therefore significant limits in the use of this strategy. In boys with Barth Syndrome, loss of the *Taz* gene is embryonic, but in TAZKD mice, expression is normal until doxycycline is administered, and the timing of administration significantly affects the pathological course in mice (156). Nevertheless, a number of studies have been performed on TAZKD mice that provide insight into the physiological role of this enzyme.

Not surprisingly, loss of the *Taz* gene caused changes in the CL content and composition of mitochondria. Cardiac tissues of TAZKD mice have a 50% decrease in the total content of CL

and a 25-fold increase in MLCL (157). Furthermore, PG (40%), PE (20%), and PI (20%) were increased in subsarcolemmal mitochondria (SSM), and intermyofibrillar (IMF) mitochondria had significant increases in PG (35%) and PE (20%) (157). When the degree of CL saturation was quantified using LC-MS/MS analysis, CL (72:8) and CL (72:7), constituted 32 and 13% of total *Wt* cardiac tissue respectively, while Tafazzin deficiency drastically reduced the 72:8 and 72:7 CL molecular species to 5 and 6%, respectively (1). Similar to effects observed in heart tissues, in *Wt* extensor digitorum longus (EDL) muscle, 72:8 and 72:7 CLs constituted 19 and 15%, respectively, of the total CL content, whereas in TAZKD EDL, these values were reduced to 2 and 3%, respectively (1). Notably, these changes in EDL were accompanied by increases in CL molecular species with shorter and asymmetric side acyl groups (1).

In the brain, TAZKD mice also have a significant decrease in brain CL content compared to littermate controls (158). Additionally, apart from PS, all phospholipids increased in the brain of TAZKD mice, with PG increasing the most (158). The amount of MLCL in TAZKD brain was significantly increased by 19-fold, resulting in a corresponding elevation in the MLCL/ CL ratio compared to the littermate controls (158). Analysis of lysophospholipids levels in the brain revealed that the amount of lysophosphatidylglycerol (LPG) was significantly increased and lysophosphatidylcholine (LPC) decreased in TAZKD mice compared to *Wt* mice (158).

As a result of changes in mitochondrial CL and lipid composition, one of the primary characteristics of TAZKD mice is altered mitochondrial morphology and function, although there are differences between tissues in the nature of these changes. TAZKD mice exhibit a significant decrease in complex I-IV activity in cardiac tissue when compared to *Wt* controls (159, 160), suggesting that the ETC is diminished in TLCL-deficient mitochondria. This

decrease in activity could partially be explained by mitochondrial TLCL deficiency reducing the electron flow rate between Complex I and Complex III by 60% (161), or because levels of nine of the polypeptides involved in oxidative phosphorylation, ETC complex assembly, and the ubiquinone biosynthesis pathway are significantly decreased in TAZKD hearts (161). Overall, TAZKD cardiomyocytes exhibit approximately 40% lower maximal respiration values than *Wt* controls (160). However, unlike cardiac tissue, when observing the respiratory capacity in brain tissue of TAZKD mice, complex I mediated respiration is elevated by 160% in mitochondria isolated from the brain of TAZKD mice compared to *Wt* controls, while state III respiration level was not significantly affected by TAZ deficiency (158).

The reductions in ETC activity are not due to a reduction in mitochondria. Quantitative PCR analysis revealed a 4-fold increase of mtDNA content in hearts of 2-month-old TAZKD mice compared with *Wt* controls, while in EDL, the mtDNA content was elevated by 30% in TAZKD when compared to *Wt* controls (1). EDL of TAZKD mice display an increased number of mitochondria, but they have various inner membrane abnormalities (*i.e.*, swollen cristae, honeycomb-like structures, concentric layers, and vacuoles), while these changes were not observed cardiac muscle (1, 158).

Tissue mitochondrial deficits in TAZKD mice resulted phenotypically to deficits in exercise capacity. In a forced treadmill exercise test, TAZKD mice repeatedly failed to stay on the belt at 15 m/min and 10% inclination, and none of the TAZKD mice were able to sustain running when the treadmill speed passed 20 m/min, where the *Wt* control mice had no difficulty maintaining this speed (160). Additional calorimetric analysis revealed that VO₂ values sharply rose with increased workload in TAZKD animals, while those for *Wt* mice remained relatively steady (160). However, as the running speed increased in the exercise test, VO₂ values for

TAZKD mice declined, while VO₂ values continued to rise for *Wt* mice (160). Lactate was also significantly elevated in blood samples of TAZKD mice compared to *Wt* controls (160).

Behavioural and neurological assessments of TAZKD mice have also been performed. Using the open field test, the movement patterns of the TAZKD mice indicated that they experienced greater anxiety, since they spent significantly more time at the edges and less time in the centre of the open field (158). It was also found Tafazzin deficiency impairs the ability to distinguish a novel object from a familiar one, potentially resulting because the hippocampal neurons of TAZKD mice show reduced protein content of synaptophysin, a presynaptic vesicle protein, as well as significant derangement of the hippocampal CA1 neuronal layer (158). Furthermore, the percentage of densely organized CA1 neurons was reduced in TAZKD mice compared to *Wt* controls (158).

The more recent generation of *Taz* knockout (*Taz*-KO) mice is less studied, but has provided a more comparable model to Barth syndrome, providing a model with embryonic *Taz* deletion (162). These mice were produced by breeding heterozygous females with a germline deletion of exons 5–10 of the *Taz* gene with wild-type male C57BL/6J mice (162). Using this model, *Taz*-KO mice displayed lower bodyweights due to an overall reduction in adiposity and smaller organs and tissues, as well as higher energy expenditure measures and respiratory exchange ratios (163). These *Taz*-KO mice were also shown to have diminished exercise capacity that deteriorated at a faster rate when compared to *Wt* controls (163). Finally, these mice displayed reduced viability as well as shortened lifespans (163). In another study using this same model, it was found that tafazzin deficiency rendered murine neutrophils more susceptible to ER stress induced apoptosis (164).

ALCAT1 Gene Ablation

As with Tafazzin deficiency, ALCAT1 deficiency causes stark changes in mitochondrial structure and function. However, unlike in Tafazzin deficiency, the total content of cardiac CL from ALCAT1^{-/-} mice was higher, and was significantly more enriched in linoleic acid compared to *Wt* control mice, suggesting appropriate, or even beneficial compensatory remodelling in ALCAT1^{-/-} mice (13). In fact, ALCAT1 deficiency studies have revealed that the normal function of this enzyme can be detrimental to mitochondria, cells, tissues, and even to the organism (13, 14). With regards to mitochondrial function, it was found that ALCAT1 deficiency rescued impaired complex I citrate synthase activity that was caused by ALCAT1 overexpression, and that isolated liver mitochondria from the ALCAT1^{-/-} mice oxidized palmitoyl-carnitine faster than mitochondria from the *Wt* control mice on a high-fat diet, indicating better mitochondrial function in the absence of ALCAT1 (13). In a murine model of non-alcoholic fatty liver disease (NAFLD), NAFLD caused mitochondrial fragmentation in isolated hepatocytes in *Wt* control mice, but ALCAT1 deficiency completely prevented this by increasing MFN2 expression in the liver, and also mitigated mtDNA depletion and the development of mutations observed in *Wt* control mice (14).

Benefits of ALCAT1 deficiency extend to the modulation of disease processes. In high fat feeding models, it was reported that when compared to *Wt* mice, the ALCAT1^{-/-} mice were more sensitive to the glucose lowering effects of insulin injection (13), and consumed 62% more food per kg of body weight than *Wt* controls (13). Protein Kinase B (PKB) phosphorylation was significantly enhanced in liver, adipose tissue, and skeletal muscle of ALCAT1^{-/-} mice relative to that from the *Wt* controls, indicating enhanced insulin sensitivity in multiple tissues (13). Overall, the energy expenditure rate was also significantly elevated in the ALCAT1^{-/-} mice, since

the ALCAT1^{-/-} mice were also more active when compared to *Wt* controls (13), and a higher respiratory exchange ratio (RER) in ALCAT1^{-/-} mice indicated improved utilization of carbohydrates as the major fuel source (13). Importantly, after 18 weeks on a high-fat diet (HFD), *Wt* controls developed NAFLD, while ALCAT1^{-/-} mice were completely protected (14).

ALCAT1^{-/-} mice have also been utilized in a murine model of Parkinson's disease (165). MPTP is a neurotoxin that creates symptoms characteristic of Parkinson's disease, and it also upregulates ALCAT1 (165). Following injection with MPTP for a 7-day period, it was found that ALCAT1 deficiency attenuated the effects of impairment in locomotor activities and coordination skills that was induced in *Wt* controls (165). Additionally, in studies of 10-week-old C57BL/6J mice, pre-treatment for three days with the potent ALCAT1 inhibitor drug was found to attenuate motor deficits caused by MPTP (165). MPTP treatment models Parkinson's disease by causing a depletion of dopaminergic neurons, but ALCAT1 inhibition by A320 prevents this loss (165). In addition, MPTP treatment also models the disease by decreasing expression of the autophagic initiator protein LC3II, but ALCAT1 inhibition normalized that expression (165). Finally, ALCAT1 inhibition serves to improve mitochondrial architecture in the MPTP model of Parkinson's disease (165). Mitochondrial architecture is regulated by a family of mitochondrial guanosine triphosphate hydases (GTPases), including mitofusion 2 (MFN2) and DRP1, that regulate the mitochondrial fusion and fission process (165). MFN2 is depleted in Parkinson's disease patients, whereas DRP1 inhibition protects against neurotoxicity (165). In this regard, ALCAT1 deficiency not only restored MFN2 to regular expression, but also significantly attenuated the mitochondrial association of DRP1 in the midbrain of MPTP mice (165). Together, this indicates a role for ALCAT1 in mitochondrial architecture.

In a study of hypertrophic cardiomyopathy, hyperthyroidism caused cardiac hypertrophy in *Wt* mice, but ALCAT1 deficiency significantly attenuated the T4-induced cardiac enlargement, and partially normalized the heart-weight to body-weight ratio (166). Chronic hyperthyroidism caused severe ventricular fibrosis as a result of cardiomyopathy, but this was significantly attenuated by ALCAT1 deficiency (166). Furthermore, while the onset of T4-induced cardiomyopathy in *Wt* mice was associated with left ventricular dysfunction characterized by a significant decrease in left ventricular fractional shortening (LVFS), ALCAT1 deficiency significantly increased LVFS (166). Cardiomyopathy also significantly increased the size of cardiomyocytes in *Wt* mice, but the hypertrophic growth of cardiomyocytes was significantly attenuated in ALCAT1^{-/-} mice (166). In *Wt* controls, chronic hyperthyroidism significantly increased mRNA expression of all hypertrophic biomarkers in *Wt* mice but ALCAT1 deficiency significantly attenuated the expression of these biomarkers (166). It was observed that hyperthyroid cardiomyopathy is associated with mitochondrial swelling, disorganized cristae, and abnormal ultrastructure of the mitochondria in *Wt* mice, but these damages were mitigated by ALCAT1 deficiency (166). However, chronic hyperthyroidism caused significant downregulation of Akt-mTOR signaling pathways in heart tissue of WT control mice but not in ALCAT1^{-/-} mice (166).

Alpha Trifunctional Protein (α TFP) and MLCL-AT1 Gene Ablation

One research group examined the contribution of α TFP to CL remodelling and mitochondrial supercomplex formation in heart and liver mitochondria from *Wt* and α TFP heterozygous [Mtpa^(+/-)] mice (167). Compared to *Wt* mice, Mtpa^(+/-) mouse heart and liver exhibited ~55% and ~50% reductions in α TFP levels, respectively (167), while MLCL AT-1 protein derived from α TFP saw reduction of approximately 30% in Mtpa^(+/-) mouse heart but not in liver (167).

To explain this contrast in tissue expression, the authors hypothesized that the expression pattern of MLCL AT-1 likely differs between heart and liver (167). Additionally, *in vitro* acylation of MLCL was reduced in heart but not in liver mitochondria of *Mtpa*^(+/-) mice compared with *Wt* (167). CL mass was also reduced in heart and liver mitochondria of *Mtpa*^(+/-) mice and, specifically, there were reductions in linoleate-containing CL species, in particular, the TLCL and L3-MLCL species (167). Cardiac and liver mitochondrial supercomplex assembly and NADH dehydrogenase (complex I) activity within these supercomplexes were unaltered in both *Mtpa*^(+/-) mouse heart and liver compared with *Wt* (167). The results indicate either that α TFP may modulate CL molecular species composition in murine heart and liver, TLCL may not be an essential requirement for mitochondrial supercomplex assembly, or that TLCL within mitochondria must decline below a threshold level before supercomplex assembly becomes destabilized (167). Overall, however, this work demonstrates a role for MLCL AT1 in the regulation of cardiac and hepatic CL total content and composition.

Chapter 3: Thesis Study I – Characterizing the O-transacylase Activity of PLAAT1 in Cardiolipin Remodeling Using Affinity-Purified Protein

Background and Rationale:

The PLAAT family of proteins have been shown to demonstrate O-transacylase activity, described as the acyl-CoA-independent transacylation of a lysophospholipid using a fatty acyl chain donated from another phospholipid (89). All PLAAT enzymes have demonstrated O-acylation of LPC at the sn-1 position (39, 104), but O-acylation of other phospholipids has not been explored. In 2011, Shinohara and colleagues reported that purified human PLAAT1 displays *in vitro* O-transacylase activity, as well as N-transacylase activity and PLA1/2 phospholipase activity (39). Among these, the O-transacylase activity of PLAAT1 predominated, and this was shown when 2-[¹⁴C]palmitoyl-lyso PC was used as the acyl acceptor in the O-transacylation reaction with unlabelled PC as the acyl donor (39). This is notably similar to the transacylase activity of Tafazzin, which uses PC as an acyl donor, but MLCL as an acyl acceptor (71). However, O-acylation activity by any PLAAT enzyme with MLCL or DLCL as fatty acyl acceptors has, to the best of my knowledge, not yet been reported.

PLAAT1 is most highly expressed in mouse heart, brain, skeletal muscle (38) - all tissues that have substantial energetic demands and abundant mitochondria. Prior work from our lab has demonstrated that PLAAT1 overexpression in cells results in an increased capacity for CL synthesis in crude lysates derived from those cells, suggesting that PLAAT1 may be able to catalyze the O-transacylation of MLCL, and therefore have direct actions in CL remodeling (38). On the other hand, our laboratory has also found that PLAAT1 overexpression in cells increases the gene expression of multiple enzymes involved in CL synthesis, suggesting that PLAAT1 could

also regulate CL remodelling indirectly, potentially through modulation of cellular signaling pathways. This could occur, theoretically, through PLAAT1's function as a N-transacylase, potentially impacting CL through NAE-regulated induction of enzymes involved in either remodeling or synthesis. It is important to note that these two potential roles for PLAAT1 in CL regulation – *i.e.* direct activity in CL remodeling through O-transacylase mediated acylation of MLCL and indirect regulation of pathways that promote CL synthesis are not mutually exclusive, and could both potentially occur *in vivo*. Thus, investigation of direct enzyme activity would require separation of the enzyme from any cellular system influences.

Our laboratory had previously made a pilot attempt at assessment of the PC:MLCL O-transacylase activity of PLAAT1 using an *in vitro* reticulocyte lysate transcription/translation system, in order to generate the enzyme free of other cellular genomic effects (38). In this, it was found that the PC:MLCL transacylase activity of reticulocyte lysates overexpressing PLAAT1 was approximately a third higher than control lysates when using [9,10-³H]-distearoyl-PC as an acyl donor. However, this experiment tested only a single PC concentration, and the sample size used for this experiment was inadequate to detect statistical significance. Thus, this first study aimed to design an enzyme assay using purified lysates, to determine if PLAAT1 exhibits direct PC:MLCL O-transacylase activity *in vitro*, and if so, to determine enzyme kinetics with different acyl donors

Objectives and Hypotheses

1. Objective: To determine if PLAAT1 has direct PC:MLCL O-transacylase activity.

Hypothesis: Affinity purified PLAAT1 will have *in vitro* PC:MLCL O-transacylase activity using MLCL as an acyl acceptor and [9,10-³H]-18:1n-9/18:1n-9-PC, [9,10-³H]-18:0/18:0-PC, and 16:0/[¹⁴C]18:2n-6-PC as acyl donors.

Study Design and Development:

Reticulocyte Lysate System

Initially, I used a reticulocyte lysate *in vitro* transcription/translation system to produce recombinant PLAAT1. This system uses reticulocyte lysates that are anucleate to transcribe and translate proteins from plasmids coding for specific proteins. It was chosen for two reasons. First, this commercial system is used extensively in synthetic biology, since it has the capacity to generate plasmid-encoded proteins at high levels and, second, since it lacks nuclear transcription capabilities, will not transcribe or translate other proteins in response to any signals provided by the plasmid-encoded protein. A major concern with using crude lysates in initial studies on the characterization of PLAAT1 was the potential for confounding that could result from increased production of NAE signaling molecules, down-stream of the known N- transacylase activity of this enzyme. Since some NAE can act as transcription factors to alter the nuclear transcription of genes involved in lipid metabolism, utilization of a system that precluded this confounding activity was essential. Thus, the TNT ® Coupled Reticulocyte Lysate System was employed. However, limitations were encountered. After significant troubleshooting, it was determined that expression of PLAAT1 in this system was variable, and in some instances the recombinant protein was even undetectable. Since inconsistencies in yield were hindering progress, a different system, with higher, more consistent yields, was needed.

Adenoviral Overexpression System and Affinity Purification

HEK293 cells express the coxsackie-adenovirus receptor that allows for efficient transduction with adenovirus (168). Adenoviral infection of these cells will yield a high level of expression of proteins encoded by the viral genome, and can be used as a method to synthesize

abundant recombinant protein. HEK293 cells were infected at a multiplicity of infection (MOI) of 20 infectious units (IFU) per cell with viral PLAAT1 (containing a separately transcribed viral green fluorescent protein (GFP) reporter) or viral GFP alone, and allowed to incubate for 72 hours. Cells were then harvested, and HRASLS1 was affinity purified. Initially, immobilized metal affinity chromatography (iMAC) was used to purify PLAAT1, since PLAAT1 has a C-terminal 6xHis tag. However, after further troubleshooting, it was determined that this method resulted in the partial purification of non-functional proteins, and it was suspected that the presence of residual metal ions following elution were impairing activity of the enzyme in subsequent assays. Thus, agarose beads coated with monoclonal anti-HA-antibodies were next tested as a means to affinity purify PLAAT1 protein, via the C-terminal region tag that is also present in the virally-transcribed protein.

In vitro PC:MLCL Transacylase Activity Assay

The assay was performed essentially as described by Uyama *et al*, with minor modifications (15). A substrate mixture containing 100 nmol of MLCL, and variable amounts of either [9,10-³H]-18:0/18:0 phosphatidylcholine (distearoyl-PC), [9,10-³H]-18:1n-9/18:1n-9 phosphatidylcholine (dioleoyl-PC), or 16:0/[¹⁴C]18:2n-6 phosphatidylcholine (1-palmitoyl-2-[¹⁴C]-linoleoyl-PC), respectively, was mixed and dried under N₂ and then reconstituted by sonification at an amplitude of 60 Hz for six 5-second bursts in 100 μL of pre-warmed (37°C) Transacylase Reaction Buffer (50 mM Tris-HCl, pH 8, 2 mM DTT, 0.1% Nonidet P-40). Reactions were initiated by addition of 100 μL of pre-warmed substrate mixture to an aliquot of 100 μL immunoprecipitated PLAAT1-bead complex. Immunoprecipitate-bead complexes prepared from HEK-293 cells infected with only adenoviral GFP were used as controls in reactions, at all concentrations. Reactions were mixed gently, and incubated in a 37°C water bath for 30 minutes.

Reactions were then quenched by addition of 0.75 mL of methanol:chloroform (2:1, v/v), and lipids were extracted by the method of Blythe and Dyer [250]. Lipids were resolved and separated by thin layer chromatography (TLC). Individual phospholipid bands were identified using known standards, and bands corresponding to CL were scraped and quantified by liquid scintillation counting.

Results:

Affinity purified PLAAT1 catalyzes the dose-dependent transacylation of MLCL using distearoyl-PC and dioleoyl-PC.

The PC:MLCL transacylase reaction was repeated using affinity purified protein generated by immunoprecipitation of the C-terminal HA fusion tag attached to virally transcribed PLAAT1, synthesized in infected HEK293 cells. It was found that affinity purified PLAAT1 produced more CL than control reactions by incorporating [³H]18:0 and [³H]18:1 derived from [9,10-³H]-distearoyl-PC and [9,10-³H]-dioleoyl-PC respectively into MLCL. PLAAT1 O-transacylase activity in reactions using 1-palmitoyl-2-[¹⁴C]-linoleoyl-PC as an acyl donor was not different than control levels at any concentration of substrate tested. To analyze kinetic parameters of PLAAT1, enzyme reactions were performed with increasing concentrations of [9,10-³H]-distearoyl-PC and [9,10-³H]-dioleoyl-PC, and enzyme velocity were determined and depicted using a Lineweaver-Burk plot (Figure 5). The calculated K_m for [9,10-³H]-distearoyl-PC as a substrate was 252.46 μM , while the V_{max} was 1.614 $\mu\text{mol}/\text{min}/\text{mg}$ protein (Table1). The calculated K_m for [9,10-³H]-dioleoyl-PC as a substrate was 31.878 μM , while the V_{max} was 0.6064 $\mu\text{mol}/\text{min}/\text{mg}$ protein (Table 1).

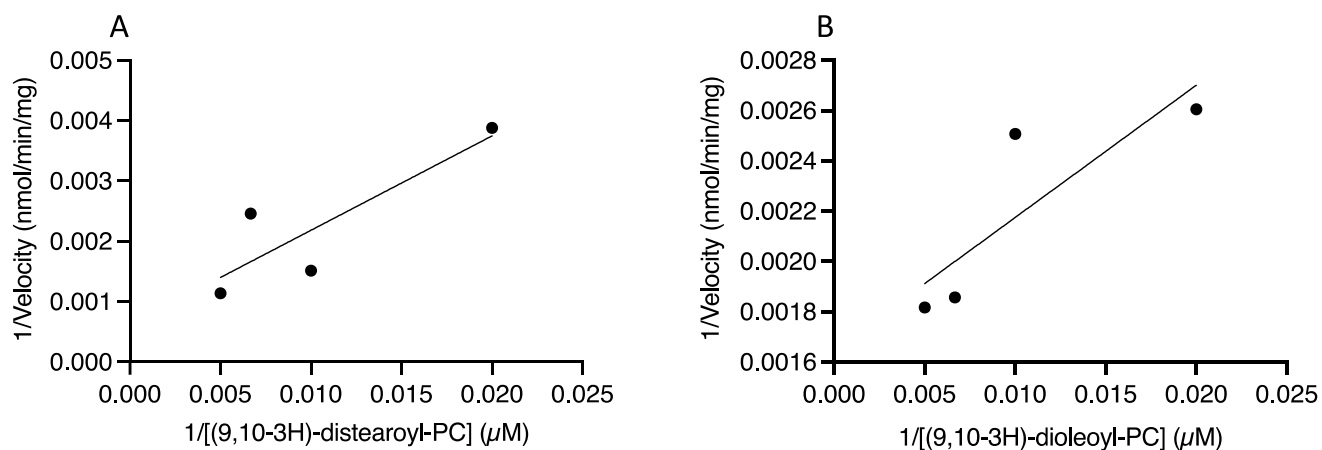


Figure 5: Lineweaver-Burk plots displaying the reciprocal PLAAT1 CL O-transacylase activity. Velocity rates (y axes) detected corresponding to reciprocal concentrations of substrates used (x axes) for reactions containing 100 μM MLCL as an acyl acceptor and either (A) [9,10-³H]-distearoyl-PC, or (B) [9,10-³H]-dioleoyl-PC as acyl donors.

Table 1. Kinetic parameters for PLAAT1 with different substrates

Substrate	V_{\max} (μmol/min/mg pro)	K_m (μM)	V_{\max} / K_m
[9,10- ³ H]-distearoyl-PC	1.614	252.46	0.0064
[9,10- ³ H]-dioleoyl-PC	0.6064	31.878	0.01902
1-palmitoyl-2-[¹⁴ C]-linoleoyl-PC	ND	ND	ND

Transacylase activity parameters of PLAAT1 were calculated from Lineweaver–Burke plots generated by assaying activity of affinity-purified enzyme using 100 μM MLCL reacted with 0–200 μM PC (n = 2–3). ND = not determined.

Discussion

PLAAT1 shares sequence similarities including catalytically critical residues, with the enzyme lecithin:retinol acyltransferase, which is an O-transacylase that catalyzes the acylation of retinol using PC as an acyl donor. Based on this homology, initial investigations of PLAAT1 (39) and other PLAAT family enzymes (89, 169), assumed that they would have PC-dependent O-transacylase activity, which was determined experimentally with PC as an acyl donor and LPC as an acyl acceptor (89, 169). However, whether PLAAT1 has activity in other O-transacylase type reactions had not been tested.

In this work, we found evidence that affinity purified PLAAT1 has O-transacylase activity *in vitro* using PC as an acyl donor and MLCL as an acyl acceptor. When compared to other CL remodelling enzymes, our findings show that PLAAT1 operates most similarly to Tafazzin that also acts as a PC:MLCL transacylase, while ALCAT1, MLCL AT-1, and α TFP, all exhibit acyl-CoA-dependent acyltransferase activity (21). However, our assay findings indicate that PLAAT1 exhibits a distinct substrate specificity that differs from tafazzin. Our *in vitro* findings on the catalytic activity of PLAAT1 using affinity-purified enzyme indicated substrate preference for distearoyl PC and dioleoyl PC over 1-palmitoyl-2-linoleoyl-PC, in contrast to tafazzin, which preferentially utilizes linoleate residues from PC (21). This activity also differs from that of MLCL AT-1 and α TFP, which prefer to use linoleoyl-CoA, and ALCAT1, which prefers HUFA, forgoing 16–18 carbon saturated, monounsaturated, and polyunsaturated fatty acids (21). Thus, the enzyme activity exhibited in this analysis suggests a preference by PLAAT1 for utilization of PC species containing saturated and monounsaturated rather than n-6 polyunsaturated 18-carbon fatty acyl chains but may also indicate some additional preference for fatty acyl moieties esterified at the *sn*-1 position of PC.

Chapter 4: Thesis Study II - Characterization of Cardiolipin Content and Composition in PLAAT1-Deficient Heart, Brain, and Skeletal Muscle

Introduction and Study Rationale

At a molecular level, animal models of tafazzin deficiency are most commonly described by the aberrant CL composition characterized in the heart and skeletal muscle tissues (1, 157, 159-161). However, recent work by our research group, as well as others, has shown that these characteristics further manifest as profound changes in growth patterns, organ weights, as well as overall survival when the effects of tafazzin deficiency are studied *in vivo* (162, 163, 170). Our *in vitro* work using affinity-purified enzyme in a transacylase assay system has shown that PLAAT1, similar to tafazzin, can also act as a PC:MLCL O-transacylase enzyme. Thus, it is rational to hypothesize that PLAAT1 may play a direct role in CL remodeling *in vivo*. Furthermore, PLAAT1 has been demonstrated to have PLA_{1/2} and N-transacylase activities. Since the latter can modify NAE production, and NAEs and their downstream targets can regulate bioenergetic processes (171), phospholipid biosynthesis (172, 173), and mitochondrial biogenesis (174), it is also rational to hypothesize that PLAAT1 may play an indirect role in CL metabolism *in vivo*.

The generation of knockout mouse models has demonstrated that loss of CL remodeling enzymes can profoundly alter the content and composition of CL species found in different tissues. For instance, one study observing TAZKD mice observed that in heart tissues of *Wt* controls, the major molecular species with C18 acyl side chains constituted 45% of total CL, while Tafazzin deficiency drastically reduced that to 11%, along with a 50% decrease in the total content of heart CL (1). Alterations in content of C18 CL were also accompanied by accumulation of molecular species with shorter acyl side chains and with higher degrees of

saturation (1). Like in heart tissues, in *Wt* EDL muscle, CL with C18 acyl side chains constituted 34% of total CL species, whereas in TAZKD EDL, these values were reduced to 5% (1). Similarly, these changes in EDL were also accompanied by increases in CL molecular species with shorter and asymmetric side acyl groups (1).

Recently, the effects of PLAAT1 ablation at the level of the organism have been reported. In a study aiming to examine the effects of PLAAT1 deficiency on HFD-induced obesity and hepatic lipid accumulation, the authors found that PC, PE, PS, and PI tended to be higher in the livers of *Plaat1*^{-/-} mice fed either a standard low fat diet or a HFD when compared to their *Wt* counterparts, while most lysophospholipids were lower in PLAAT1 deficient livers (155). They did not, however, examine CL levels or composition. Since PLAAT1 is most highly expressed in brain, heart, and skeletal muscle, these tissues were the primary focus for study in this series of experiments. Thus, to test whether PLAAT1 deficiency alters tissue CL levels, we also generated a *Plaat1*^{-/-} mouse model.

Objectives and Hypotheses

The objectives and hypothesis for this study were as follows:

1. Objective 1: To compare the total amount of CL in brain, heart, and skeletal muscle of *Plaat1*^{-/-} mice in comparison to *Wt* mice.

Hypotheses: *Plaat1*^{-/-} mice will display decreased total CL in brain, heart, and skeletal muscle tissues in comparison to *Wt* mice. Since our enzyme assay results indicated that PLAAT1 displays a preference for PC containing 18:0 and 18:1n-9 as acyl substrates, the ablation of the enzyme would suggest that CL would decrease in tissues where these acyl chains are one of the preferred substrates for CL remodelling.

2. Objective 2: To compare the CL fatty acyl profiles of brain, heart, and skeletal muscle, in *Plaat1*^{-/-} mice with *Wt* mice.

Hypotheses: Since our first study using a purified system indicated that PLAAT1 preferentially incorporates saturated and mono-unsaturated fatty acids onto MLCL, the CL fatty acyl profile of PLAAT1 deficient tissues is expected to have an increased ratio of n-6 to SFA and MUFA species, and thus a decreased ratio of saturated to polyunsaturated fatty acids.

Study Design:

Animals:

To generate *Plaat1* knockout (*Plaat1*^{-/-}) mice, exon 3 of the *Plaat1* gene was deleted in C57Bl/6J zygotes using CRISPR by technicians at The Centre for Phenogenomics (TCP), Toronto, ON, CA, producing *Plaat1*^{+/-} (heterozygous) mice. Exon 3 was targeted because deletion of this region will disrupt enzymatic activity of the PLAAT1 protein, since at least 2 catalytically critical residues are present in this domain. *Plaat1*^{+/-} mice were maintained on a C57Bl/6J background by routinely crossing them with *wildtype* C57Bl/6J mice, and then *Plaat1*^{-/-} mice were produced by intercrossing male and female *Plaat1*^{+/-} mice taken from the 7th generation of sequential crosses. Thus, the animals used for this study were male and female *Plaat1*^{-/-} mice and *Wt* controls. Animal procedures were performed with the approval of the University of Waterloo Animal Care Committee (AUPP#43325, approved 03 June 2021, renewed June 04, 2023) and comply with guidelines of the Canadian Council on Animal Care. Mice were ear notched at 4 weeks of age and genotyped to determine the total number of *Plaat1*^{-/-} and *Wt* male and female mice. At 20 weeks of age, this subset of mice was sacrificed, and organs and tissues from euthanized mice were excised, weighed, and snap-frozen in liquid nitrogen and stored at - 80°C.

Lipid Extraction, Thin Layer Chromatography (TLC), and Gas Chromatography (GC)

Total lipids were isolated from the tissue samples of *Plaat1*^{-/-} and *Wt* mice using Folch's method (175). In summary, tissue was homogenized using a Polytron® at top speed, in 3 mL of a chloroform:methanol mixture in a 2:1 ratio, supplemented with butylated hydroxytoluene as an antioxidant, sourced from Sigma-Aldrich, Bellfonte PA. These samples were then vortexed for 15 seconds at the highest speed. Subsequently, 500 µL of Na₂PO₄ was added, then the samples

were inverted three times and centrifuged at 3,000 x rpm for a period of 5 minutes to segregate the organic and aqueous phases. The lower organic phase was extracted to a newly labeled tube. These samples were then dried under a gentle nitrogen stream and dissolved in 50 µL of chloroform. Individual lipid classes were then separated by thin layer chromatography (TLC). Samples were reconstituted in 50 µL of chloroform, applied to a silica gel HF plate (20cm × 20 cm, 250 µM; Analtech Inc., Cole-Parmer Canada, Montreal, Quebec), then resolved using a chloroform:methanol:2-propanol:0.25% KCl:trimethylamine solvent front (30:9:25:6:18, v/v/v/v/v). CL bands were visualized by UV illumination after spraying with 0.1% 2,7-dichlorofluorescein in methanol (w/v), and identified and scraped based on comparison with CL standards (Avanti Polar Lipids, Millipore Sigma, Mississauga, Ontario, Canada). In preparation for gas chromatography (GC), the fatty acyl species within CL were derivatized to fatty acyl methyl esters by a transesterification method using 14% boron trifluoride in methanol and hexane (Thermo Scientific, Bellfonte PA), containing nonadecanoic acid (19:0) ethyl ester as an internal standard (Nu-Check Prep, Elysian, MN). This was then heated at 95 °C for 1 h. This product was centrifuged at 3000 × rpm for 5 min, then the top layer was transferred to a fresh tube, dried under a N₂ stream, and resuspended in 65 µL of heptane. Analysis using gas chromatography with flame ionization detection was performed using the Agilent 7890A gas chromatograph equipped with a DB-FFAP 15 m × 0.10 mm injected dose × 0.10 µm film thickness nitroterephthalic acid modified polyethylene glycol capillary column (J&W Scientific/Agilent Technologies, Mississauga, Ontario, Canada) with hydrogen as the carrier gas. Briefly, 1 µL of samples were introduced by an Agilent 7693A autosampler into the injector and heated to a temperature of 250 °C with a split ratio of 50:1. Initial temperature was 150 °C with a 0.25-min hold followed by a 35 °C/min ramp to 200 °C, a 1 °C/min ramp to 211 °C, and then a

80 °C/min ramp up to 245 °C with a 4-min hold at the end. The flame ionization detector temperature was set at 300 °C with air and nitrogen make-up gas flow rates of 300 and 10 mL/min, respectively, sampled at a frequency of 50 Hz.

Statistical Analysis:

Fatty acyl composition was expressed in two ways: concentrations (measured in µg of fatty acids per mg of protein) and as relative weight percentages (as a percentage of the total fatty acid mass analyzed). Total CL content was calculated based on the total mass of all CL fatty acyl species within each sample. Differences in the total content and relative percentages of fatty acyl species and lipid categories between *Wt* and *Plaat1*^{-/-} mice were analyzed using an unpaired Student's t-test to determine differences between genotypes.

Results

PLAAT1 deficiency results in higher total CL content in the female mouse brain and changes CL fatty acyl content to a less saturated composition.

The effects of PLAAT1 deficiency on the total amount of CL in the brain tissues of *Plaat1*^{-/-} mice were evaluated. Notably, where the total amount of CL in the brain tissues of female *Plaat1*^{-/-} mice compared to their *Wt* counterparts was 154% greater (*Wt*, 437.2 ± 50.36 µg CL/ g of tissue versus *Plaat1*^{-/-}, 1109 ± 193.4 µg CL/ g of tissue, P=0.0152) (Fig. 6B). This alteration in total CL content in brain tissue did not extend to the male mice, where brain tissues from the *Plaat1*^{-/-} mice displayed 31.2% higher CL content, but this change was not found to be statistically significant for the tested sample size (Fig. 6A).

Tissue contents of major classes of fatty acids and individual species within those classes were analyzed, and the data are shown both as total concentrations (in µg/g of tissue analyzed) and as relative mass percentages by mass. The total concentration of SFA were lower in male *Plaat1*^{-/-} mice (Fig. 7A) but were not different in female *Plaat1*^{-/-} mice (Fig. 7C). Our analysis of the relative mass percentage of different CL species revealed a lower abundance of SFA species in CL isolated from the brains of male *Plaat1*^{-/-} mice, in comparison to their *Wt* counterparts (*Wt*, 30.67 ± 0.88 wt/wt % of total CL versus *Plaat1*^{-/-}, 17.21 ± 0.76 wt/wt % of total CL, P<0.0001) (Fig. 7B, 3A). The lower SFA content was predominantly attributable to less CL acylation by 18:0 fatty acid (FA) species, which were quantitatively the most abundant SFA species in brain CL, where a relative reduction of 65.76% was recorded in *Plaat1*^{-/-} males (*Wt*, 15.91 ± 0.65 wt/wt % of total CL versus *Plaat1*^{-/-}, 5.45 ± 0.36 wt/wt % of total CL, P<0.0001) (Fig. 8A). A comparable effect was observed in the relative brain CL composition in female *Plaat1*^{-/-} mice, where the relative proportion of both the total SFA species (*Wt*, 31.86 ± 2.96 wt/wt % of total CL versus *Plaat1*^{-/-}, 21.51 ± 0.83 wt/wt % of

total CL, $P=0.0073$) (Fig. 2D, 3B) and 18:0 species (*Wt*, 18.05 ± 0.91 wt/wt % of total CL versus *Plaat1*^{-/-}, 6.48 ± 0.60 wt/wt % of total CL, $P<0.0001$) was found to be less when compared to *Wt* mice (Fig. 8B). In addition to these changes, relative reductions were also seen in less abundant SFAs, such as the 20:0, 22:0, and 24:0 FAs, in both male and female *Plaat1*^{-/-} mice (Fig. 8A, B).

We evaluated the impact of PLAAT1 deficiency on the total content of MUFA species in CL extracted from mouse brains and found no significant differences in concentrations in either male or female *Plaat1*^{-/-} mice. However, we noted significantly lower percentage of CL comprised of MUFA, as well as differences in the composition of MUFA species in CL. Specifically, in *Plaat1*^{-/-} male brains, there was substantially less relative composition by MUFA species (*Wt*, 29.94 ± 0.62 wt/wt % of total CL versus *Plaat1*^{-/-}, 20.01 ± 0.68 wt/wt % of total CL, $P<0.0001$) (Fig. 7B, 9A). A similar change was also seen in the *Plaat1*^{-/-} female brains (*Wt*, 28.38 ± 0.34 wt/wt % of total CL versus *Plaat1*^{-/-}, 23.35 ± 1.42 wt/wt % of total CL, $P=0.0062$) (Fig. 7D, 9B). The majority of this compositional shift can be attributed to less acylation by 18:1n-9 FAs, which was found to be 36.1% lower in *Plaat1*^{-/-} males (*Wt*, 19.58 ± 0.59 wt/wt % of total CL versus *Plaat1*^{-/-}, 12.52 ± 0.57 wt/wt % of total CL, $P<0.0001$) (Fig. 9A), and 22.2% lower in *Plaat1*^{-/-} female mice (*Wt*, 21.07 ± 0.71 wt/wt % of total CL versus *Plaat1*^{-/-}, 16.38 ± 1.05 wt/wt % of total CL, $P=0.0064$) (Fig. 9B). In male *Plaat1*^{-/-} mice, relative amounts of 20:1n-7 and 22:1n-9 were also less, while in female *Plaat1*^{-/-} mice, we observe reduced 20:1n-9 species (Fig. 9A, B).

We examined alterations in the CL composition of FA categories in the brains of *Wt* and *Plaat1*^{-/-} mice. In *Wt* mice, the SFA 18:0 and the MUFA 18:1n-9 constituted the most abundant acyl chains of CL (Fig. 7A, C). However, *Plaat1*^{-/-} mice exhibited a significant shift in this pattern. In both male and female *Plaat1*^{-/-} mice, the total concentration and relative abundance of n-6 PUFA in

brain CL was ≥ 2 -fold greater (Fig. 7A, C). Thus, the lesser relative abundance of SFA and MUFA were offset by proportionally higher total N-6 species. Specifically, the total concentration of N-6 PUFA in brain CL from male and female *Plaat1*^{-/-} mice was found to be 196% and 233% greater, respectively (Fig. 7A, C). In relative terms, male *Plaat1*^{-/-} mice demonstrated a 135% higher mass percentage of brain CL that was comprised of N-6 PUFA (*Wt*, 22.99 \pm 0.97 wt/wt % of total CL versus *Plaat1*^{-/-}, 53.93 \pm 1.06 wt/wt % of total CL, P<0.0001) (Fig. 7B, 10A), while for the female *Plaat1*^{-/-} mice it was 105% more (*Wt*, 22.43 \pm 0.79 wt/wt % of total CL versus *Plaat1*^{-/-}, 45.90 \pm 2.19 wt/wt % of total CL, P<0.0001) (Fig. 7D, 10B).

Interestingly, despite greater amounts of N-6 species, we noted significantly lower relative amounts of AA (20:4n-6), which was the most abundant N-6 fatty acyl species in CL isolated from brains of *Wt* mice. Specifically, male *Plaat1*^{-/-} mice have 83.14% less of this species compositionally (*Wt*, 15.13 \pm 0.84 wt/wt % of total CL versus *Plaat1*^{-/-}, 2.55 \pm 0.58 wt/wt % of total CL, P<0.0001) (Fig. 10A), while in female *Plaat1*^{-/-} mice it was found to be 73.61% less (*Wt*, 11.18 \pm 2.14 wt/wt % of total CL versus *Plaat1*^{-/-}, 2.95 \pm 0.43 wt/wt % of total CL, P=0.0055) (Fig. 10B). But perhaps most interestingly, we see that compensation by N-6 FA's is almost exclusively driven by a 996% (*Wt*, 4.31 \pm 0.28 wt/wt % of total CL versus *Plaat1*^{-/-}, 47.22 \pm 0.98 wt/wt % of total CL, P<0.0001) (Fig. 5A), and a 372% (*Wt*, 8.49 \pm 1.73 wt/wt % of total CL versus *Plaat1*^{-/-}, 40.09 \pm 1.76 wt/wt % of total CL, P<0.0001) (Fig. 10B) greater relative abundance of linoleic acid (18:2n-6) in brain CL of male and female *Plaat1*^{-/-} mice. This is of note because TLCL is the most ubiquitous form of mature CL in tissues *outside* of the brain, but the deletion of PLAAT1 resulted in a compositional change wherein linoleate became the most abundant CL fatty acyl species within the brain.

N-3 fatty acyl species were the least abundant category in brain CL both from *Wt* and *Plaat1^{-/-}* mice. Regardless, our examination of brain CL acylation by N-3 fatty acids revealed notable alterations associated with PLAAT1 deficiency. Male *Plaat1^{-/-}* mice had a 27.96% lower relative abundance of total N-3 in brain CL (*Wt*, 9.54 ± 0.44 wt/wt % of total CL versus *Plaat1^{-/-}*, 6.87 ± 0.64 wt/wt % of total CL, $P=0.0091$) (Fig. 7B, 11A). Furthermore, 41.69% lower levels of 22:6n-3 (DHA) were also evident (*Wt*, 7.61 ± 0.37 wt/wt % of total CL versus *Plaat1^{-/-}*, 4.44 ± 0.72 wt/wt % of total CL, $P=0.0045$) (Fig. 11A). Female mice exhibited similar patterns in these respective compositions, though the differences were not statistically significant (Fig. 11B). On the other hand, CL isolated from brain tissues of female *Plaat1^{-/-}* mice contained 314% more 22:5n-3 (EPA) than was evident in CL isolated from *Wt* female brains (*Wt*, 0.14 ± 0.05 wt/wt % of total CL versus *Plaat1^{-/-}*, 0.60 ± 0.12 wt/wt % of total CL, $P=0.0097$) (Fig. 11B), and these differences were not seen in males. In both male and female mice, the relative proportion of 18:3n-3 in CL approximately twice as much in *Plaat1^{-/-}* mice, but this fatty acyl constituted less than 1% of total brain CL (Fig. 11A, B). Despite these changes, total N-3 concentrations did not differ between either male or female *Plaat1^{-/-}* mice when compared to *Wt* controls (Fig. 11B, D).

Alterations caused by PLAAT1 in relative PUFA content in the male mice to be 86% higher (*Wt*, 32.67 ± 1.37 wt/wt % of total CL versus *Plaat1^{-/-}*, 60.85 ± 1.49 wt/wt % of total CL, $P<0.0001$) (Fig. 7B), and 77% higher in female mice (*Wt*, 29.2 ± 1.75 wt/wt % of total CL versus *Plaat1^{-/-}*, 51.70 ± 2.37 wt/wt % of total CL, $P<0.0001$) (Fig. 7D), mostly due to greater acylation specifically by 18:2n-6 (Fig. 10A, B). In contrast, the relative abundance of HUFA species was 57% less in *Plaat1^{-/-}* male brains (*Wt*, 27.22 ± 1.35 wt/wt % of total CL versus *Plaat1^{-/-}*, 11.57 ± 1.17 wt/wt % of total CL, $P<0.0001$), and 51% less in *Plaat1^{-/-}* female brains (*Wt*, 19.71 ± 3.48 wt/wt % of total

CL versus *Plaat1*^{-/-}, 9.67 ± 1.39 wt/wt % of total CL, $P=0.028$) (Fig. 7B, D). Although docosapentaenoic acid (22:5n-3) was significantly more abundant in CL in female *Plaat1*^{-/-} brains, this fatty acyl species constituted less than 1% of total CL. Thus, the difference in HUFA abundance between *Wt* and *Plaat1*^{-/-} brain CL was largely due to lower proportions of DHA (22:6n-3) and AA (20:4n-6) that are quantitatively more substantial in CL in this tissue.

PLAAT1 deficiency in mouse heart tissue results in lower total CL contents and a shift in CL fatty acyl content to a more saturated composition with a lowered relative abundance of linoleoyl CL species.

After examining various tissues, the most remarkable alteration due to PLAAT1 deficiency was observed in cardiac tissue, where total CL content was substantially lower in both male and female *Plaat1*^{-/-} mice. In male mice, we documented 95% less total CL content (*Wt*, 18321 ± 5196 $\mu\text{g CL/ g}$ of tissue versus *Plaat1*^{-/-}, 995.7 ± 240.9 $\mu\text{g CL/ g}$ of tissue, $P=0.0158$), and in female mice 82% less (*Wt*, 9402 ± 1854 $\mu\text{g CL/ g}$ of tissue versus *Plaat1*^{-/-}, 1672 ± 415.6 $\mu\text{g CL/ g}$ of tissue, $P=0.0066$) (Fig. 6A, B). The lower total CL is associated with significant lesser concentrations of all major classes of fatty acyl species in male *Plaat1*^{-/-} mice, and in total concentrations of SFA, MUFA, and N-6 PUFA in female *Plaat1*^{-/-} mice. Male *Plaat1*^{-/-} mice had 90%, 96%, 97%, and 83% lower concentrations of total SFA, MUFA, N-6 PUFA, and N-3 PUFA respectively (Fig. 12A). *Plaat1*^{-/-} female mice had 66% lower total masses of SFA, 88% lower total MUFA, and 87% lower total N-6 PUFA in CL per gram of brain tissue analyzed (Fig. 12C).

In heart CL from *Plaat1*^{-/-} mice, the relative abundance of N-6 species was considerably less. Specifically, male and female *Plaat1*^{-/-} mice had 44% (Fig. 12B, 15A) and 37% (Fig.12D, 15B) lower relative proportions of N-6 PUFA, respectively. Male *Plaat1*^{-/-} mice had 83% lower relative abundance of 18:2n-6 (*Wt*, 35.79 ± 0.79 wt/wt % of total CL versus *Plaat1*^{-/-}, 6.04 ± 0.77 wt/wt %

of total CL, $P < 0.0001$) (Fig. 15A). Similarly, in female *Plaat1*^{-/-} mice, 18:2n-6 relative abundance was 87% lower (*Wt*, 29.73 ± 1.19 wt/wt % of total CL versus *Plaat1*^{-/-}, 3.95 ± 0.38 wt/wt % of total CL, $P = 0.0158$) (Fig. 15B). This change likely indicates a reduction in tetra-linoleoyl species of CL in mouse hearts from both sexes, although this was not directly investigated in the current work. Surprisingly, the abundance of other N-6 PUFA species tended to be *higher* in *Plaat1*^{-/-} mice. AA levels were substantially higher in both sexes. Male *Plaat1*^{-/-} mice exhibited an approximate 18-fold higher level of 20:4n-6 (*Wt*, 0.63 ± 0.11 wt/wt % of total CL versus *Plaat1*^{-/-}, 11.38 ± 1.36 wt/wt % of total CL, $P < 0.0001$), and female *Plaat1*^{-/-} mice, this difference was 20-fold (*Wt*, 0.63 ± 0.03 wt/wt % of total CL versus *Plaat1*^{-/-}, 12.86 ± 1.44 wt/wt % of total CL, $P < 0.0001$) (Fig. 15A, B).

We also observed significant compositional differences in an array of saturated fatty acyl species in CL from *Plaat1*^{-/-} mouse hearts. Although the total concentration of SFA in CL in heart tissue was lower in *Plaat1*^{-/-} mice compared to *Wt* controls, total heart CL content was less, and therefore when SFA was examined as a relative proportion of the total mass of CL present, the relative abundance of SFA in CL from *Plaat1*^{-/-} mice was higher than the relative abundance in CL from *Wt* mice. In other words, in *Plaat1*^{-/-} mice, despite the drastic reduction in total CL concentrations in heart (which was associated with reductions in concentrations of all classes of fatty acids in heart CL) the relative content of SFA in analyzed CL was greater in mice deficient in PLAAT1. The relative mass percentage of SFA in heart CL was 74% higher in male *Plaat1*^{-/-} mice (*Wt*, 17.16 ± 0.40 wt/wt % of total CL versus *Plaat1*^{-/-}, 29.84 ± 1.96 wt/wt % of total CL, $P = 0.0002$) (Fig. 12B, 13A) and 101% higher in female *Plaat1*^{-/-} mice (*Wt*, 18.45 ± 0.19 wt/wt % of total CL versus *Plaat1*^{-/-}, 37.11 ± 3.29 wt/wt % of total CL, $P = 0.0005$) (Fig. 12D, 13B). The predominant SFA species detected in heart CL in *Wt* mice was 16:0, and the relative content of this lipid did not differ significantly between *Wt* and *Plaat1*^{-/-} mice (Fig. 13A, B). In contrast, stearate

(18:0) levels in heart CL were approximately 12 fold higher in both male (*Wt*, 1.36 ± 0.19 wt/wt % of total CL versus *Plaat1*^{-/-}, 16.99 ± 1.33 wt/wt % of total CL, $P < 0.0001$) and female (*Wt*, 1.90 ± 0.07 wt/wt % of total CL versus *Plaat1*^{-/-}, 22.63 ± 2.57 wt/wt % of total CL, $P < 0.0001$) mice lacking PLAAT1, and this difference resulted in 18:0 becoming the most abundant SFA in heart CL in *Plaat1*^{-/-} mice (Fig. 13A, B). With regards to less abundant SFA's, namely 20:0, 22:0, and 24:0, each constituting less than 1% of total CL fatty acyl species, we see significantly greater relative levels when PLAAT1 is deficient (Fig. 13A, B).

The concentrations and relative abundances of MUFA species in CL isolated from the hearts of *Plaat1*^{-/-} mice were substantially lower compared to *Wt* mice. The observed differences were found in both male and female mice. In male *Plaat1*^{-/-} mice, the relative abundance of total MUFA species was 34.7% less (*Wt*, 39.58 ± 1.19 wt/wt % of total CL versus *Plaat1*^{-/-}, 25.83 ± 2.71 wt/wt % of total CL, $P = 0.0017$) (Fig. 12B, 14A) and in female mice 41.4% less (*Wt*, 45.14 ± 1.48 wt/wt % of total CL versus *Plaat1*^{-/-}, 26.46 ± 1.78 wt/wt % of total CL, $P < 0.0001$) (Fig. 12D, 14B). The lower amount of MUFA abundance was primarily due to lesser relative abundance of oleate (18:1n-9), which is typically the second most highly enriched fatty acyl chain in heart CL. The relative amounts of 18:1n-9 were 36.7% lower in male *Plaat1*^{-/-} mice (*Wt*, 27.79 ± 0.90 wt/wt % of total CL versus *Plaat1*^{-/-}, 17.64 ± 1.63 wt/wt % of total CL, $P = 0.0006$), and 48.4% lower in female *Plaat1*^{-/-} mice (*Wt*, 35.28 ± 1.34 wt/wt % of total CL versus *Plaat1*^{-/-}, 18.22 ± 1.40 wt/wt % of total CL, $P < 0.0001$) (Fig. 14A, B).

PLAAT1 deficiency resulted in a lower total concentration of omega-3 species in heart CL in male mice, although this difference did not reach statistical significance in females. However, the relative percentage of N-3 PUFA levels as a mass percentage of total fatty acyl species in heart CL

was 153% greater in male *Plaat1*^{-/-} mice (*Wt*, 2.84 ± 0.07 wt/wt % of total CL versus *Plaat1*^{-/-}, 7.19 ± 1.14 wt/wt % of total CL, P=0.0053) (Fig. 12B, 16A) and 196% greater in female *Plaat1*^{-/-} mice (*Wt*, 2.38 ± 0.08 wt/wt % of total CL versus *Plaat1*^{-/-}, 7.06 ± 0.98 wt/wt % of total CL, P=0.0014) (Fig. 12D, 16B). In *Wt* mice, 18:3n-3 was the most abundant N-3 PUFA species in CL, in both males and females, followed by DHA (22:6n-3). In PLAAT1 deficient mice, however, the level of DHA was much higher. In both male and female *Plaat1*^{-/-} mice, DHA levels were 14-fold higher (male *Wt*, 0.49 ± 0.12 wt/wt % of total CL versus *Plaat1*^{-/-}, 6.70 ± 1.16 wt/wt % of total CL, P=0.0007, female *Wt*, 0.49 ± 0.05 wt/wt % of total CL versus *Plaat1*^{-/-}, 6.63 ± 1.06 wt/wt % of total CL, P<0.0001) (Fig. 16A, B).

Total CL PUFA concentrations in heart and relative PUFA concentrations in heart CL were both significantly lower when PLAAT1 was deficient, and these effects were common to both sexes (Fig. 12). The relative proportion of PUFA in heart CL was 29.5% lower in male *Plaat1*^{-/-} mice compared to male *Wt* mice (*Wt*, 40.16 ± 0.59 wt/wt % of total CL versus *Plaat1*^{-/-}, 28.3 ± 2.05 wt/wt % of total CL, P=0.0005) and 19.9% lower in female *Plaat1*^{-/-} versus *Wt* mice (*Wt*, 33.53 ± 1.27 wt/wt % of total CL versus *Plaat1*^{-/-}, 26.87 ± 2.54 wt/wt % of total CL, P=0.0472) (Fig. 12B, D). This difference is mostly driven by lower acylation by 18:2n-6 species.

Interestingly, in both males and females the total HUFA species in heart CL isolated from *Plaat1*^{-/-} mice comprised a substantially higher percentage of the total fatty acyl species within that CL, although the concentrations of total CL HUFA per gram of brain tissue did not differ significantly by genotype, suggesting relatively high conservation of CL enriched in this class of fatty acyl chains after PLAAT1 loss. For male *Plaat1*^{-/-} mice, the relative mass percentage of heart CL HUFA species was approximately 11-fold higher than in *Wt* mice (*Wt*, 1.96 ± 0.31 wt/wt % of total

CL versus *Plaat1*^{-/-}, 20.94 ± 2.15 wt/wt % of total CL, P<0.0001) (Fig. 12B). Similarly, female *Plaat1*^{-/-} mice had an approximately 12-fold greater relative enrichment of heart CL with HUFA species compared to their sex-matched *Wt* controls (*Wt*, 1.78 ± 0.12 wt/wt % of total CL versus *Plaat1*^{-/-}, 22.27 ± 2.35 wt/wt % of total CL, P<0.0001) (Fig. 12D). The substantial enrichment of heart CL by HUFA species appears to be driven primarily by greater relative mass percentages of the 20:4n-6 and 22:6n-3 species.

PLAAT1 deficiency results in greater CL concentrations in the gastrocnemius muscle of both male and female mice, including higher relative composition by MUFA species and lower relative composition by N-6 PUFA species.

PLAAT1 deficient male and female mice have a significantly higher concentration of CL in gastrocnemius muscle. In male *Plaat1*^{-/-} mice, we see a 185% higher concentration of total CL (*Wt*, 596.2 ± 90.71 µg CL/ g of tissue versus *Plaat1*^{-/-}, 1704 ± 317 µg CL/ g of tissue, P=0.015), while in female *Plaat1*^{-/-} mice we observe a 364% greater concentration of total CL (*Wt*, 899.2 ± 33.51 µg CL/ g of tissue versus *Plaat1*^{-/-}, 4127 ± 1132 µg CL/ g of tissue, P=0.0142) (Fig. 6A, B). This can be further separated into specific differences in fatty acyl classes, where we observed that the concentration of SFA was 192% higher, and the concentration of MUFA was 463% higher in male *Plaat1*^{-/-} mice, while the concentrations of SFA, MUFA, and N-6 PUFA in female *Plaat1*^{-/-} mice were higher by 347%, 760%, and 215%, respectively (Fig. 17A, C).

Despite the higher concentrations of CL SFA in male and female *Plaat1*^{-/-} gastrocnemius muscle, these concentrations were proportionate to the overall greater CL concentration in this tissue, and as a result, the relative abundance of SFA expressed as a mass percentage of total fatty acyl chains in analyzed CL did not differ significantly between *Plaat1*^{-/-} and *Wt* mice, and this was observed in both sexes (Fig. 17B, D and 18A, B). Within the SFA species, differences in

the abundance of specific fatty acyls were evident. We observed a lesser relative proportion of 18:0 in both male (*Wt*, 5.55 ± 0.12 wt/wt % of total CL versus *Plaat1*^{-/-}, 1.55 ± 0.34 wt/wt % of total CL, $P < 0.0001$) and female (*Wt*, 5.71 ± 0.31 wt/wt % of total CL of tissue versus *Plaat1*^{-/-}, 2.26 ± 0.47 wt/wt % of total CL, $P = 0.0003$) mice (Fig. 18A, B). Although differences in the proportions of palmitate (16:0) did not reach statistical significance, modestly higher levels of this FA species, as well as myristate (14:0) together seem to have contributed to offsetting the lower 18:0 levels, so that total SFA proportions did not differ significantly in gastrocnemius CL between genotypes.

Total gastrocnemius CL MUFA concentrations were nearly 6-fold and 9-fold higher in male and female *Plaat1*^{-/-} mice, respectively (Fig. 17A, C). We observed that male *Plaat1*^{-/-} mice have a 98% higher relative MUFA content compared to *Wt* mice as a proportion of total CL fatty acyl species analyzed (*Wt*, 21.42 ± 1.01 wt/wt % of total CL versus *Plaat1*^{-/-}, 42.37 ± 1.81 wt/wt % of total CL, $P < 0.0001$), and an 83% higher relative MUFA proportion in total fatty acyl species analyzed in female *Plaat1*^{-/-} mice (*Wt*, 22.16 ± 1.13 wt/wt % of total CL versus *Plaat1*^{-/-}, 40.55 ± 0.83 wt/wt % of total CL, $P < 0.0001$) (Fig. 17B, D and 19A, B). This difference stems primarily from greater relative proportions of 18:1n-9 species, which are 92% higher in proportional content in CL from male *Plaat1*^{-/-} mouse gastrocnemius muscle (*Wt*, 15.08 ± 1.04 wt/wt % of total CL versus *Plaat1*^{-/-}, 29.01 ± 2.32 wt/wt % of total CL, $P = 0.0016$), and 81% higher in female *Plaat1*^{-/-} mouse gastrocnemius muscle CL (*Wt*, 15.98 ± 0.98 wt/wt % of total CL versus *Plaat1*^{-/-}, 28.95 ± 0.76 wt/wt % of total CL, $P < 0.0001$) (Fig. 19A, B).

Higher concentrations of total N-6 PUFA in CL isolated from the gastrocnemius muscle of *Plaat1*^{-/-} mice were statistically significant in females, but did not reach this threshold in males (Fig. 17A, C). Regardless, these higher levels were not as elevated as the total CL concentration

elevation that was observed overall, and therefore the relative proportional abundance of N-6 acylated onto CL (analyzed by mass percentage) was 33.2% lower in male *Plaat1^{-/-}* mice (*Wt*, 50.58 ± 1.78 wt/wt % of total CL versus *Plaat1^{-/-}*, 33.80 ± 1.68 wt/wt % of total CL, $P=0.0003$) and by 31.1% in female *Plaat1^{-/-}* mice (*Wt*, 50.31 ± 1.30 wt/wt % of total CL versus *Plaat1^{-/-}*, 34.64 ± 0.47 wt/wt % of total CL, $P<0.0001$) (Fig.17B, D and 20A, B). Most of the relatively lower level of N-6 PUFA content results from differences in linoleic acid, where we see that the relative mass percentage of 18:2n-6 in total gastrocnemius CL is 27.8% lower in male *Plaat1^{-/-}* mice (*Wt*, 44.34 ± 2.59 wt/wt % of total CL versus *Plaat1^{-/-}*, 32.00 ± 1.67 wt/wt % of total CL, $P=0.0042$), and 26.1% lower in female *Plaat1^{-/-}* mice (*Wt*, 44.38 ± 0.89 wt/wt % of total CL versus *Plaat1^{-/-}*, 32.79 ± 0.35 wt/wt % of total CL $P<0.0001$) (Fig. 20A, B). In both sexes, we also observe relative lower mass percentages of 20:2n-6, 20:3n-6, 20:4n-6, 22:4n-6, and 22:5n-6 species, but these fatty acyl species were substantially less abundant than 18:2n-6 in terms of relative composition (Fig. 20A, B).

The relative mass percentage of total N-3 PUFA species was approximately 48% lower in both male (*Wt*, 5.97 ± 0.47 wt/wt % of total CL versus *Plaat1^{-/-}*, 2.86 ± 0.17 wt/wt % of total CL, $P=0.0002$), and female (*Wt*, 6.11 ± 0.48 wt/wt % of total CL versus *Plaat1^{-/-}*, 2.99 ± 0.20 wt/wt % of total CL, $P=0.0003$) *Plaat1^{-/-}* mice (Fig.17B, D and 21A, B). Within this class, the most significant difference in the relative proportion of any single fatty acyl species was an 82% lower level of DHA in both male (*Wt*, 3.89 ± 0.44 wt/wt % of total CL versus *Plaat1^{-/-}*, 0.68 ± 0.09 wt/wt % of total CL $P<0.0001$) and female *Plaat1^{-/-}* mice (*Wt*, 4.43 ± 0.47 wt/wt % of total CL versus *Plaat1^{-/-}*, 0.80 ± 0.14 wt/wt % of total CL $P<0.0001$) (Fig. 21A, B). Only one N-3 species displayed higher relative content, and this was alpha-linolenic acid, where a near 2 – fold higher

proportional content was seen in the gastrocnemius CL analyzed from both male and female *Plaat1*^{-/-} mice (Fig. 21A, B).

Both HUFA and PUFA species were relatively less abundant in CL isolated from gastrocnemius muscles from both male and female *Plaat1*^{-/-} mice, due to the relatively lower levels of total N-6 and N-3 contents. We observe 35% less PUFA species in male *Plaat1*^{-/-} mice (*Wt*, 56.63 ± 1.43 wt/wt % of total CL versus *Plaat1*^{-/-}, 36.66 ± 1.83 wt/wt % of total CL $P < 0.0001$), and 33% less in female *Plaat1*^{-/-} mice (*Wt*, 56.47 ± 1.58 wt/wt % of total CL versus *Plaat1*^{-/-}, 37.67 ± 0.60 wt/wt % of total CL $P < 0.0001$) (Fig. 17B, D). HUFA are more drastically different in *Plaat1*^{-/-} mice, since these highly unsaturated species are 77.5% lower in proportional abundance in gastrocnemius CL isolated from male mice (*Wt*, 10.51 ± 1.24 wt/wt % of total CL versus *Plaat1*^{-/-}, 2.37 ± 0.24 wt/wt % of total CL $P = 0.0002$), and 74.9% lower in female mice (*Wt*, 10.21 ± 0.91 wt/wt % of total CL versus *Plaat1*^{-/-}, 2.56 ± 0.37 wt/wt % of total CL $P < 0.0001$) (Fig. 17B, D).

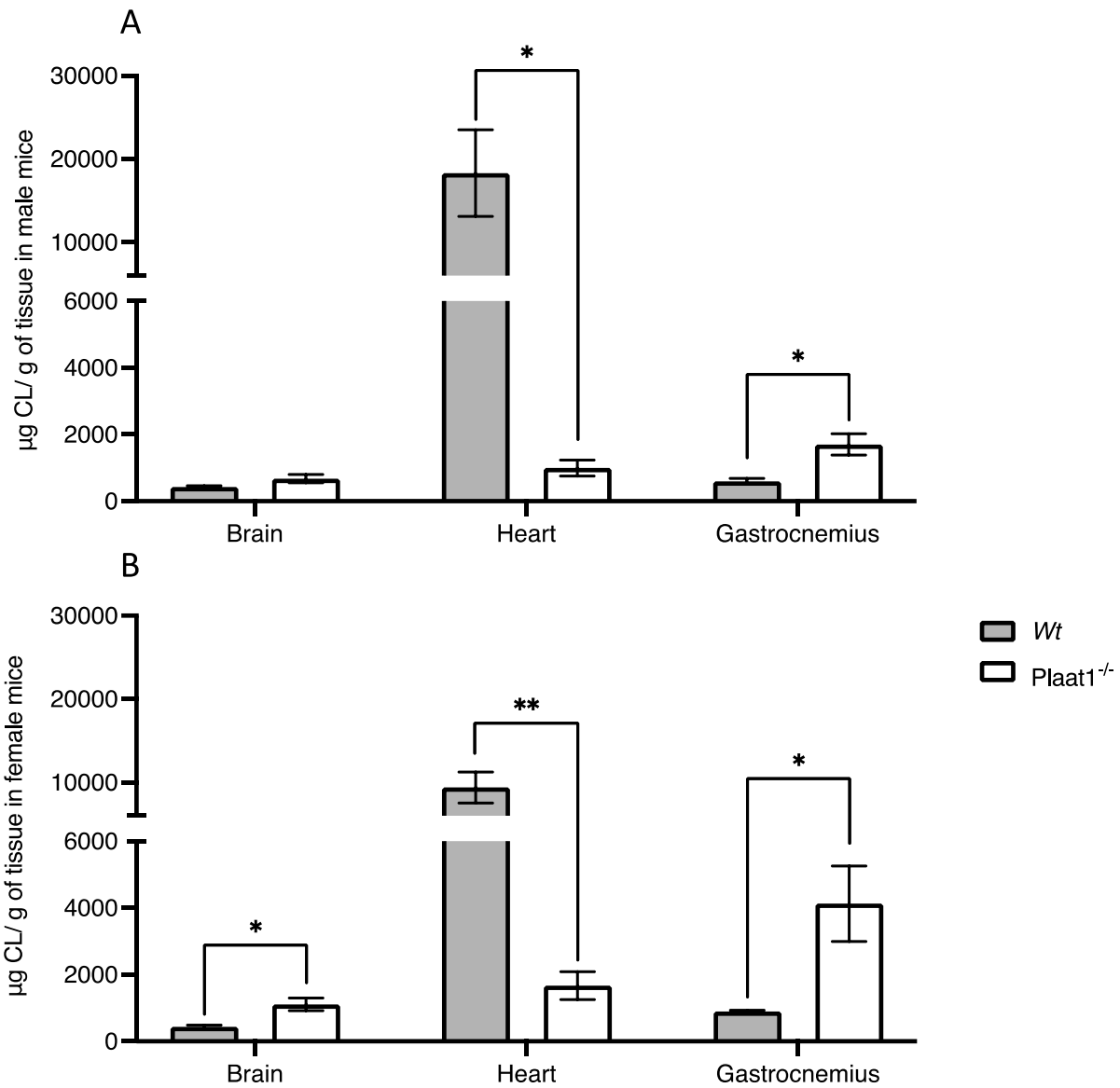


Figure 6: PLAAT1 deficiency alters total CL concentrations in various mouse tissues.

Total CL concentrations in brain, heart and gastrocnemius tissues of *Wt* and *Plaatt1^{-/-}* male (A) and female (B) Data are means ± S.E.M; n = 4-5. *P < 0.05, **P < 0.01.

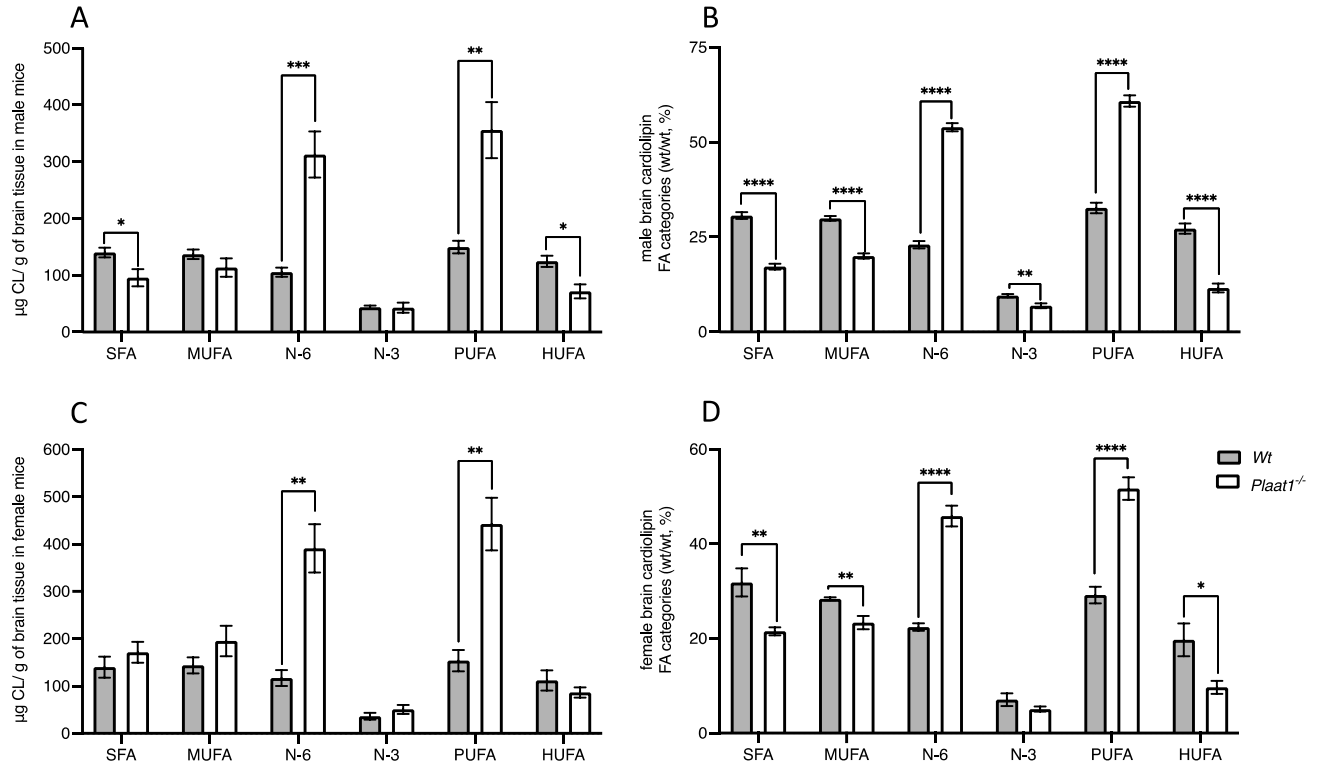


Figure 7: PLAAT1 deficiency alters the concentration of CL in brain and relative proportional abundance of major classes of fatty acyls in isolated CL.

CL was isolated from brain, and the fatty acyl content and composition were analyzed by gas chromatography in tissues taken from *Wt* and *Plaati*^{-/-} mice. The total mass of CL was quantified as micrograms of fatty acyl chains for male (B) and female (D) mice per gram of tissue analyzed. The relative proportional abundances of fatty acyl classes were analyzed as mass percentages for male (A) and female (C) mice. Data are means \pm S.E.M; n = 5. *P < 0.05, **P < 0.01, ***P < 0.001, ****P < 0.0001.

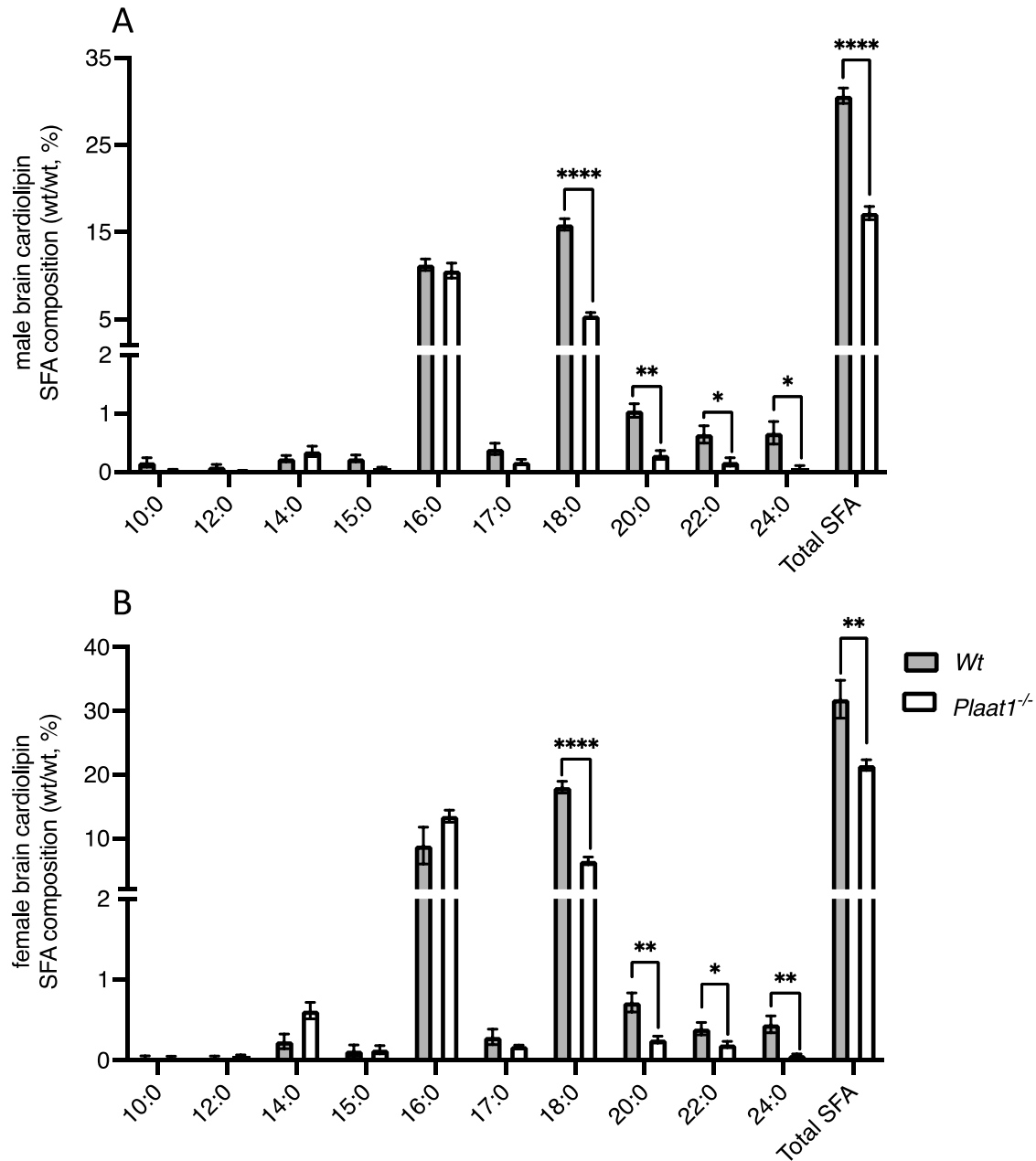


Figure 8: PLAAT1 deficiency displays lowered relative proportional composition of specific SFA species in CL isolated from the brain.

Relative mass percentages of different SFA species in isolated CL derived from brains of male (A) and female (B) *Wt* and *Pla1*^{-/-} mice. Data are means ± S.E.M; n = 5. *P < 0.05, **P < 0.01, ****P < 0.0001.

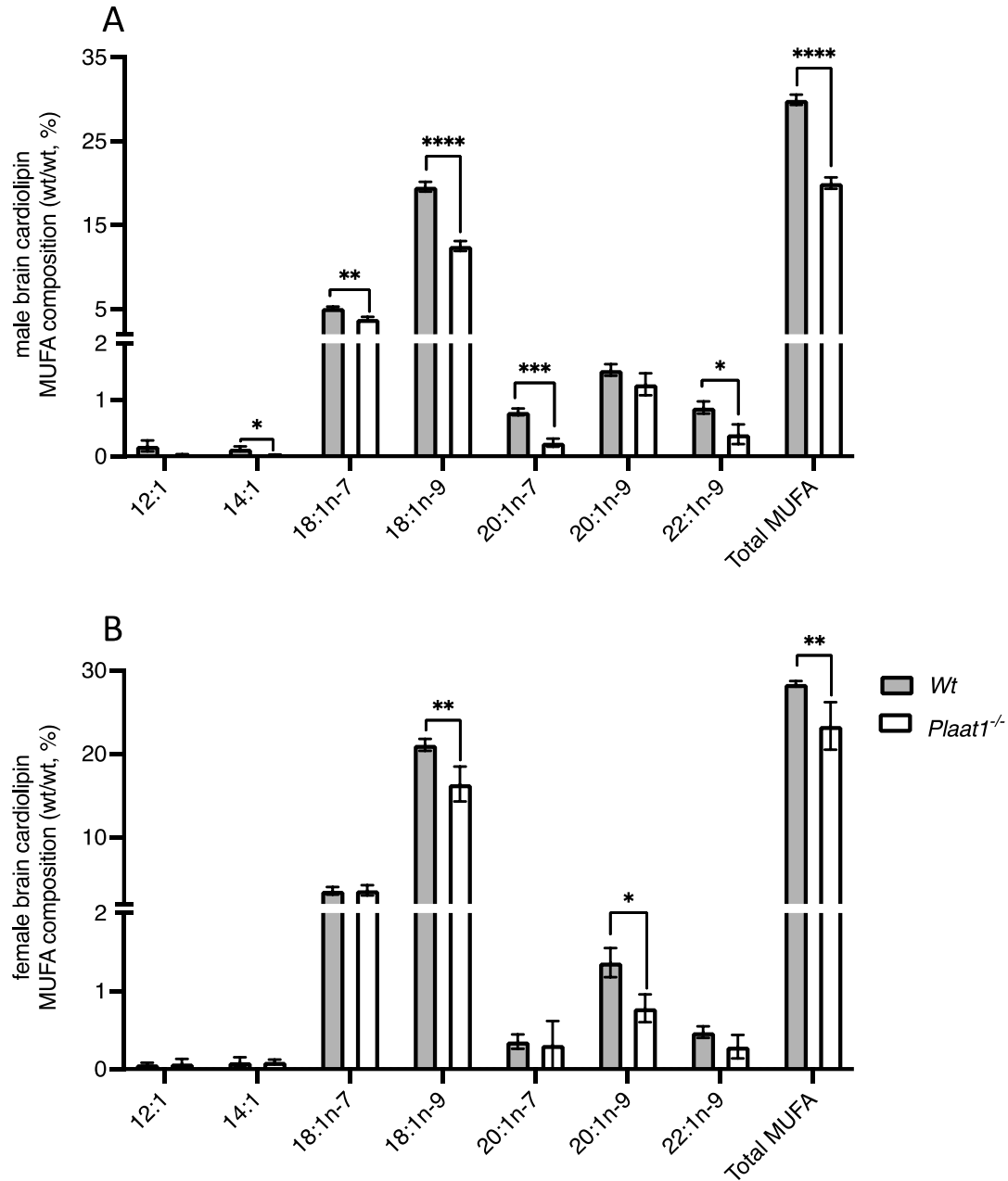


Figure 9: PLAAT1 deficiency displays lowered relative proportional composition of specific MUFA species in CL isolated from the brain.

Gas chromatography analysis of alterations in the relative mass percentage of MUFA species present in CL isolated from brain tissues derived from *Wt* and *Plaati*^{-/-} mice. Relative mass percentage of different MUFA species in isolated CL derived from brains of male (A) and female (B) *Wt* and *Plaati*^{-/-} mice. Data are means \pm S.E.M; n = 5. *P < 0.05, **P < 0.01, ***P < 0.001, ****P < 0.0001.

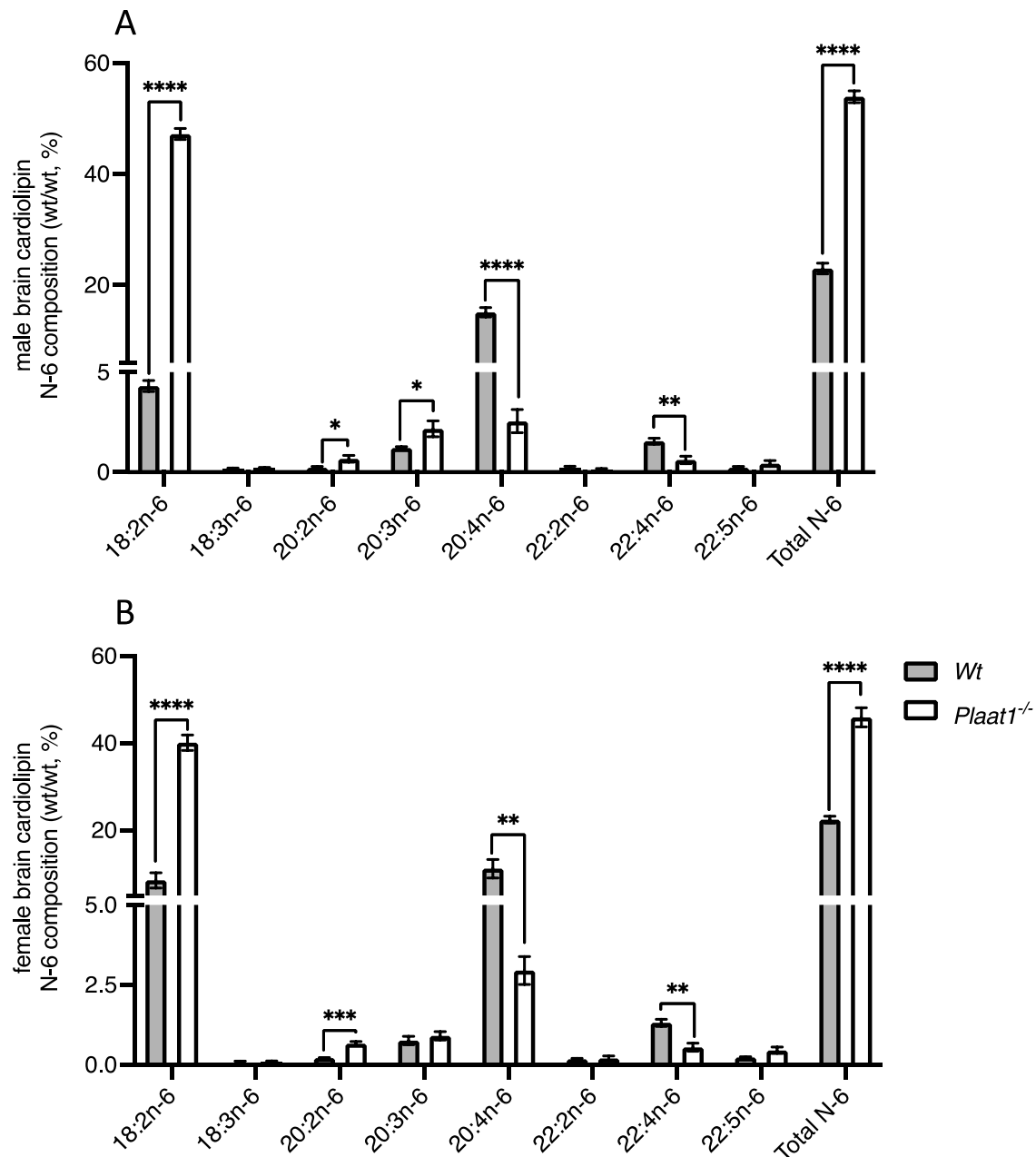


Figure 10: PLAAT1 deficiency alters relative proportional composition of specific N-6 PUFA species in CL isolated from the brain.

Relative mass percentages of different N-6 PUFA species in isolated CL derived from brains of male (A) and female (B) *Wt* and *Pla1*^{-/-} mice. Data are means \pm S.E.M; n = 5. *P < 0.05, **P < 0.01, ***P < 0.001, ****P < 0.0001.

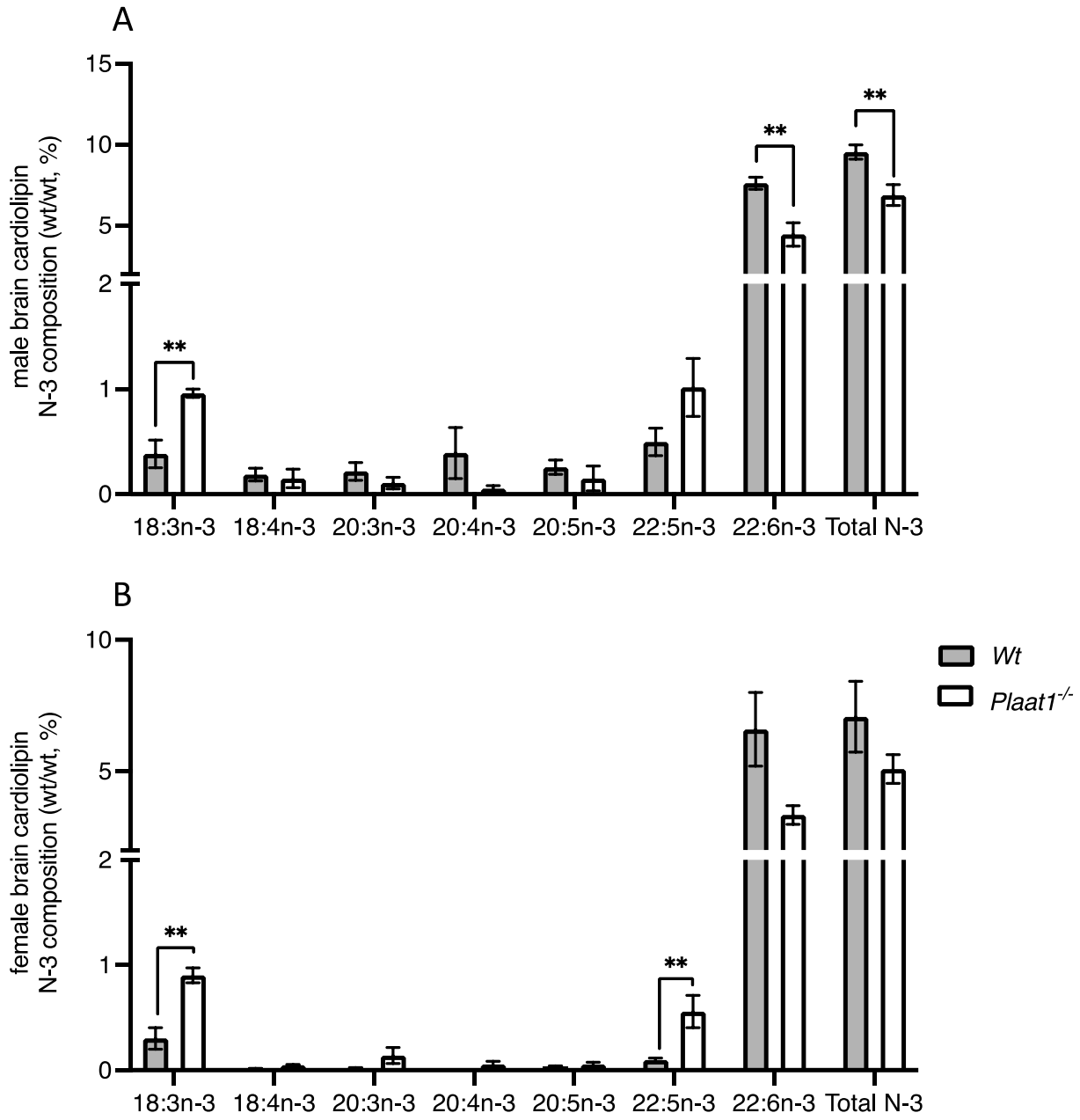


Figure 11: PLAAT1 deficiency alters relative proportional composition of specific N-3 PUFA species in CL isolated from the mouse brain.

Relative mass percentages of N-3 PUFA species in isolated CL derived from brains of male (A) and female (B) *Wt* and *Plaati^{-/-}* mice. Data are means \pm S.E.M; n = 5. **P < 0.01.

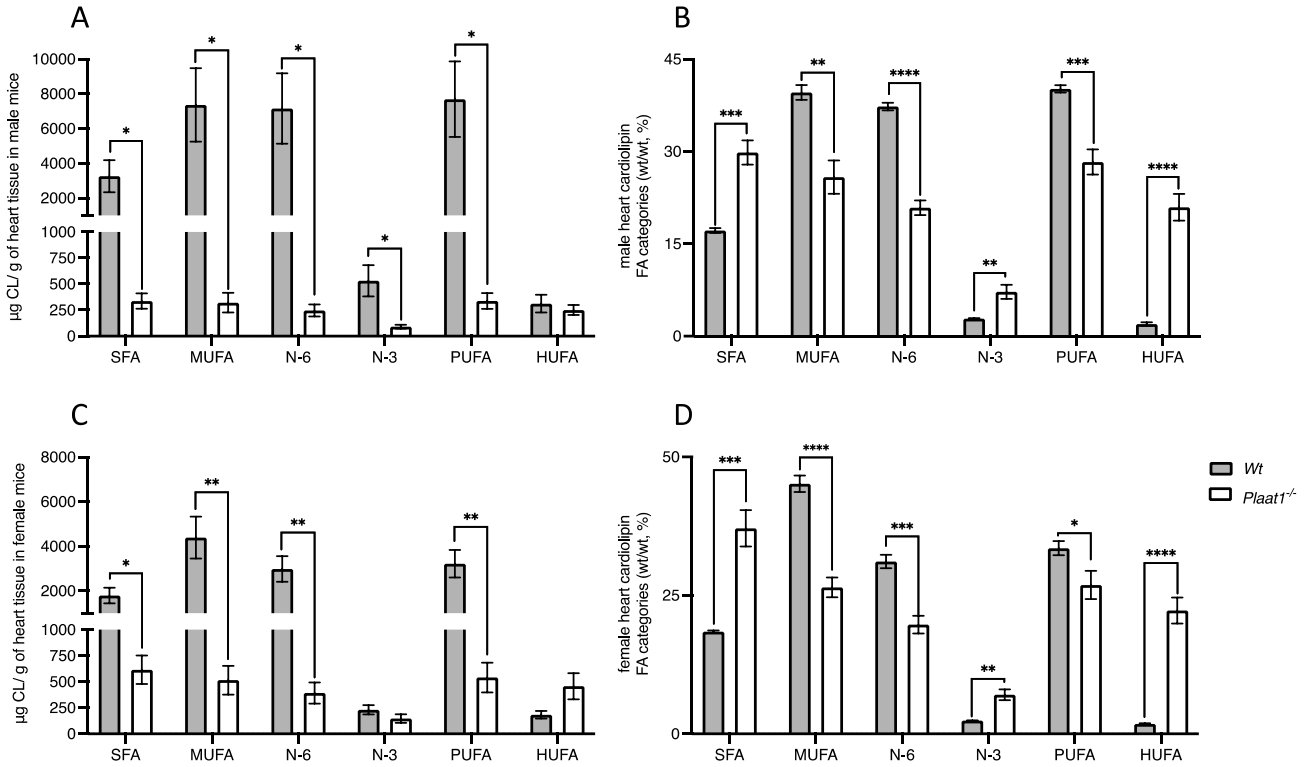


Figure 12: PLAAT1 deficiency alters the concentration of CL in cardiac tissue and relative proportional abundance of major classes of fatty acyls in isolated CL.

CL isolated from *Wt* and *Plaatt*^{-/-} mouse hearts was analyzed by gas chromatographs for fatty acyl content and composition. The total mass of CL was quantified as micrograms of fatty acyl chains for male (A) and female (C) mice per gram of tissue. The relative proportional abundances of fatty acyl classes were analyzed as mass percentages for male (B) and female (D) mice. Data are means \pm S.E.M; n = 5. *P < 0.05, **P < 0.01, ***P < 0.001, ****P < 0.0001.

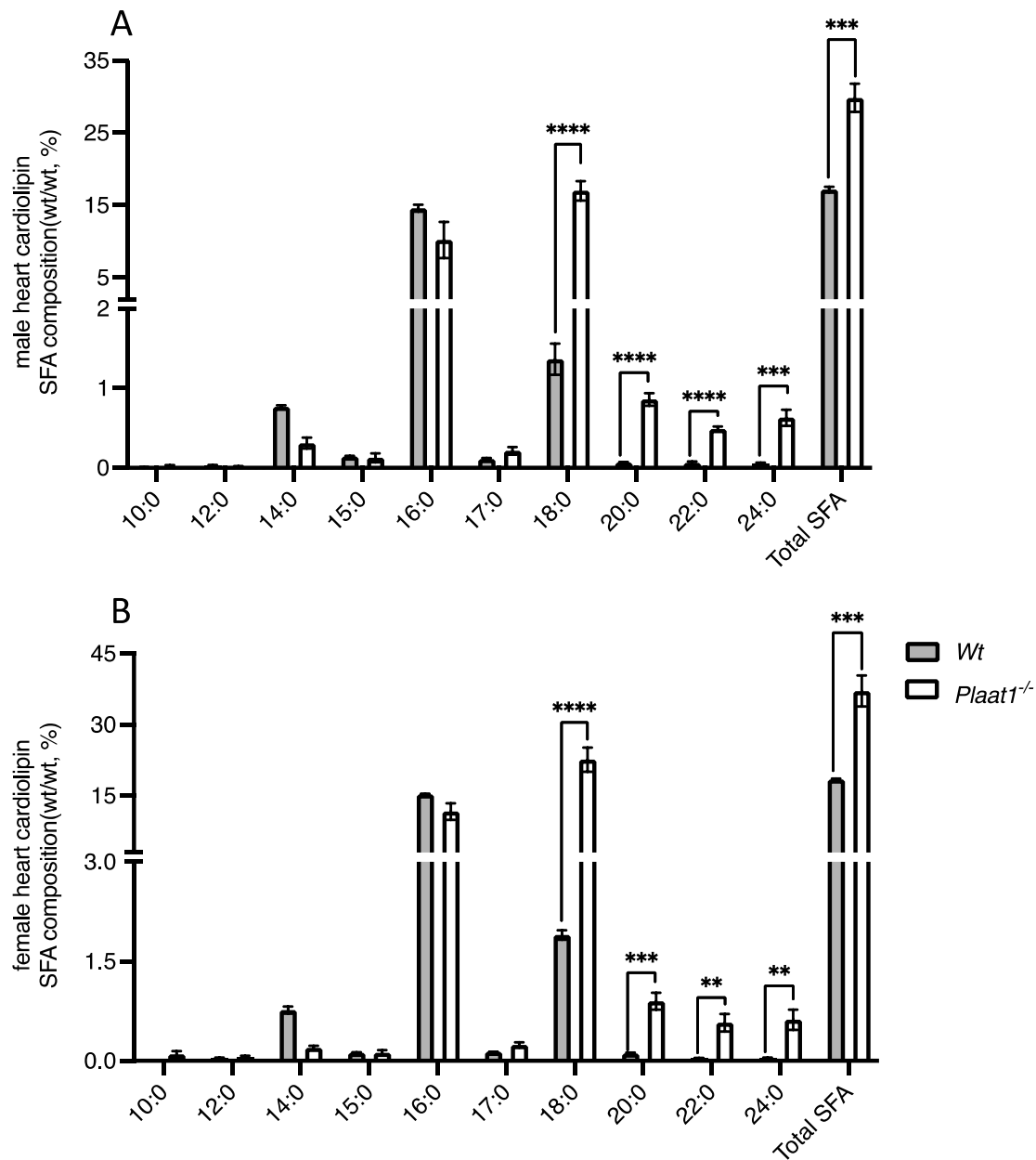


Figure 13: PLAAT1 deficiency displays higher relative proportional composition of specific SFA species in CL isolated from the heart.

Relative mass percentages of different SFA species in isolated CL derived from hearts of male (A) and female (B) *Wt* and *Plaat1*^{-/-} mice. Data are means \pm S.E.M; n = 5. **P < 0.01, ***P < 0.001, ****P < 0.0001.

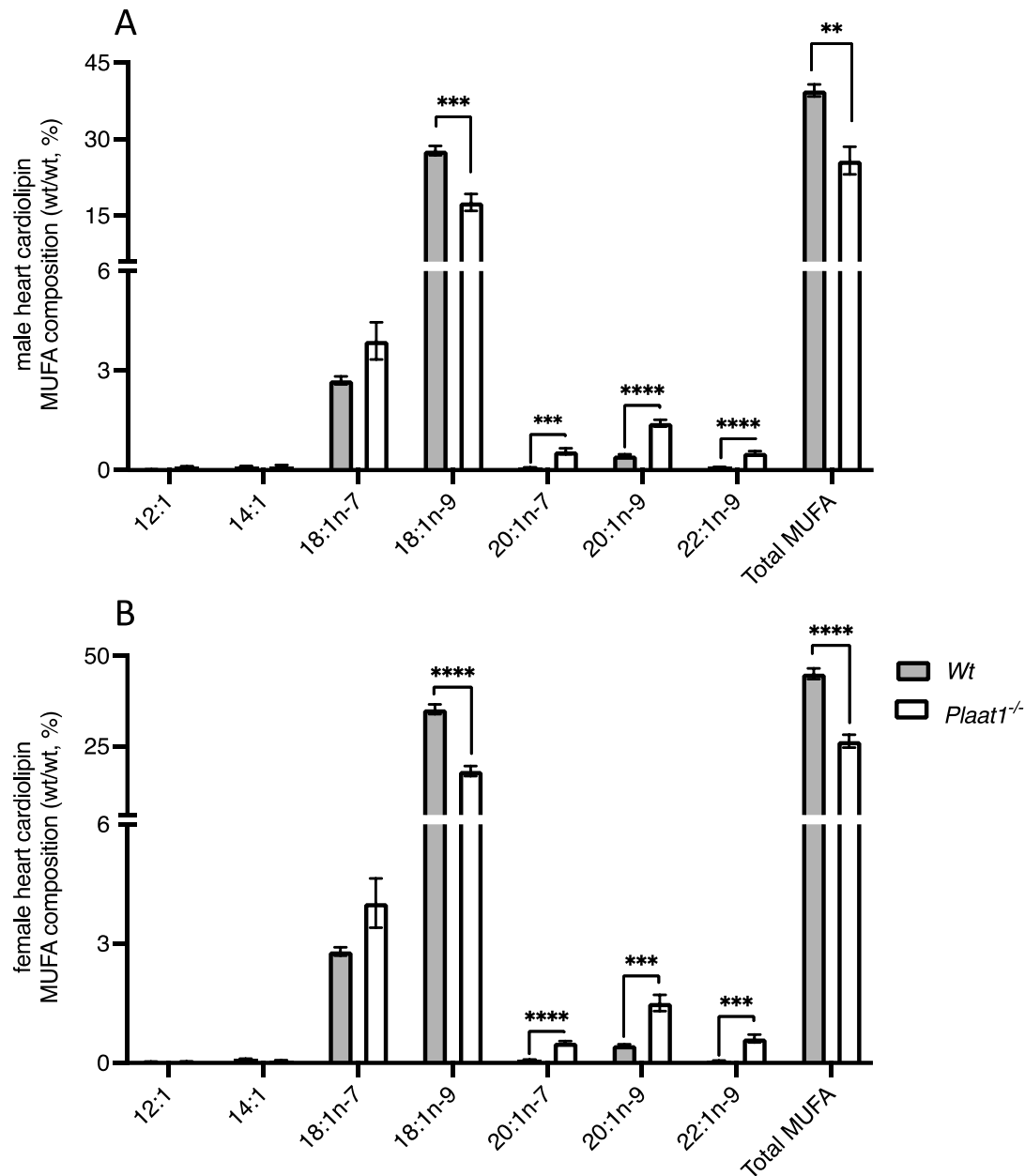


Figure 14: PLAAT1 deficiency alters relative proportional composition of specific MUFA species in CL isolated from the heart.

Using gas chromatography, the fatty acyl species composition of mouse heart CL was analyzed, and the relative mass percentages of different MUFA species in this isolated heart CL from male (A) and female (B) *Wt* and *Plaatt1^{-/-}* mice were graphed. Data are means \pm S.E.M; n = 5.

P < 0.01, *P < 0.001, ****P < 0.0001.

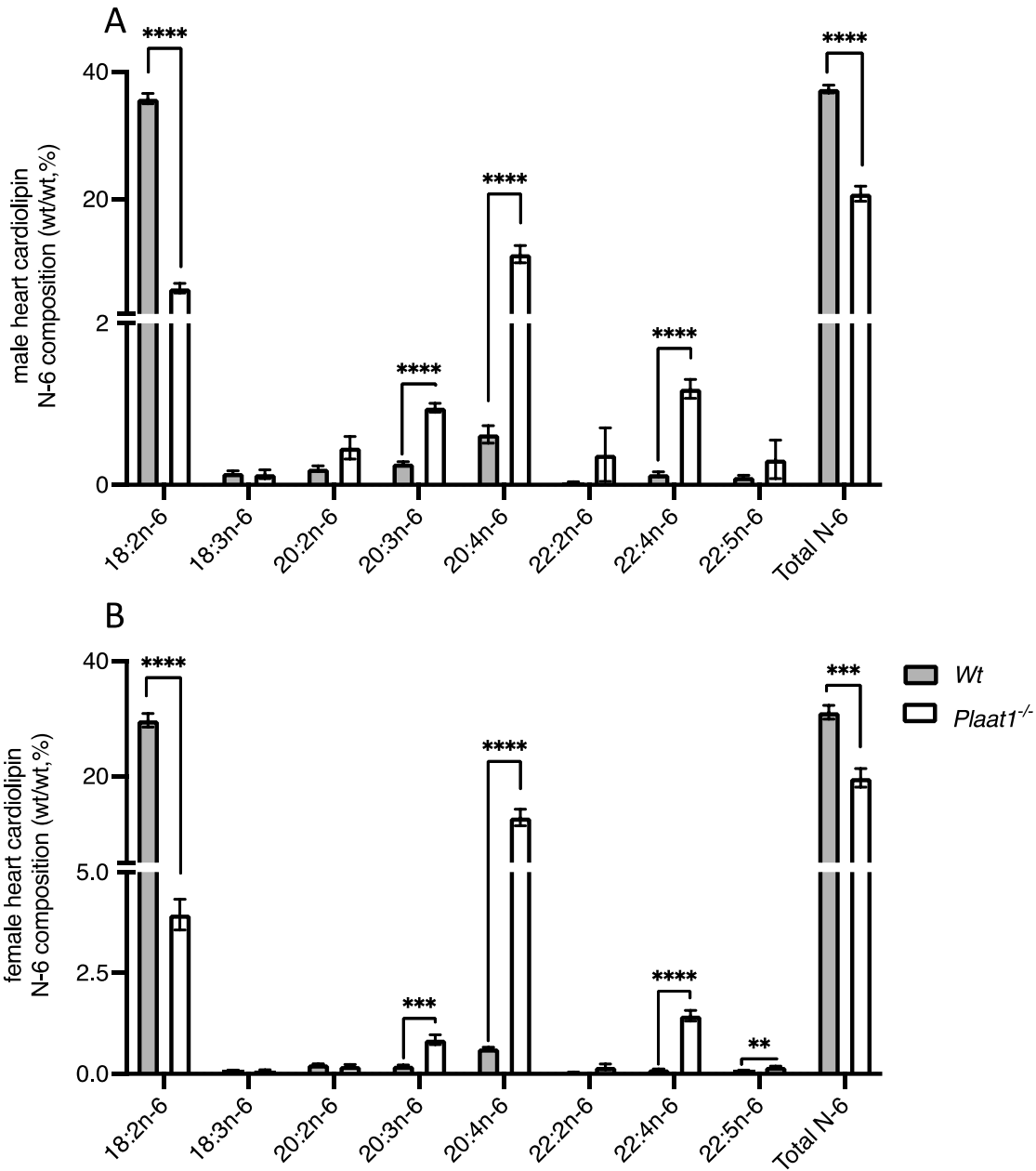


Figure 15: PLAAT1 deficiency alters relative proportional composition of specific N-6 PUFA species in CL isolated from the heart.

Relative mass percentages of different N-6 PUFA species in CL isolated from hearts of male (A) and female (B) *Wt* and *Plaati^{-/-}* mice. Data are means \pm S.E.M; n = 5. **P < 0.01, ***P < 0.001, ****P < 0.0001.

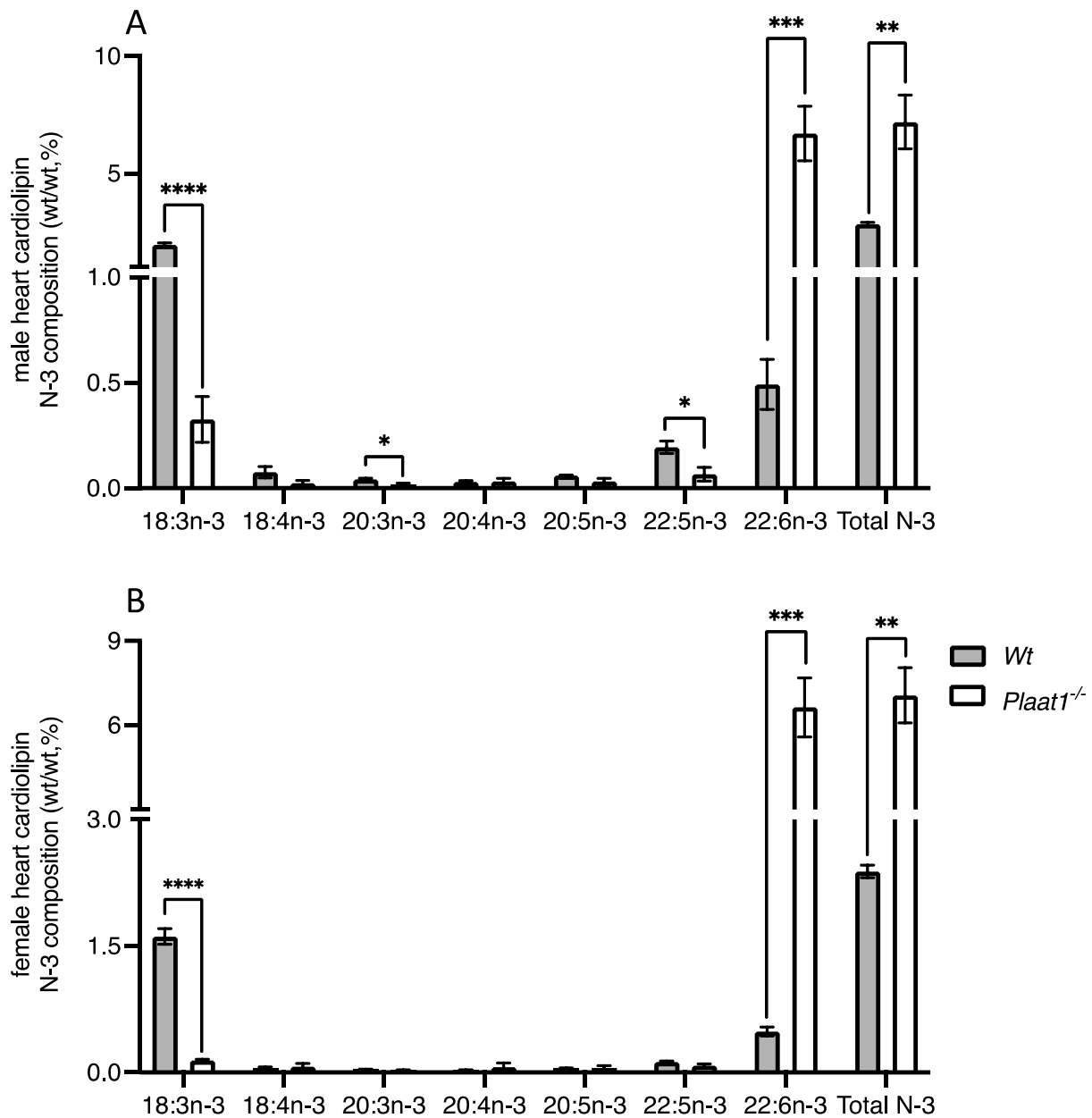


Figure 16: PLAAT1 deficiency alters relative proportional composition of specific N-3 PUFA species in CL isolated from the heart.

Relative mass percentages of N-3 PUFA species as a proportion of total CL fatty acyl species in CL isolated from hearts of male (A) and female (B) *Wt* and *Plaati*^{-/-} mice. Data are means \pm S.E.M; n = 5. *P < 0.05, **P < 0.01, ***P < 0.001, ****P < 0.0001.

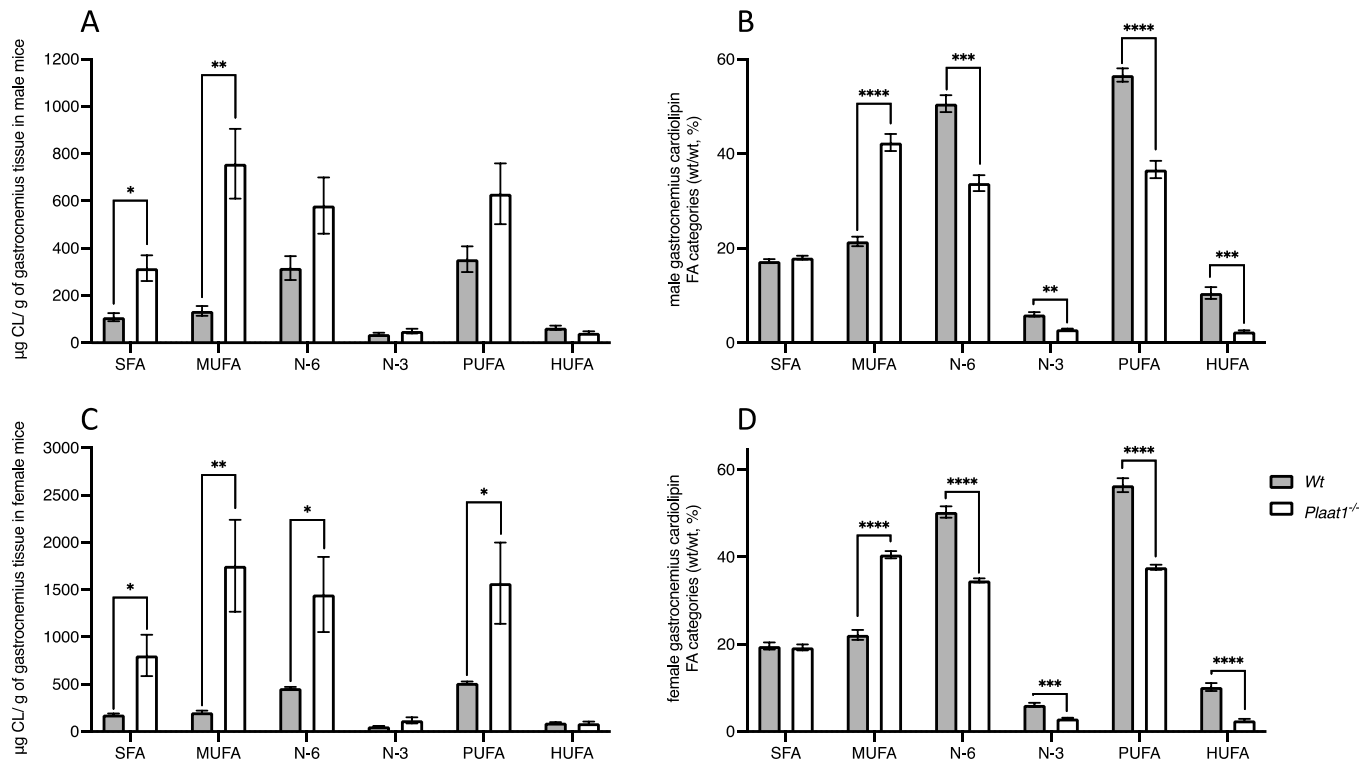


Figure 17: PLAAT1 deficiency alters the concentration of CL in gastrocnemius muscle and relative proportional abundance of major classes of fatty acyls in CL isolated from this tissue.

CL isolated from *Wt* and *Plaati*^{-/-} mouse gastrocnemius muscle was analyzed by gas chromatographs for fatty acyl content and composition. The total mass of CL was quantified as micrograms of fatty acyl chains for male (A) and female (C) mice per gram of tissue. The relative proportional abundances of fatty acyl classes were analyzed as mass percentages for male (B) and female (D) mice. Data are means \pm S.E.M; n = 5. *P < 0.05, **P < 0.01, ***P < 0.001, ****P < 0.0001.

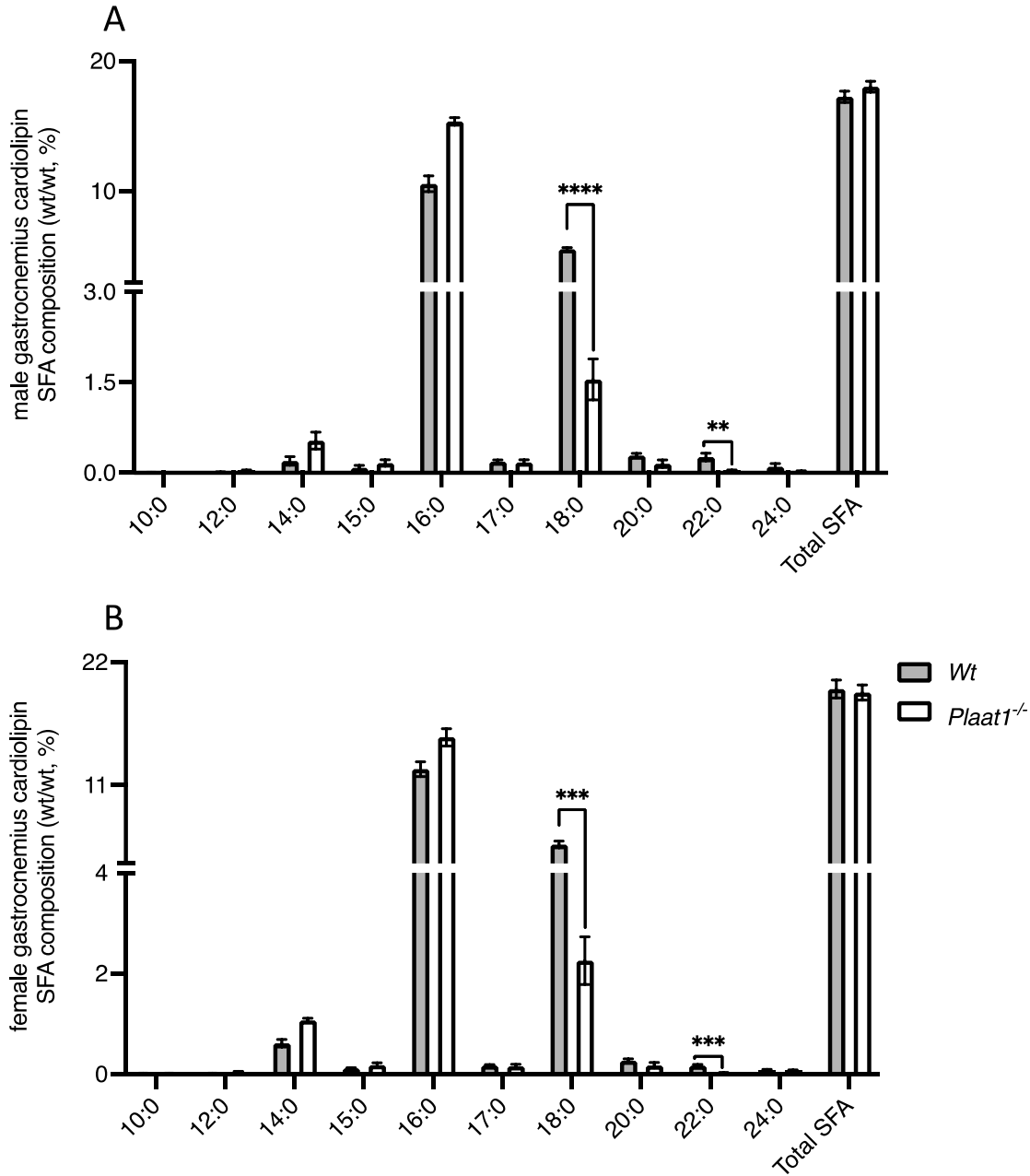


Figure 18: PLAAT1 deficiency displays lowered relative proportional composition of specific SFA species in CL isolated from gastrocnemius muscle.

Shown are relative mass percentages of SFA species as a proportion of total CL fatty acyl species in CL isolated from gastrocnemius muscles of male (A) and female (B) *Wt* and *Plaat1*^{-/-} mice. Data are means ± S.E.M; n = 5. **P < 0.01, ***P < 0.001, ****P < 0.0001.

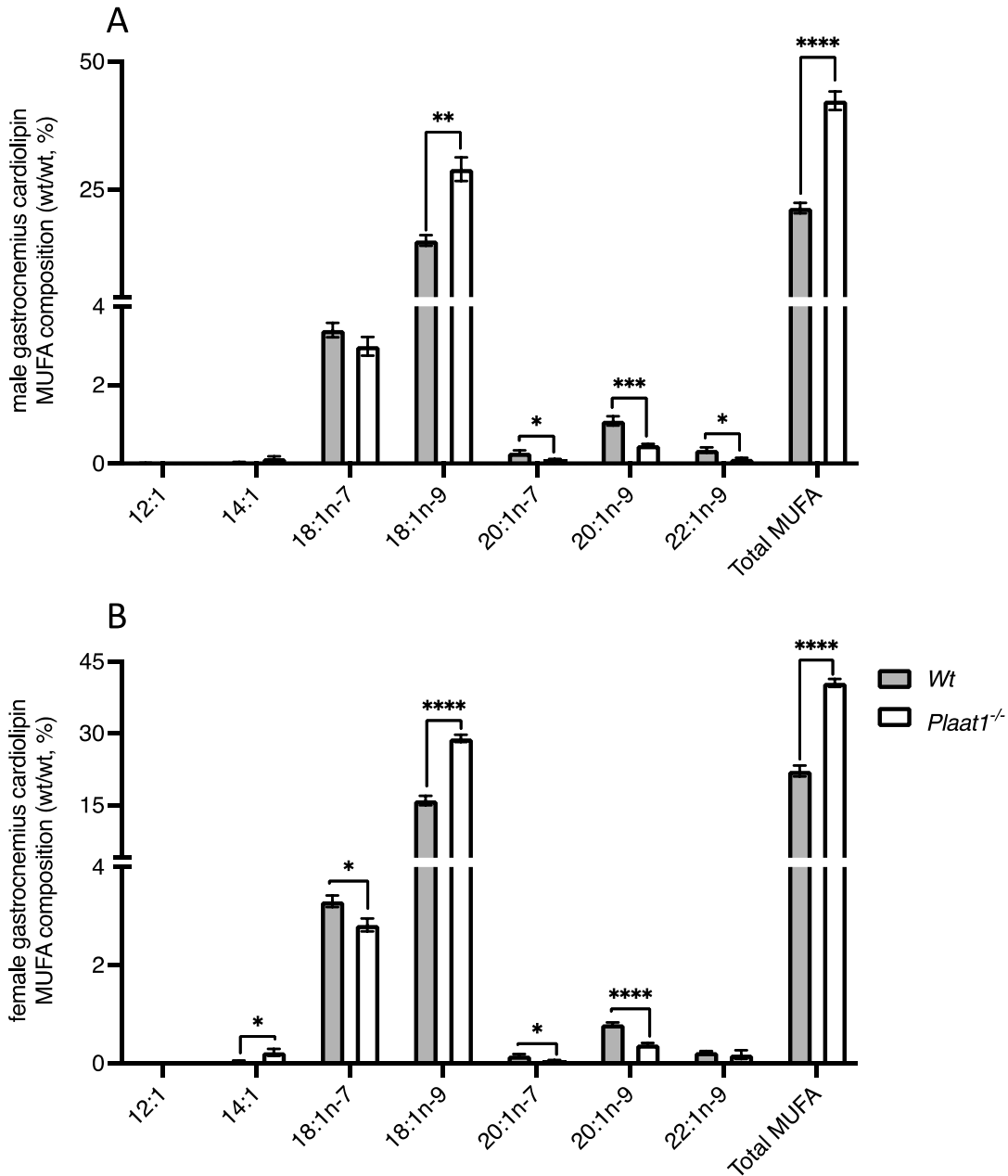


Figure 19: PLAAT1 deficiency alters relative proportional composition of specific MUFA species in CL isolated from gastrocnemius muscle.

Shown are relative mass percentages of MUFA species as a proportion of total CL fatty acyl species in CL isolated from gastrocnemius muscles of male (A) and female (B) *Wt* and *Plaati^{-/-}* mice. Data are means \pm S.E.M; n = 5. **P < 0.01, ***P < 0.001, ****P < 0.0001.

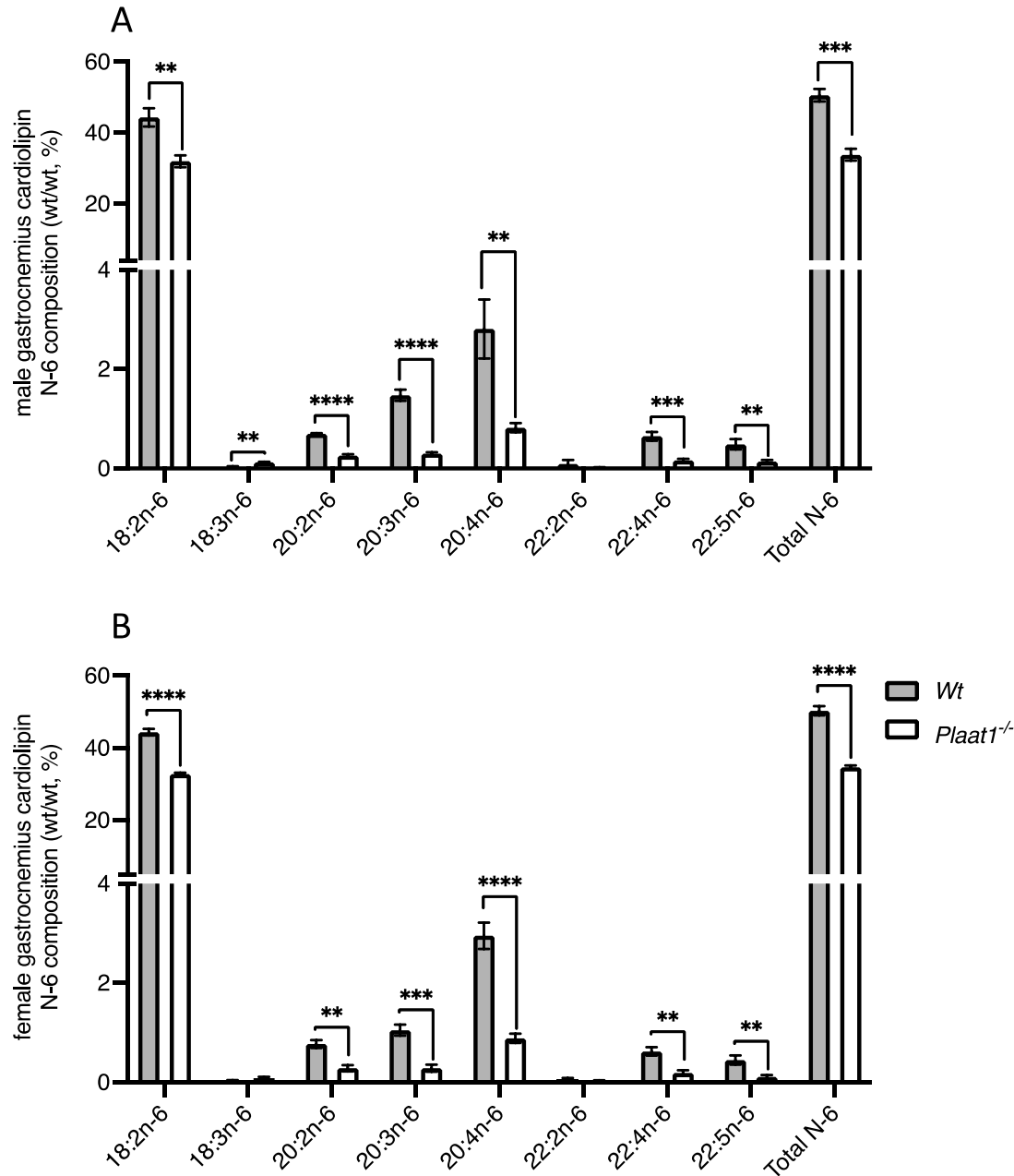


Figure 20: PLAAT1 deficiency alters relative proportional composition of specific N-6 PUFA species in CL isolated from gastrocnemius muscle.

Shown are relative mass percentages of N-6 PUFA species as a proportion of total CL fatty acyl species in CL isolated from gastrocnemius muscles of male (A) and female (B) *Wt* and *Plaati^{-/-}* mice. Data are means \pm S.E.M; n = 5. **P < 0.01, ***P < 0.001, ****P < 0.0001.

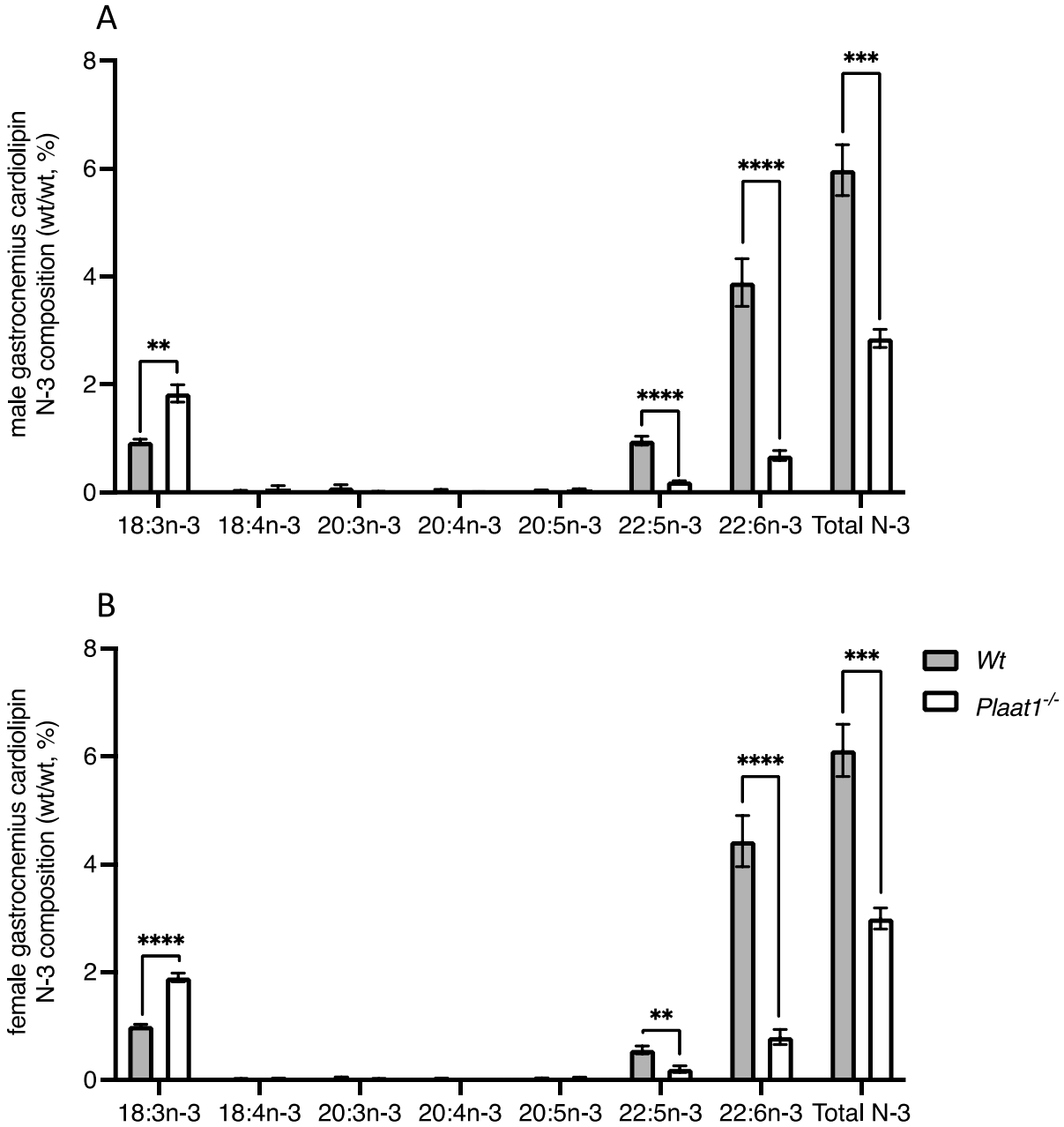


Figure 21: PLAAT1 deficiency alters relative proportional composition of specific N-3 PUFA species in CL isolated from gastrocnemius muscle.

Shown are relative mass percentages of N-3 PUFA species as a proportion of total CL fatty acyl species in CL isolated from gastrocnemius muscles of male (A) and female (B) *Wt* and *Plaat1*^{-/-} mice. Data are means ± S.E.M; n = 5. **P < 0.01, ***P < 0.001, ****P < 0.0001.

Discussion

The major objectives of this study were to compare the total concentration of CL in brain, heart and gastrocnemius muscle of *Plaat1*^{-/-} mice in to *Wt* controls, as well as to compare the CL fatty acyl profiles of those tissues between genotypes in sex-matched mice. To do this, I extracted total lipids from the brain, heart, and gastrocnemius muscle of *Wt* and *Plaat1*^{-/-} mice, and then isolated CL using TLC for further analysis through GC. GC analysis provided measures of the total mass of individual fatty acyl species contained in isolated CL, which allowed for a sub-analysis of the relative mass percent of individual species, in order to compare the concentrations of total CL and CL major class and fatty acyl species in tissues, as well as the relative proportional enrichment of individual fatty acyl species within a given mass of CL. This study has demonstrated a cogent case for a role for PLAAT1 in CL remodelling, in at least these three different tissues.

The findings of this study reveal intriguing variations in the amount and composition of CL in male and female *Plaat1*^{-/-} mice across different tissues, with the most pronounced changes observed in heart. This tissue exhibited striking differences between *Wt* and *Plaat1*^{-/-} mice, with 95% and 82% lower total CL concentrations measured in male and female mice, respectively. Significantly lower relative proportions of SFA, MUFA, and N-6 PUFA contributed to this decrease. One of the most noteworthy aspects of these results is the dramatic 83% and 87% lower relative amount of linoleate in the hearts of male and female *Plaat1*^{-/-} mice. TLCL, as a predominant CL species, is typically the most abundant species in the heart (1, 176, 177). However, the observed deficiency of PLAAT1 was correlated with a significantly lower relative amount of the acyl species that comprises TLCL, where it constitutes less than 7% of total CL fatty acyl species by mass percentage in both sexes. This was in turn correlated with an elevated

proportion of AA and DHA, by approximately 18-20-fold and 14-fold, respectively. This shift is functionally important because it renders the CL more susceptible to ROS and other apoptotic stimuli, which can have negative effects on tissue health (14, 51). The effect is strongly reminiscent of the effects resulting from increased CL remodeling by the ALCAT1 enzyme, which results in decreased TLCL and increased AA and DHA (17). Given that both ALCAT1 and PLAAT1 share localization to the endoplasmic reticulum (ER) and mitochondria-associated membranes (MAM) (165), there may be underlying connections between these proteins. The resemblance between the observed effects due to PLAAT1 deficiency and the characteristic features of ALCAT1 remodeling suggests a potential interplay between these two enzymes. The results may suggest a novel role for PLAAT1 in inhibiting the expression of ALCAT1 in heart tissue, which may be lost when PLAAT1 is deficient. Alternately, ALCAT1 activity may undergo a compensatory increase with PLAAT1 activity loss.

In brain tissue of *Plaat1*^{-/-} mice, the changes are particularly marked in omega-6 acylated CL species, predominantly driven by the increase in 18:2n-6 species, which surged by 196% and 233% in male and female mice, respectively. This elevation drastically reshaped the relative composition of CL, diminishing the prevalence of previously dominant species such as 18:1 and 18:0 acylated species and reducing the amounts of AA (20:4n-6) and DHA (22:6n-3), which in *Wt* mice are unique in their prevalence to brain tissue. This led to linoleate becoming the most predominant species, constituting 47% and 40% of total brain CL in male and female mice, respectively, a significant shift from previously making up less than 10%. This alteration might have profound implications for brain function and cellular integrity, but the exact effects remain to be fully elucidated. Overall, total CL concentration is higher in the brain tissue of *Plaat1*^{-/-}

female mice, and though brain CL in the male mice also appears to be higher, these differences there do not reach significance.

Analysis of gastrocnemius muscle reveals that this tissue had the highest relative difference between genotypes in total CL concentration, with 185% and 365% higher levels of total CL concentration in male and female *Plaat1*^{-/-} mice, respectively. This elevation in total CL can be further broken into significantly higher quantities of the MUFA, SFA, and N-6 species, in order of abundance. In relative terms, the most significant changes are seen in the 18:1n-9 species, where a near 2-fold higher mass percentage within isolated CL was observed in both sexes, and in the 18-2n:6 species, where relative content is 26-28% lower.

The observation of varying CL species composition amongst the analyzed tissues of *Wt* mice, with an even more complex pattern in PLAAT1 deficient mice, raises intriguing questions regarding the underlying mechanisms that govern these differences. Notably, while the heart and gastrocnemius muscle typically demonstrate a certain similarity in CL composition, the alterations in *Plaat1*^{-/-} mice trended more closely between the brain and gastrocnemius muscle. This apparent discrepancy highlights a more complex regulatory environment that may be influenced by tissue-specific factors.

Chapter 5: Thesis Study III - Gross Morphology and Survival Analysis of *Plaat1*^{-/-} Mice

Introduction and Study Rationale

In Study 1 of this thesis, I demonstrated that PLAAT1 has PC:MLCL transacylase activity *in vitro*. In Study 2, I demonstrated that deficiency in this enzyme profoundly alters the CL composition of brain, heart, and skeletal muscle. Interestingly, loss of PLAAT1 did not uniformly *decrease* CL levels in all tissues tested, but rather resulted in significant *increases* in CL total content in brain and skeletal muscle. This indicates important complexity in the role of PLAAT1 in CL regulation. Study 2 was designed to evaluate CL levels only, and from that work it is not possible to determine the source of the changes in CL levels. Although extensive further studies will be needed to investigate all of the potential contributors, and therefore fall outside of the scope of this thesis, potential sources of the variation can be postulated. For example, the decline in cardiac total CL levels in PLAAT1 deficient mice could indicate that this enzyme is directly involved in CL remodeling in this tissue, and that loss of this activity was not compensated by increased activity from other CL remodeling enzymes, while increased compensatory activity in brain and skeletal muscle could explain the elevated CL levels in those tissues. Alternatively, tissue-specific differences in the regulation of NAE species and levels by PLAAT1 could result in tissue-specific differences in CL metabolism when this enzyme is deleted. Regardless, the sizeable differences in tissue CL levels strongly suggest that phenotypic alterations would manifest in our *Plaat1*^{-/-} mice.

Objectives and Hypothesis:

1. Objective: To determine if there are differences in growth patterns, tissue weights, and food intakes between *Plaat1*^{-/-} mice and *Wt* controls.

Hypotheses: *Plaat1*^{-/-} mice will exhibit lower total body weights at all ages. The heart is expected to increase in weight due to cardiac hypertrophy, and skeletal muscles to decrease due to atrophy. Liver weight is also expected to decrease. Food intakes are expected to be decreased due to lower N- transacylase activity that may diminish the production of NAEs that are active in satiety regulation.

2. Objective: To determine viability of male and female *Plaat1*^{-/-} mice by determining sex and genotypes of mice at birth.

Hypotheses: Genotypic and phenotypic ratios of the *Plaat1*^{-/-} mice will follow the expected 1:2:1 genotypic ratio and 3:1 phenotypic ratio.

3. Objective: To compare survival and natural life span of *Plaat1*^{-/-} mice with *Wt* controls as well as perform a qualitative analysis observing causes of death in both groups.

Hypotheses: *Plaat1*^{-/-} mice will display shorter life spans due to CL-related mitochondrial dysfunction in cardiac tissue.

Study Design:

Animals:

Plaat1^{-/-} mice were generated as described in thesis study 2. The animals used for this study were male and female *Plaat1*^{-/-} mice and *Wt* controls. Animal procedures were performed with the approval of the University of Waterloo Animal Care Committee (AUPP#43325, approved 03 June 2021, renewed June 04, 2023) and comply with guidelines of the Canadian Council on Animal Care. Mice were ear notched at 4 weeks of age and genotyped to determine the total number of *Plaat1*^{-/-} and *Wt* male and female mice. A growth curve was generated by measuring body weight from 4 until 20 weeks of age. At week 18 mice were single housed for acclimatization and from week 19-20, average food intake was measured daily over a 7-day period to determine average daily food intake. Food intake was then normalized to mouse body weight. At 20 weeks of age, this subset of mice was sacrificed, and organs and tissues from euthanized mice were excised, weighed, and snap-frozen in liquid nitrogen and stored at - 80°C. A second subset of mice chosen for the evaluation of longevity were not subjected to other physiological evaluations. These mice were permitted to live their natural lifespans either until spontaneous death occurred, or until humane endpoints pre-defined in our approved animal use protocols necessitated euthanasia. Age at death was recorded as their survival endpoint.

Statistical Analysis

Growth curve comparisons between *Wt* and *Plaat1*^{-/-} were conducted using a repeated measures ANOVA to detect interactions between genotype and age as main factors. Tissue weight comparisons (normalized to bw) and average 24-hr food intake between *Wt* and *Plaat1*^{-/-} mice were conducted using an unpaired Student's t-test to determine differences between genotypes. The observed distribution of offspring genotypes produced from crosses of *Plaat1*^{-/+} females with

Plaat1^{-/+} males was compared to expected genotypic ratios by chi-square test. Survival of mice is depicted using Kaplan–Meier survival distributions, and significance was analyzed by the log-rank Mantel-Cox test. When a *Plaat1*^{-/-} mouse reached the humane lifespan endpoint before a *Wt* control, a *Wt* control was also entered as censored data for survival analysis.

Results:

PLAAT1 deficiency does not alter body weights but results in sex-specific differences in organ weights and food intakes

Body weights of mice were measured weekly from 4-weeks of age until sacrifice at 20-weeks of age. Differences in growth were not observed between sex-matched *Wt* and *Plaat1*^{-/-} mice (Fig. 22A, B). At 20 weeks of age, these mice were euthanized and their organs and tissues were weighed. After normalizing to mouse bodyweight, we found that livers from male *Plaat1*^{-/-} mice were 22.1% smaller (*Wt*, 0.0435 ± 0.0024 g/ g bw versus *Plaat1*^{-/-}, 0.0339 ± 0.0013 g/ g bw, P=0.0039), kidneys were 15.2% smaller (*Wt*, 0.0118 ± 0.0007 g/ g bw versus *Plaat1*^{-/-}, 0.0100 ± 0.0006 g/ g bw, P=0.0259), hearts were 13.6% smaller (*Wt*, 0.0046 ± 0.0002 g/ g bw versus *Plaat1*^{-/-}, 0.0040 ± 0.0001 g/ g bw, P=0.0100), and soleus muscles were 27.6% smaller (*Wt*, 0.00063 ± 0.00006 g/ g bw versus *Plaat1*^{-/-}, 0.00045 ± 0.00003 g/ g bw, P=0.0191) (Fig. 23A). Differences between female *Wt* and *Plaat1*^{-/-} mice were not observed, although differences in kidney (P=0.0793) and soleus (P=0.0762) size did approach statistical significance when comparing the two genotypes (Fig. 24B).

From 19 to 20 weeks of age, mice were single housed and food intake was recorded daily to calculate average 24-hr food intake over a 7-day period. Male *Plaat1*^{-/-} mice had 14.8% lower total 24-hr food intakes (*Wt*, 3.188 ± 0.1296 g versus *Plaat1*^{-/-}, 2.716 ± 0.0731 g, P=0.0131) (Fig. 24A), and 17.5% lower 24-hr food intakes when values were expressed normalized to mouse bodyweights (*Wt*, 0.0989 ± 0.0065 g/ g bw versus *Plaat1*^{-/-}, 0.0815 ± 0.0033 g/ g bw, P=0.0444) (Fig. 24B). Age-matched female mice, on the other hand, did not display a difference between food intakes when genotypes were compared (Fig. 24C, D).

Proportions of offspring genotypes were not significantly different from the expected 1:2:1 genotypic ratio and 3:1 phenotypic ratio.

To produce *Plaat*^{1-/-} mice, male and female *Plaat*^{1+/-} mice were bred together. In total, 296 mice were produced and genotyped (Table 2). In total, male and female *Plaat*^{1-/-} mice, and male *Plaat*^{1+/-} mice, made up 15.5%, 14.5% and 28.1%, of the offspring genotypes, respectively, all of which are larger proportions than the expected 1:2:1 genotypic ratio. Female *Plaat*^{1+/-} mice, as well as male and female *Wt* mice, made up 19.9%, 11.5% and 10.5%, of the offspring genotypes, respectively, all of which are smaller proportions than the expected 1:2:1 genotypic ratio. However, Chi-squared analysis indicated that discrepancies from the expected genotypic ratios are not statistically significant (Table 2). When comparing to the 3:1 phenotypic, *Plaat*^{1+/-} and *Wt* mice (possessing the dominant *Wt* trait) made up 39.5% and 30.4% of the male and female offspring genotypes, respectively (Table 3). On the other hand, *Plaat*^{1-/-} mice (possessing the recessive *Plaat*^{1-/-} trait) made up 15.6% and 14.5% of the male and female offspring genotypes, respectively (Table 3). Here, we find that the male mice, as well as female *Plaat*^{1-/-} mice, constituted larger proportions than the expected 3:1 phenotypic ratio, while female *Plaat*^{1+/-} and *Wt* were over 7% lower than their expected proportions (Table 3). The deviations in the phenotypic ratios approached but did not reach significant threshold (P=0.0586).

Plaat^{1-/-} mice experienced premature mortality

The subset of mice chosen for evaluation of longevity were not used in other experiments and lived until either spontaneous death occurred, or until they were euthanized at the end of their humane lifespan limits, as predetermined in our approved animal use protocols. When comparing survival between male *Plaat*^{1-/-} and *Wt* mice, using Kaplan–Meier survival curves, log-rank test

analysis determined that the lifespan of male *Plaat1*^{-/-} mice was significantly shorter (P=0.0455) (Fig. 4A). The median lifespan for male *Plaat1*^{-/-} mice was 26 months, in contrast to their *Wt* counterparts that had a median lifespan of 32 months (Fig. 25A). Log-rank test analysis comparing survival of female *Plaat1*^{-/-} and *Wt* mice did not find statistically significant differences in survival, despite approaching statistical significance (P=0.0522) (Fig. 25B). The median lifespan for female *Plaat1*^{-/-} mice was 25.5 months, in contrast to their *Wt* counterparts that had a median lifespan of 31.5 months (Fig. 25B).

The humane lifespan limits of the mice were established by veterinarians in our animal care facility, who determined whether a specific disease or condition qualified the mouse for euthanasia. Among these conditions, dermatitis was cited as a rationale for euthanasia in 5 male *Plaat1*^{-/-} mice (Table 4). Notably, this condition was observed almost exclusively in males and exclusively in *Plaat1*^{-/-} mice, appearing just one other time in a female *Plaat1*^{-/-} mouse (Table 4). Similarly, eye ulcers were uniquely present only in female *Plaat1*^{-/-} mice (Table 4). In *Wt* mice, one male was euthanized due to the presence of a tumor, and one female was euthanized due to the presence of ascites. All other deaths in *Wt* mice were spontaneous, with mice found dead in their cages during daily monitoring.

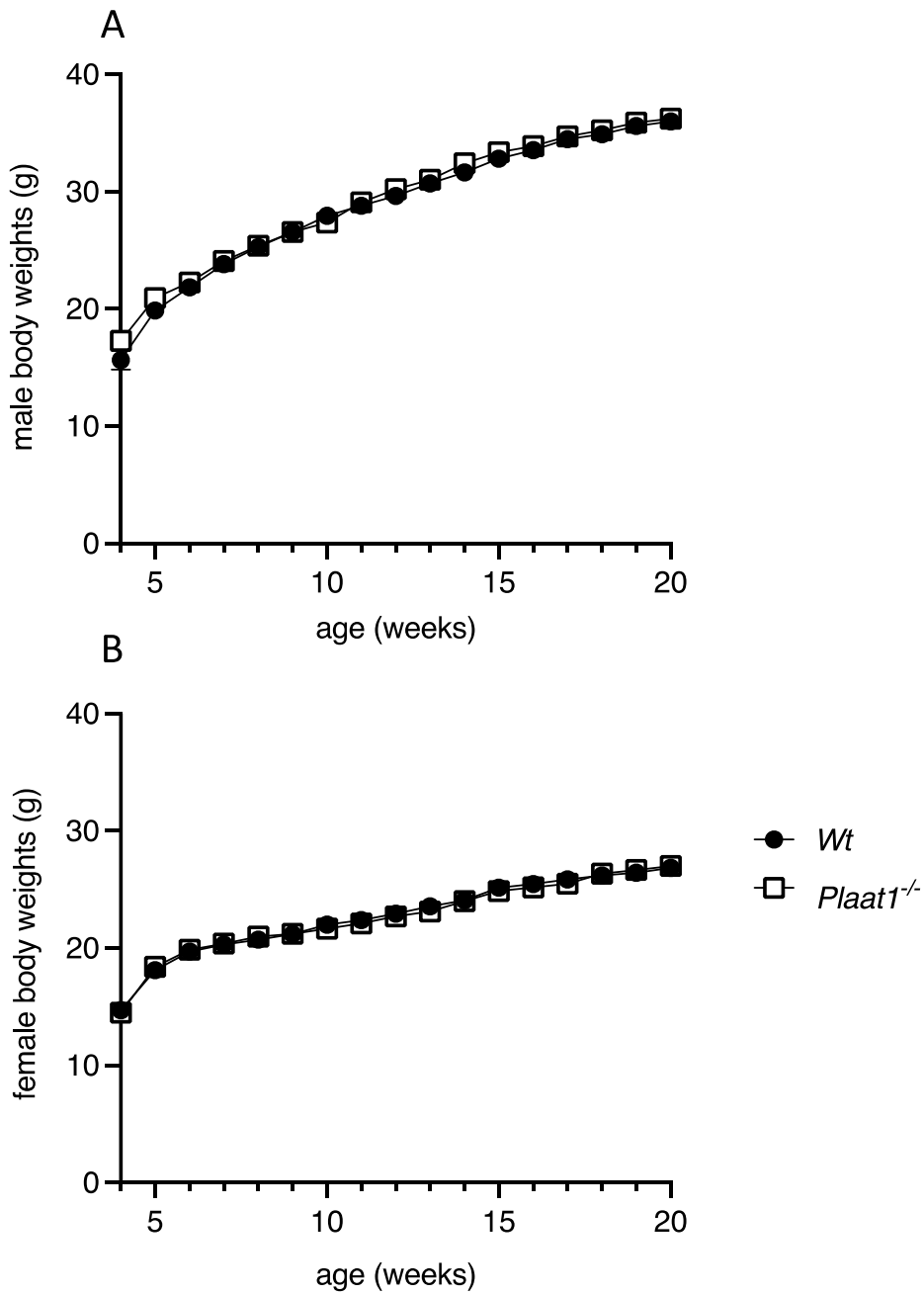


Figure 22: Female and male body weights from 4 to 20 weeks of age. Male (A) and female (B) mice were weighed and plotted over time to observe growth patterns. Data are means \pm SEM. n=5.

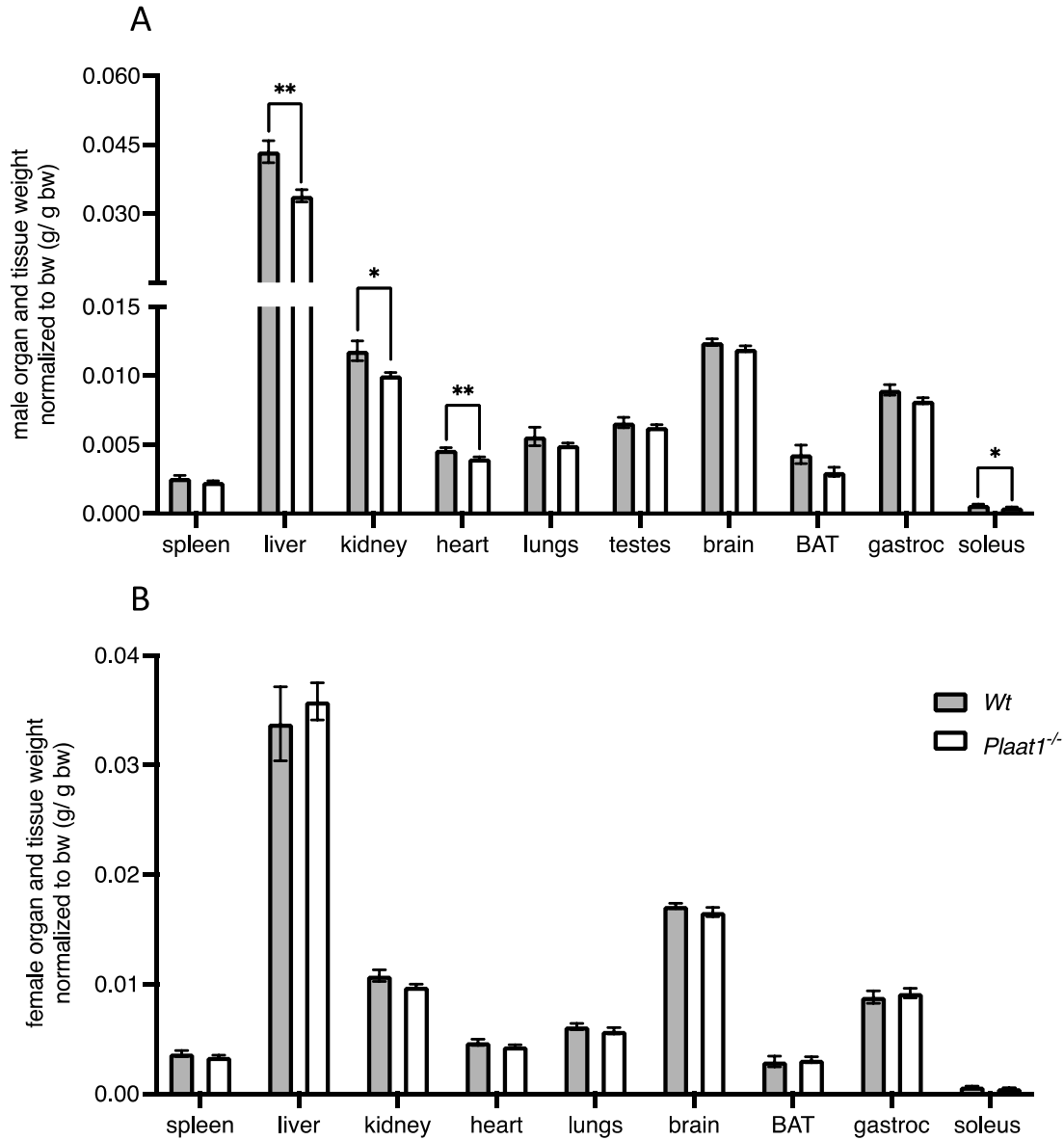


Figure 23: Organ and tissue weights in male and female mice. Male (A) and female (B) organ and tissue weights were recorded at 20 weeks of age and are expressed relative to body weight (bw). Data are means \pm SEM. * $P < 0.05$, ** $P < 0.01$. $n = 6-8$.

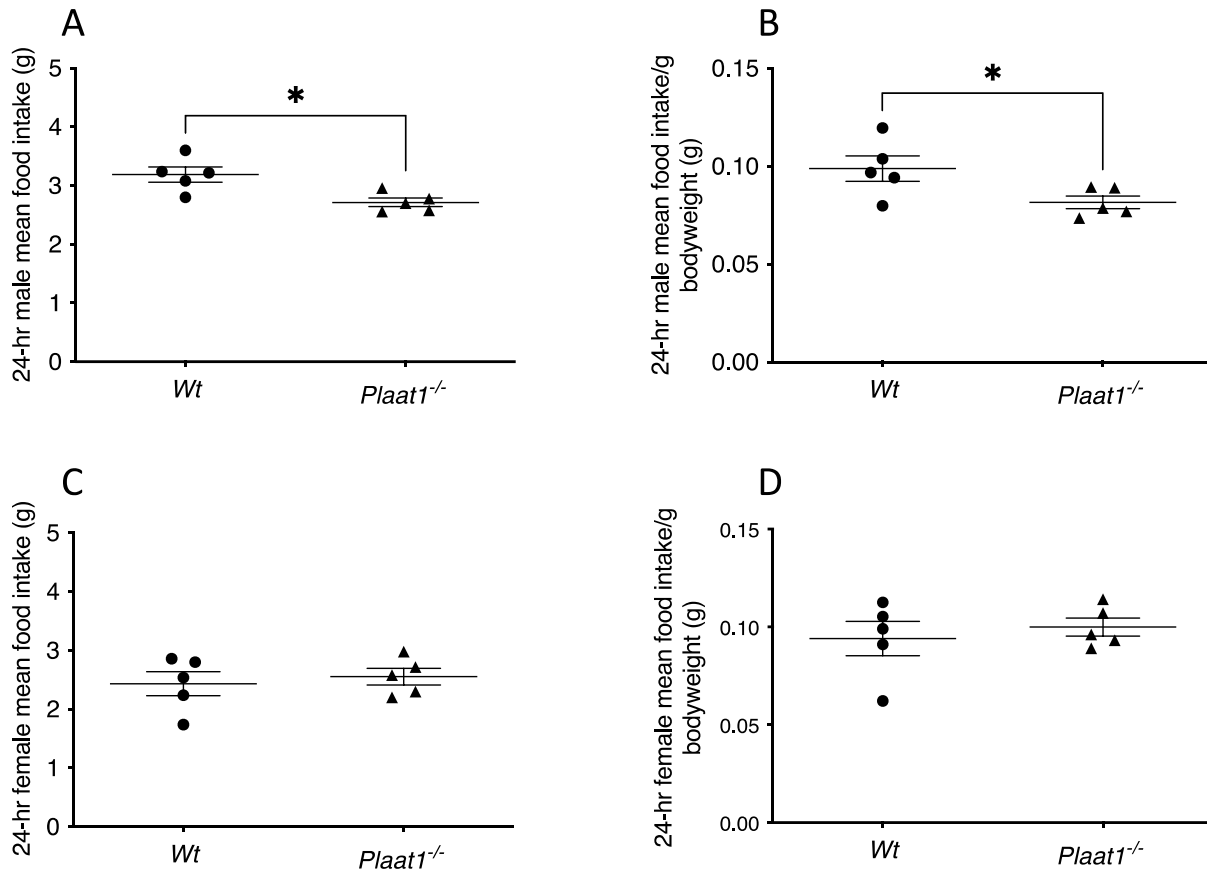


Figure 24: Daily measures of food intakes. Food intakes from male (A, B) and female (C, D) mice were recorded over a 7-day period. Measures within sexes were recorded as mean daily (24 h) food intakes (A, C) or as food intakes normalized to body weights (B, D). Data are means \pm SEM. * $P < 0.05$. $n = 5$.

Table 2. Ratio of genotypes at the time of weaning.

Sex	Genotype	Expected Number of Mice	Observed Number of Mice
Male	<i>Wt</i>	37 (12.5%)	34 (11.5%)
	<i>Het</i>	74 (25%)	83 (28.1%)
	<i>Plaat1^{-/-}</i>	37 (12.5%)	46 (15.5%)
Female	<i>Wt</i>	37 (12.5%)	31 (10.5%)
	<i>Het</i>	74 (25%)	59 (19.9%)
	<i>Plaat1^{-/-}</i>	37 (12.5%)	43 (14.5%)

Genotypic ratio of offspring at weaning resulting from heterozygous (*Plaat1^{-/+}*) male and female breeding. Total numbers of expected and observed mice are shown with expected and observed percentages indicated in parentheses. The expected number of mice was calculated according to the total number of mice sexed and was based on the expected 1:2:1 genotypic ratio.

Table 3. Phenotypic ratio at the time of weaning.

Sex	Genotype	Expected Number of Mice	Observed Number of Mice
Male	<i>Wt & Het</i>	111 (37.5%)	117 (39.5%)
	<i>Plaat1^{-/-}</i>	37 (12.5%)	46 (15.6%)
Female	<i>Wt & Het</i>	111 (37.5%)	90 (30.4%)
	<i>Plaat1^{-/-}</i>	37 (12.5%)	43 (14.5%)

Phenotypic ratio of offspring at weaning resulting from heterozygous (*Plaat1^{-/+}*) male and female breeding. Total numbers of expected and observed mice are shown with expected and observed percentages indicated in parentheses. The expected number of mice was calculated according to the total number of mice sexed and was based on the expected 3:1 phenotypic ratio.

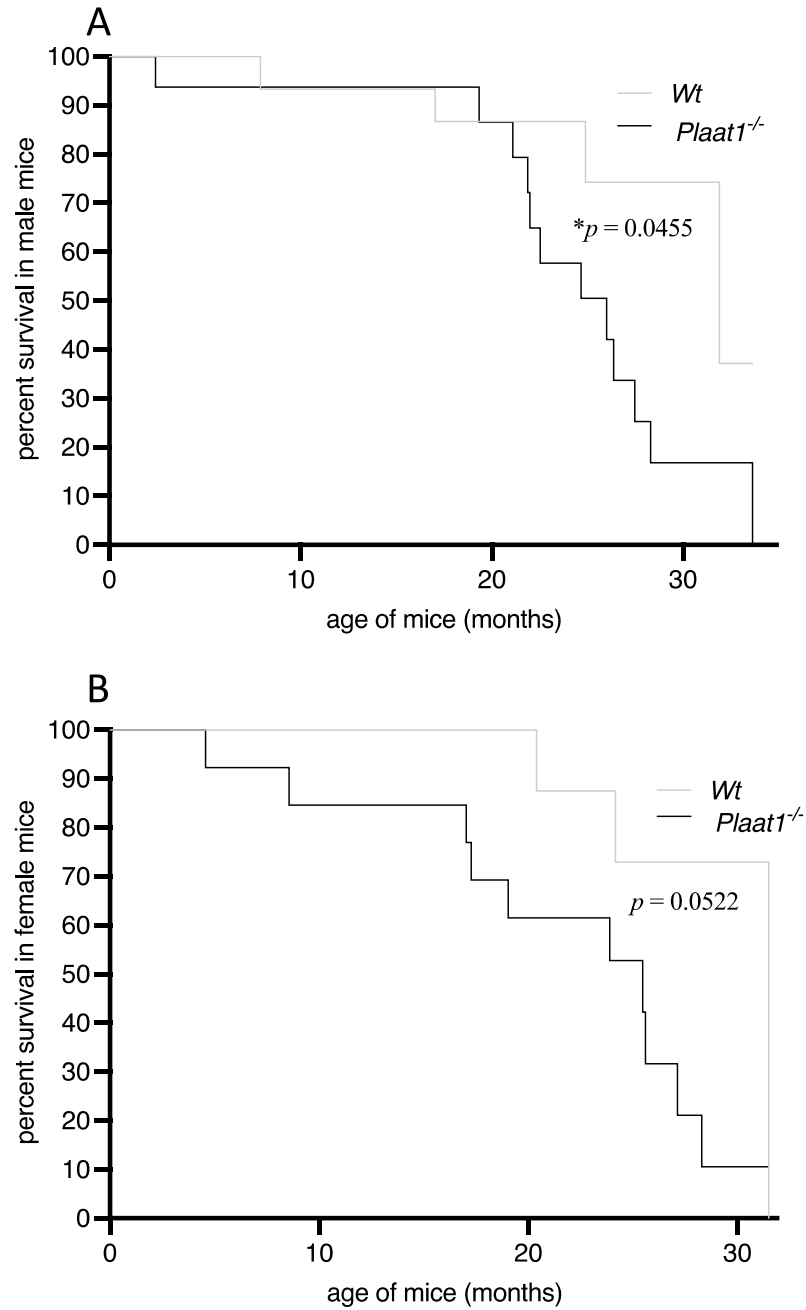


Figure 25: Kaplan–Meier survival curves. Age at spontaneous death or ethically required euthanasia was recorded, from weaning until 32 months of age. Differences between genotypes were assessed by log-rank test for male (A), and female (B) mice. * $P < 0.05$. $n = 3-12$.

Table 4: Cause of death for male and female *Plaat1*^{-/-} and *Wt* mice

	FD	Tumor	Eye ulcer	Head tilt	Dermatitis	Ascites
Male <i>Wt</i>	3	1	-	-	-	-
Male <i>Plaat1</i> ^{-/-}	6	-	-	-	5	1
Female <i>Wt</i>	2	-	-	-	-	1
Female <i>Plaat1</i> ^{-/-}	3	1	4	1	1	-

Cause of death or euthanasia was recorded for mice at the end of their humane lifespan limits.

Discussion:

This study aimed to characterize phenotypic differences caused by PLAAT1 deficiency, including differences in body, organ and tissue weights, food intakes, offspring genotype proportions, adult survival rates, differences in survival rates, and causes of death. This study found that PLAAT1 deficiency resulted in some notable morphological differences in male mice, while also highlighting that male and female *Plaat1*^{-/-} mice may have a predisposition for certain diseases that limit longevity.

When considering bodyweight growth for a 16-week period, no differences were observed between *Plaat1*^{-/-} or *Wt* mice for either sex. This is consistent with the findings of Rahman and colleagues, who found that male *Plaat1*^{-/-} and *Wt* mice fed a standard diet displayed no differences in bodyweights between 0 and 12 weeks of age (155). However, we did find that male *Plaat1*^{-/-} mice had smaller liver, kidney, heart, and soleus muscle masses. Rahman *et al.* similarly reported that skeletal muscle weights were lower in *Plaat1*^{-/-} mice fed a standard diet, but they did not observe lower liver weights between genotypes until mice were challenged a high-fat diet. In that work the researchers reported that in liver, PLAAT1 acts primarily as a PLA1/2, resulting in increased levels of PC and decreased levels of LPC with *Plaat1* gene deletion (155). The researchers concluded that PLAAT1 deficiency reduced hepatic lipid accumulation and given that LPC is a marker of non-alcoholic fatty liver they also concluded that PLAAT1 loss resulted in the induction of hepatocyte lipoapoptosis (155, 178, 179). The significant effect that PLAAT1 deficiency had on the liver as reported in the paper by Rahman and colleagues is intriguing, given that our previous work has found that the mRNA expression of PLAAT1 is lowest in this tissue (37), and suggests that additional tissue-specific studies in *Plaat1*^{-/-} mice are warranted.

The magnitude of reduction in weight of the soleus muscle from male *Plaat1*^{-/-} mice is similar to the reduction seen in *Taz-KO* mice (163). Tomczewski and colleagues found that tafazzin total deficiency resulted in an approximate 25% decrease in soleus weight, similar to the 27.6% decrease that we observed in male *Plaat1*^{-/-} mice. We also found that male *Plaat1*^{-/-} mice display 13.6% smaller hearts, contrary to my initial hypothesis that was predicated on a common trait of *Taz-KO* mouse models, which is that cardiomyopathy and cardiac fibrosis often lead to heart enlargement (162, 180). The reason for these reductions, will require further exploration, and future work should examine the microscopic morphology of these tissues using histopathological techniques. Furthermore, analysis of the function of tissue mitochondria, and additional molecular mechanisms examining the metabolic function and lipid composition of these tissues should be performed.

Unlike *Taz-KO* mice (163), *Plaat1*^{-/-} mice in this study had significantly lower 24-hr food intake when compared to their *Wt* counterparts, both as a total average measure, and after normalizing food intake to mouse bodyweight. A possible explanation for this could be related to PLAAT1's function as a N- transacylase enzyme (39). PLAAT1 deficiency could result in reduced NAPE and subsequently reduced NAE production and altered NAE profiles and signaling. AEA, an endocannabinoid and a well-studied NAE, has been shown to be an appetite stimulant (132, 181), and thus a decrease in its production due to diminished N-transacylase activity could result in appetite suppression and reduced food intake. However, lower food intakes did not result in lower body weights. Thus, lower food intakes could reflect better metabolic efficiency, necessitating lower levels of food intakes, or could also reflect lower energy expenditures (also necessitating reduced food intakes). Animal activity levels are addressed in Chapter 6.

A 1:2:1 genotypic ratio and 3:1 phenotypic ratio are the relative fractions of genotypes and phenotypes, respectively, among offspring following as a result of mating two heterozygotes, where each parent possesses one dominant allele and one recessive allele (182). The genotypic and phenotypic ratios differ, because Mendel's first law of inheritance, the Law of Dominance, states that in a heterozygote, one trait will conceal the presence of another trait for the same characteristic, because when two different alleles for a particular trait present together, only the dominant allele expresses, by masking the expression of the recessive allele (182). The recessive allele in this case being deletion of Exon 3 that produces *Plaat1* knockout. The phenotype in question in our case would be the successful embryogenesis, birth, and survival until weaning at 4-weeks of age, the age at which the mice are genotyped. C57BL mice have a reported 1:1 sex ratio, indicating an absence of selective mortality in embryos of either sex during embryogenesis (183). Additionally, no prior research has indicated a role of CL, PLAAT1, or NAE's in altering the 1:1 sex chromosome ratio in ejaculated spermatozoa. Furthermore, only one other study, along with this thesis, has generated *Plaat1* knockout mice, which did not report deviations from the expected 1:2:1 genotypic ratio or 3:1 phenotypic ratio when using this model. Due to these reasons, I had initially hypothesized that the offspring genotype proportions would not deviate from the expected 1:2:1 genotypic ratio or 3:1 phenotypic ratio. Our results supported this hypothesis, as the deviations from the expected genotypic ratios observed in the offspring were not reported to be different when using Chi-squared analysis. This is in line with the work of Rahman *et al*, that also reported *Plaat1*^{-/-} mice being born with the expected genotypic frequency (155). In regard to deviations from the expected phenotypic ratios, the differences found were on the cusp of statistical significance, suggesting that this analysis was underpowered and that a difference would be present with a larger sample size.

Kaplan–Meier survival curves until 32 months were generated for a subset of mice living until their humane survival endpoints within that period. It was found that within this subset, male and female *Plaat1*^{-/-} mice had 6- and 5-month shorter median lifespan, respectively, when compared to *Wt* controls. Survival between the male mice was found to be significantly different between genotypes, while differences in survival between female mice bordered on statistical significance. Analysis of leading causes of death or prescribed euthanasia for both male and female *Plaat1*^{-/-} mice resulted in interesting initial findings. For male *Plaat1*^{-/-} mice, dermatitis was the most frequent cause for euthanasia, while for female *Plaat1*^{-/-} mice, eye ulcers were the primary cause, with only one female mouse experiencing dermatitis, both of which indicating a dysfunction of the immune response. As discussed in Chapter 2, oxidized CL serves a critical role in immune responses as well as autophagy (54), such as the activation of toll-like receptor 4 (TLR4) during sepsis, promoting an inflammatory response to the bacterial infection (55). Thus an impaired autophagic process due to changes in CL content in *Plaat1*^{-/-} mice could be correlated with the observed disease conditions.

A common theme among these findings is the almost exclusively male specific outcomes when characterizing the impact of PLAAT1 deficiency in younger adult mice. Organ weights, food intake, and survival were all found to be statistically significantly different when comparing male *Wt* and *Plaat1*^{-/-} mice, while this was not the case for the female mice. In the case of survival, female *Plaat1*^{-/-} mice also exhibited earlier mortality by similar margins, suggesting that the loss of PLAAT1 can still present changes in female mice in time to affect longevity. Some other characteristics, such as reductions in kidney and soleus weight, did approach statistical significance for female *Plaat1*^{-/-} mice, suggesting that experiments may have been underpowered and that a larger sample size should be examined.

Chapter 6: Thesis Study IV - Phenotypic Characterization of *Plaat1*^{-/-} Mice

Introduction and study rationale:

Ablation of the *Taz* gene in mice is well studied and has been shown to result in profound alterations in phenotype. For instance, a recent publication by our research group reported that *Taz-KO* mice weigh almost 30% less than their *Wt* littermates at 3 months of age, and can run only half as far before exhausting (163). A TAZKD mouse model has also demonstrated diminished exercise capacity, associated with impaired oxygen consumption (160). Therefore, it is likely that mice with alterations in other genes affecting CL remodeling would also have altered phenotypic characteristics and responses to exertion.

Study 1 of this thesis demonstrates that PLAAT1 functions directly in CL remodeling, while study 2 displayed stark changes in both total CL content as well as compositional changes within CL in the brain, heart, skeletal muscle tissues derived from *Plaat1*^{-/-} mice. Finally, in study 3 we found that PLAAT1 deficiency is correlated with reduced weight of the liver, heart, kidney and soleus muscle, decreased food intake, as well as lower survival rates when compared to *Wt* mice. Thus, loss of PLAAT1 is expected to directly affect physiological functions related to mitochondrial activity and energy metabolism. Additionally, since PLAAT1 has an established impact on NAE synthesis, there is reason to believe that *Plaat1* gene ablation could also alter metabolic and behavioral outcomes by modulating levels of these bioactive signaling molecules. There are too many possible alterations to comprehensively review in this work, but some examples related specifically to exercise and metabolism include: i) Alterations in AEA levels can affect anxiety in mice (184) and may influence pain control within the central nervous system by activating CB1 cannabinoid receptors, which could alter perceived exertion levels in exercise (185); ii) AEA also displays vasodilatory effects through the endothelial CB1 receptor,

and could impact blood flow to muscles, thereby affecting exercise performance (186); iii) Like AEA, OEA is involved in pain sensation, and alterations in its synthesis could modify pain perception during and after exercise, affecting the ability to perform strenuous activities and recover from intense physical exertion (187); iv) Decreased AEA and OEA levels in mouse hippocampus have been associated with increased anxiety-like behaviours, which can affect behavioural and metabolic measures both during exercise and at rest (188); v) PEA is recognized for anti-inflammatory effects, acting through the peroxisome proliferator-activated receptor alpha (PPAR- α) (189), and therefore could influence inflammatory responses to exercise and subsequent recovery times and muscle repair.

Considering the multifaceted connections between PLAAT1, CL, NAEs, and various physiological functions, there is a clear rationale for exploring effects of PLAAT1 deficiency in an animal model. I therefore conducted an initial phenotypic characterization of male and female *Plaat1* deficiency in mice, including measures of behavior, metabolism, and exercise capacity.

Objectives and Hypothesis:

1. Objective 1: To determine if *Plaat1*^{-/-} mice have alterations in metabolic measures relative to *Wt* controls, including oxygen utilization, carbon dioxide production, RER, and energy expenditure.

Hypotheses: *Plaat1*^{-/-} mice are predicted to have increased oxygen consumption rates and carbon dioxide production, with an elevated RER indicating greater dependence on glycolysis. Increased total energy expenditure is also predicted due to an expected increased dissipation of the proton gradient due to altered CL content.

2. Objective 2: To determine if *Plaat1*^{-/-} mice exhibit altered locomotor and ambulatory activity, and rearing behaviour.

Hypotheses: Changes in N-acylethanolamide synthesis in the brains of *Plaat1*^{-/-} mice could affect behaviour, which is expected to manifest as increased anxiety-like behaviour and culminate as increased rearing activity. Aberrant CL remodelling is expected to influence energy metabolism resulting in decreased voluntary locomotor and ambulatory movements.

3. Objective 3: To determine if *Plaat1*^{-/-} mice exhibit altered exercise capacity as well as exercise recovery when compared to *Wt* controls.

Hypotheses: Impairments in mitochondrial function due to altered CL remodelling are expected to impair exercise tolerance, leading to reduced exercise capacity in *Plaat1*^{-/-} mice. Furthermore, *Plaat1*^{-/-} mice are also expected to exhibit poorer recovery, resulting in a greater reduction in distance and maximum speed from the first to the second exercise capacity test.

Study Design

Animals:

Male and female *Plaat1*^{-/-} mice and their *Wt* controls were studied. At 8 – weeks of age, mice underwent assessment by indirect calorimetry, and at 12 – weeks of age performed the exercise capacity and exercise recovery test. Animal procedures were performed with the approval of the University of Waterloo Animal Care Committee (AUPP#43325, approved 03 June 2021, renewed June 04, 2023) and comply with guidelines of the Canadian Council on Animal Care.

Indirect Calorimetry:

The mice were subjected to indirect calorimetry using the Comprehensive Laboratory Animal Monitoring System (CLAMS, Columbus Instruments, Columbus, OH, USA). Prior to undergoing CLAMS testing, the mice were housed individually in standard cages for a duration of 24 h. Subsequently, the mice were positioned in individual, clear, and sealed chambers, equipped with free access to standard chow and water. Air was supplied to the chambers at a rate of 0.5 L/min, and the environment was maintained at a room temperature of 22–23°C, following a 12:12-hour light/dark cycle (with lights on from 07:00 to 19:00 and off from 19:00 to 07:00). Before initiating the CLAMS testing session, the gas sensors were adjusted using a standard gas mixture, comprising 20.5% oxygen, 0.5% carbon dioxide, with the balance made up of nitrogen. Throughout the investigation, the consumption of oxygen (VO_2 ; mL/Kg/h) and production of carbon dioxide (VCO_2 ; mL/Kg/h) within each chamber were measured at intervals of 28 minutes. Measure of VO_2 represents the volume of oxygen used to convert energy substrate into ATP. RER is the ratio of VCO_2 divided by VO_2 and can be used to estimate the fuel source for

energy production based on the difference in the number of oxygen molecules required for glucose versus fatty acids oxidation, where an RER of 0.7 indicates that fatty acids are the primary substrate, while an RER of 1.0 indicates that carbohydrates are the primary energy substrate. The total energy expenditure (TEE) was calculated using the Lusk equation $((3.815 + 1.232 \times \text{RER}) \times \text{VO}_2 \text{ (in liters)})$, with the TEE values adjusted according to total body weight (kg). In addition to these measures, the chambers were fitted with photobeams situated above the cage floor, designed to track the total locomotor activity through infrared beam breaks along three planes: x (locomotion), y (ambulation), and z (rearing). Activity was measured by calculating the sum of the X-axis movement counts associated with horizontal movement. The assessment of all these parameters (VO_2 , VCO_2 , RER, TEE, and total activity) was carried out over a span of 26 hours, where the initial 2-hour period was allocated to allow the mice to adapt to the new equipment, and the data collected during this acclimatization phase were excluded from the 24-hour analyses.

Treadmill Exercise Capacity and Exercise Recovery Test:

The exercise capacity of the mice was assessed through an incremental treadmill running test, adapted from a modified protocol previously used by our research group (163). Briefly, these sessions were conducted during the evening hours (17:00–21:00) in a darkened room illuminated by overhead red lighting. The testing utilized a five-lane motor-driven treadmill (Model LE8700, Panlab/Harvard Apparatus, Barcelona, Spain), set at a constant incline of 5° . The first three days were designated as an acclimatization period for the mice to become accustomed to the equipment. On the first and second days, the mice were positioned on the stationary treadmill for a period of 5 min, followed by a gradual introduction to running at

incremental speeds: 5 cm/s for 5 min, 10 cm/s for 2 min, and then 15 cm/s for a duration of 3 min. On the third day, the mice were again placed on the static treadmill for 5 min, and then their training progressed with running speeds of 5 cm/s for 3 min, 10 cm/s for 2 min, 15 cm/s for 2 min, and concluding with 20 cm/s for a 3-min interval. The fourth day was assigned as a rest day. The exercise capacity test was conducted on day 5. Mice were initially set on the stationary treadmill for 5 min, and then the exercise capacity evaluation commenced at a starting speed of 10 cm/s. This speed was subsequently increased by 3 cm/s every 2 min, continuing up to a maximum speed of 70 cm/s. The mice were encouraged to run until the point of exhaustion, identified as an inability to continue running for a consecutive 5-second period. Metrics such as the total running time until reaching exhaustion, the maximum speed achieved, and the overall distance covered were documented. For the exercise recovery analysis, mice were rested for 1 h from their initial cessation of exercise before repeating the exercise capacity test.

Statistical Analysis

Comparisons of VO_2 , VCO_2 , and TEE between *Wt* and *Plaat1^{-/-}* mice were conducted using an unpaired Student's t-test to determine differences between genotypes. Comparisons for the exercise exhaustion test was performed by 2-way ANOVA for an effect of genotype and an effect of distance and time travelled, as well as for maximum speed achieved. Following identification of significant effects, Bonferroni's multiple comparisons tests were used to identify significant differences in means within genotypes for tests 1 and 2, and significant differences between genotypes for a specific test.

Results:

Plaat1^{-/-} mice display diminished oxygen consumption, carbon dioxide production, and energy expenditure.

Indirect calorimetry was assessed in the CLAMS system, and metabolic values were analysed using mean values derived from the 28-min measuring intervals. Male *Plaat1^{-/-}* mice displayed reduced respiratory gas exchange when compared to *Wt* controls. When comparing oxygen consumption, male *Plaat1^{-/-}* mice displayed a 23.5% reduction in oxygen consumption over the 24-hour testing period (*Wt*, 4659 ± 347.6 ml/ kg/ h versus *Plaat1^{-/-}*, 3563 ± 304 ml/ kg/ hour, P=0.0390) (Fig. 26A, D). However, no significant difference was observed between groups during the light phase. Rather, the decreased VO₂ consumption is specifically derived from the dark phase, where PLAAT1 deficient mice consumed 24% less oxygen over the 12-hour period (*Wt*, 5086 ± 362 ml/ kg/ hour versus *Plaat1^{-/-}*, 3863 ± 316.2 ml/ kg/ hour, P=0.0291) (Fig. 26A, D). Similarly, a decrease in VCO₂ production was also noted in the male *Plaat1^{-/-}* mice, but this was in the 24-hour (*Wt*, 4491 ± 148.3 ml/ kg/ hour versus *Plaat1^{-/-}*, 3239 ± 297.8 ml/ kg/ hour, P=0.0037) (Fig. 26B, E), light (*Wt*, 3949 ± 133.9 ml/ kg/ hour versus *Plaat1^{-/-}*, 2927 ± 274.3 ml/ kg/ hour, P=0.0074) (Fig. 26B, E), and dark phases (*Wt*, 5044 ± 188 ml/ kg/ hour versus *Plaat1^{-/-}*, 3562 ± 325 ml/ kg/ hour, P=0.0027) (Fig. 26B, E), where decreases of 26.7%, 25.9%, and 29.4% were observed, respectively. RER was not different between PLAAT1 deficient and control mice, but TEE (calculated using gas exchange data collected in the metabolic chambers) was 23.6% lower in male *Plaat1^{-/-}*, over the 24-hour period (*Wt*, 23.02 ± 1.72 kcal/ kg/ hour versus *Plaat1^{-/-}*, 17.58 ± 1.52 kcal/ kg/ hour, P=0.0394) (Fig. 26C, F). Most of this reduction in TEE was derived from the 24.5% decrease in the dark phase (*Wt*, 25.31 ± 1.86 kcal/ kg/ hour versus *Plaat1^{-/-}*, 19.12 ± 1.59 kcal/ kg/ hour, P=0.0299), given that a significant difference was not observed during the light phase (Fig. 26C, F).

Female *Plaat1*^{-/-} mice displayed similarly clear phenotypic differences in their metabolic parameters. When comparing oxygen consumption, female *Plaat1*^{-/-} mice displayed a 21.7% reduction in oxygen consumption over the 24-hour testing period (*Wt*, 4959 ± 275.3 ml/ kg/ h versus *Plaat1*^{-/-}, 3862 ± 195.2 ml/ kg/ hour, P=0.0087) (Fig. 27A, D). However, unlike the male mice, the lower VO₂ consumption is derived from both the light and dark phase, where female PLAAT1 deficient mice consumed 25.1% less oxygen during the light phase (*Wt*, 4671 ± 312.2 ml/ kg/ hour versus *Plaat1*^{-/-}, 3500 ± 209.8 ml/ kg/ hour, P=0.0110), and 19% less oxygen during the dark phase (*Wt*, 5225 ± 250.4 ml/ kg/ hour versus *Plaat1*^{-/-}, 4232 ± 183.9 ml/ kg/ hour, P=0.0096) (Fig. 27A, D).

Carbon dioxide production was also lower in the female *Plaat1*^{-/-} mice, and this was noted in the 24-hour (*Wt*, 4359 ± 250.2 ml/ kg/ hour versus *Plaat1*^{-/-}, 3459 ± 200.6 ml/ kg/ hour, P=0.0186) (Fig. 27B, E), light (*Wt*, 4003 ± 246.3 ml/ kg/ hour versus *Plaat1*^{-/-}, 3083 ± 193.9 ml/ kg/ hour, P=0.0150) (Fig. 27B, E), and dark phases (*Wt*, 4686 ± 269.6 ml/ kg/ hour versus *Plaat1*^{-/-}, 3830 ± 212 ml/ kg/ hour, P=0.0317) (Fig. 27B, E), where decreases of 20.6%, 23%, and 18.3 % were observed, respectively. Analogous to the male mice, differences in RER were not observed, but the female *Plaat1*^{-/-} mice did display notably lower TEE, which was found to be 21.8% lower over the 24-hour period (*Wt*, 24.29 ± 1.348 kcal/ kg/ hour versus *Plaat1*^{-/-}, 18.99 ± 0.9796 kcal/ kg/ hour, P=0.0099) (Fig. 27C, F), 28% lower during the light phase (*Wt*, 22.80 ± 1.504 kcal/ kg/ hour versus *Plaat1*^{-/-}, 16.42 ± 0.8954 kcal/ kg/ hour, P=0.0072) (Fig. 27C, F), and 18.8% lower over the dark phase (*Wt*, 25.7 ± 1.278 kcal/ kg/ hour versus *Plaat1*^{-/-}, 20.87 ± 0.9480 kcal/ kg/ hour, P=0.0125) (Fig. 27C, F).

Male $Plaat1^{-/-}$ mice display decreased rearing activity.

CLAMS analysis can also measure various forms of mouse activity, including ambulation movements, such as when a mouse traverses a chamber, total locomotion movements, such as grooming and feeding in addition to ambulation, and rearing movements, which includes inspective and exploratory behaviour. Female $Plaat1^{-/-}$ mice did not demonstrate differences in locomotor, ambulatory, or rearing activities when compared to their Wt counterparts (Fig. 29). Male $Plaat1^{-/-}$ mice, however, demonstrated 44.2 % lower total rearing activity over a 24 h period (Wt , 5057 ± 879.2 versus $Plaat1^{-/-}$, 2823 ± 357.9 IR beam interruptions, $P=0.0328$) (Fig. 28A), which included a 41.4% reduction during the light phase (Wt , 689.6 ± 85.3 IR beam interruptions versus $Plaat1^{-/-}$, 403.7 ± 57.34 IR beam interruptions versus, $P=0.0186$) (Fig. 28C, F). It is worth noting that most of the reduced rearing activity displayed by male $Plaat1^{-/-}$ mice is derived from a reduction in the dark phase, which approached statistical significance ($P=0.0597$) (Fig. 28C, F). Rearing activity is an indication of inspective exploration of the mouse environment, and the reduction of this activity type in male $Plaat1^{-/-}$ mice suggests apathetic behaviour.

Male $Plaat1^{-/-}$ mice have lower exercise endurance during an initial exercise bout, but less of a loss of capacity for recurrent exercise after a 1-hr rest period.

Maximum exercise capacity was tested by having the mice run on a motorized treadmill until exhaustion, with the treadmill speed increasing at 2-minute intervals. For each test, the total distance travelled and time spent running were recorded, as well as the maximum speed achieved, which is a discrete variable when compared to the continuous measures of distance and time. Here, male $Plaat1^{-/-}$ mice exhibited a significantly lower exercise capacity, running 15.3% less total distance when compared to Wt controls (Wt , 789 ± 80.2 m versus $Plaat1^{-/-}$, 668.4 ± 21.4 m, $P=0.004$) (Fig. 30A), for 6.9% less time (Wt , 2233 ± 44.66 seconds versus $Plaat1^{-/-}$, $2078 \pm$

39.62 seconds, $P=0.0213$ (Fig. 30B), and achieving an 8.4% lower maximum speed (*Wt*, 64 ± 0.95 m/sec versus *Plaat1^{-/-}*, 58.6 ± 1.12 m/sec, $P=0.0061$) (Fig. 30C). These results indicate a reduced capacity for exercise. Exercise tolerance did not differ significantly in the female *Plaat1^{-/-}* mice.

Following a 1 h rest period, mice were tested on the treadmill again to determine if there were any differences in the ability of mice to recover after total exhaustion. Male *Wt* mice traveled a 14.6% shorter distance in their second test compared to their first test (first test, 789 ± 80.2 m versus second test, 673.8 ± 24.32 m, $P=0.0002$) (Fig. 30A). This decrease in performance for the *Wt* mice was also apparent in the 9.8% less time spent running (first test, 2233 ± 44.66 seconds versus second test, 2015 ± 45.07 seconds, $P=0.0014$) (Fig. 30B), as well as the 5.3% lower maximum speed achieved (first test, *Wt*, 64 ± 0.95 m/sec versus second test, 60.6 ± 1.17 m/sec, $P=0.0312$) (Fig. 30C). Conversely, while male *Plaat1^{-/-}* mice at their second test still ran a shorter distance, for less time, and achieved a lower maximum speed than *Wt* mice did during their first test, the performance measures of the male *Plaat1^{-/-}* mice at their first and second tests were not different, indicating no loss of exercise capacity with repeat testing in this paradigm (Fig. 30).

When comparing between the first and second exercise capacity tests, on average the male *Wt* mice travelled 113 m less, while the *Plaat1^{-/-}* mice travelled 28.2 m more during their second bout (*Wt*, -113 ± 20.69 m versus *Plaat1^{-/-}*, 28.2 ± 15.39 m, $P=0.0006$) (Fig. 30D). This trend was also observed for time spent running, where on average the male *Wt* mice ran for 172.7 seconds less, while the *Plaat1^{-/-}* mice ran for 77.4 seconds more during their second bout (*Wt*, -172.7 ± 38.8 seconds versus *Plaat1^{-/-}*, 77.4 ± 28.2 seconds, $P=0.0011$) (Fig. 30E), as well as for the maximum speed achieved, (*Wt*, -3.4 ± 1.03 m/sec versus *Plaat1^{-/-}*, 1.2 ± 1.53 m/sec, $P=0.0372$) (Fig. 30F).

When comparing baseline tests, the differences observed in the male mice were not present between female *Plaat1*^{-/-} and *Wt* mice. However, from the second tests after 1h of rest, we do see that female *Wt* mice traveled a 10.6% shorter distance compared to their first test (first test, 631 ± 28.3 m *versus* second test, 563.8 ± 52 m, P=0.0228) (Fig. 31A), and like the male mice, female *Plaat1*^{-/-} mice did not display a difference in distance travelled between their first and second tests (Fig. 31A). No differences were observed in the time spent running when comparing the first and second test for either genotype (Fig. 31B). In contrast to the male mice, the maximum speed achieved by the female *Plaat1*^{-/-} mice was 3% lower during the second test (first test, *Wt*, 59.8 ± 2.03 m/sec *versus* second test, 58 ± 2.51 m/sec, P=0.0386), while a reduction in maximum speed achieved was not observed in female *Wt* mice (Fig. 30C). Overall, differences were not observed between female *Plaat1*^{-/-} and *Wt* mice when comparing changes in their performance between test 1 and test 2 (Fig. 31D, E, F).

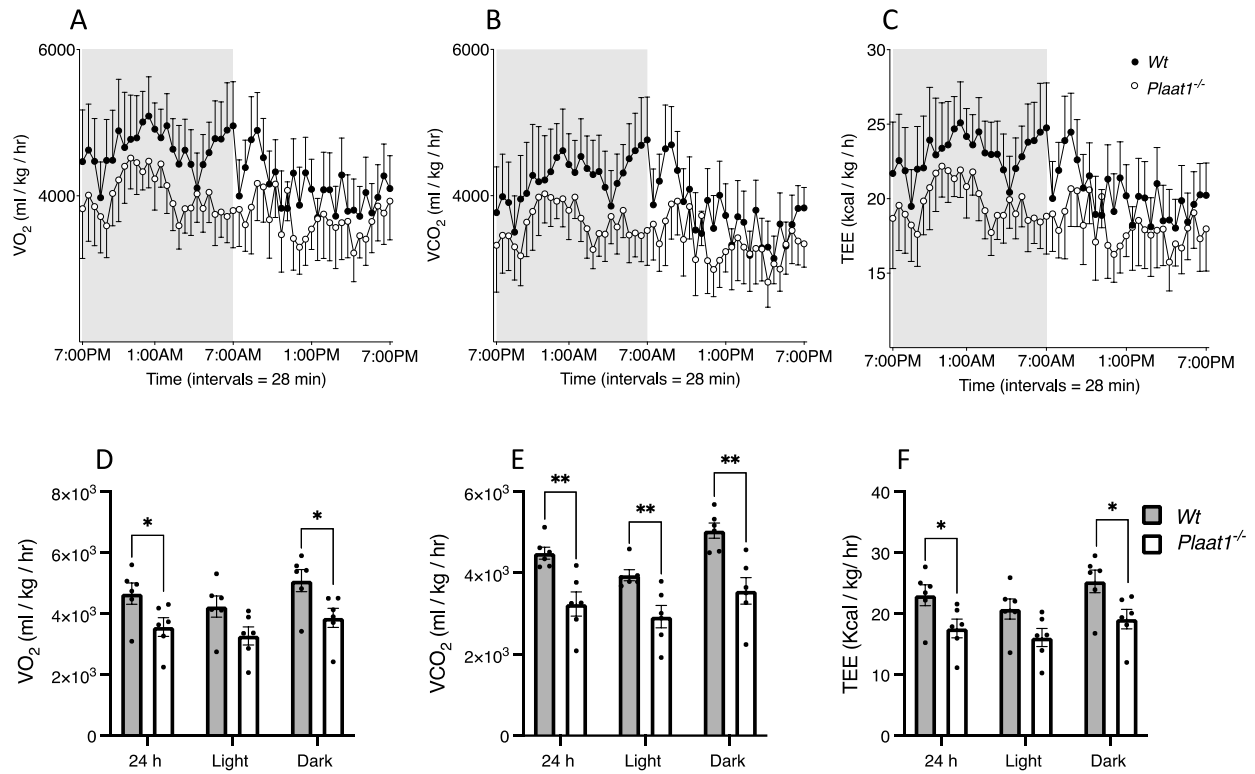


Figure 26: Respiration Measures in Male Mice Oxygen consumption and carbon dioxide production by male *Plaat1^{-/-}* and *Wt* mice. Representative plot of whole-body VO_2 (A), VCO_2 (B), and TEE (C) normalized to total body weight. Dark (denoted by shaded background) and light (denoted by unshaded background) cycles are shown. The bar graphs of the daily averages, in addition to averages by photoperiod, of VO_2 (D), VCO_2 (E), and TEE (F) are also shown. Data are means \pm SEM, n=6. *P<0.05, **P<0.01.

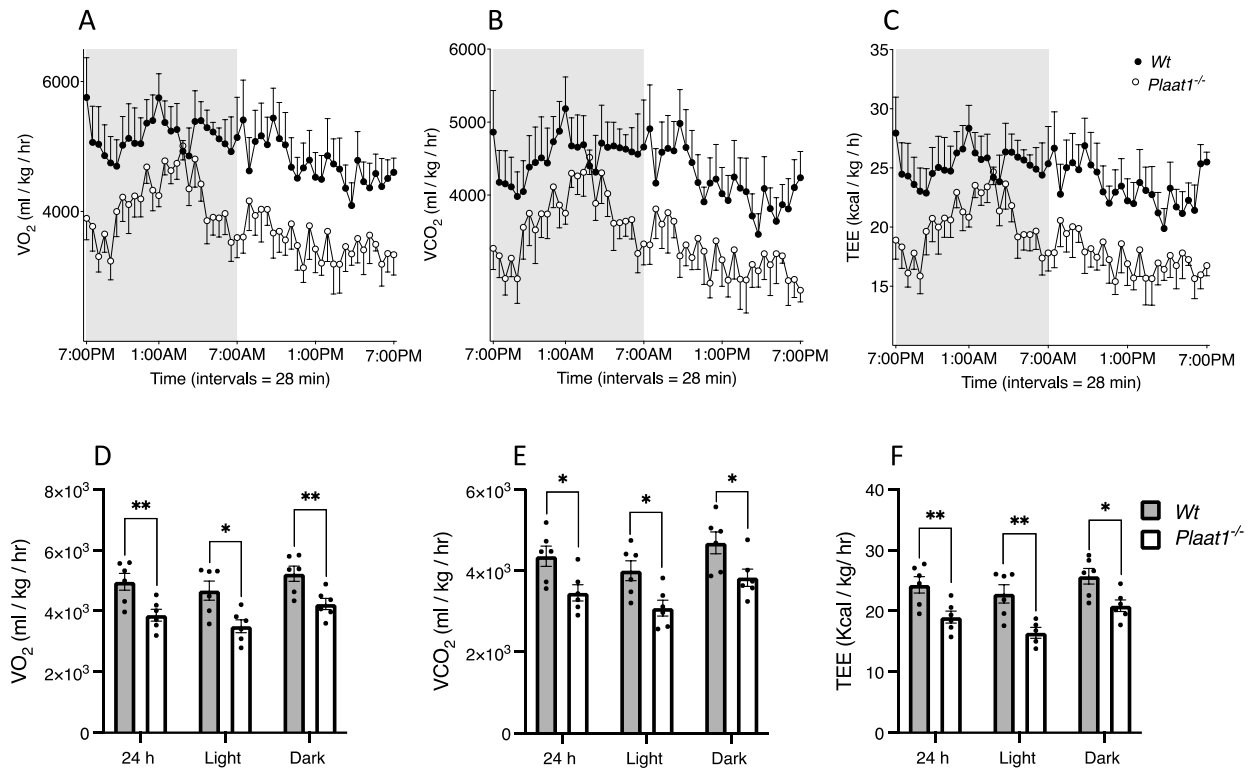


Figure 27: Respiration Measures in Female Mice Oxygen consumption and carbon dioxide production by female *Plaat1^{-/-}* and *Wt* mice. Representative plot of whole-body VO_2 (A), VCO_2 (B), and TEE (C) normalized to total body weight. Dark (denoted by shaded background) and light (denoted by unshaded background) cycles are shown. The bar graphs of the daily averages, in addition to averages by photoperiod, of VO_2 (D), VCO_2 (E), and TEE (F) are also shown. Data are means \pm SEM, n=6. *P<0.05, **P<0.01.

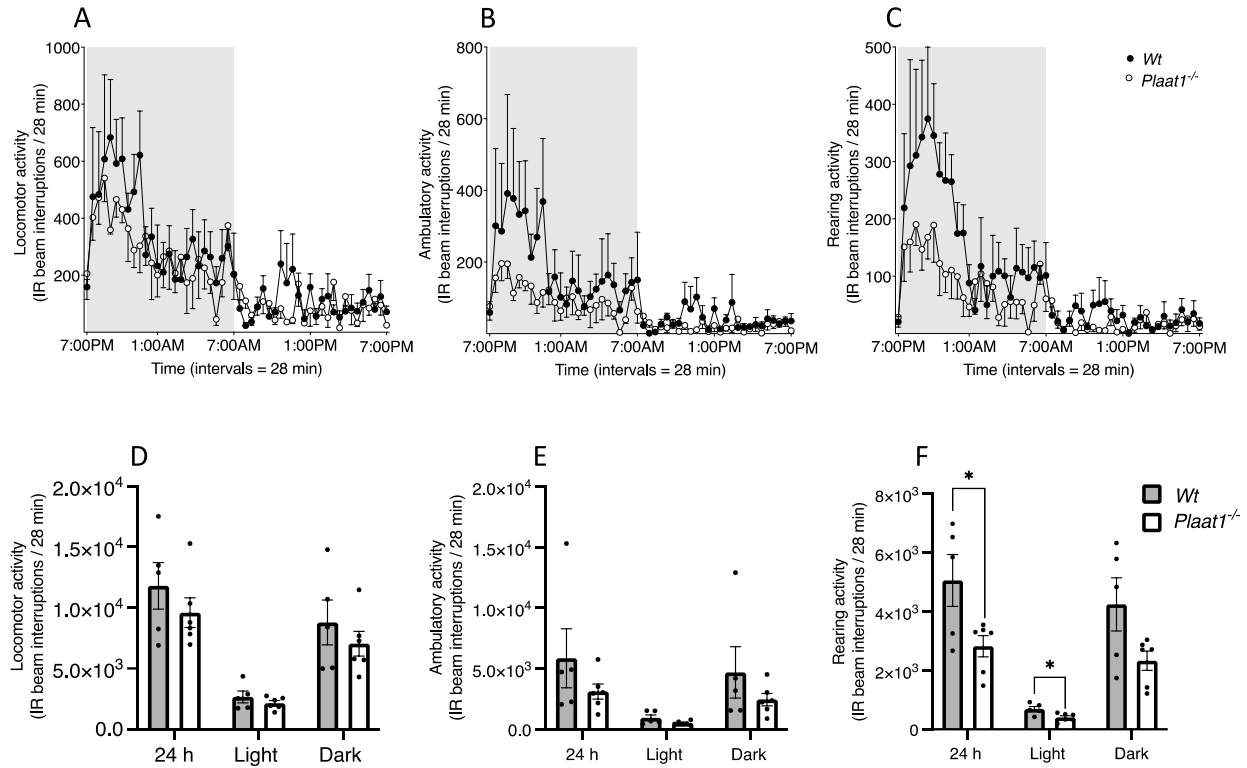


Figure 28: Voluntary Activity Measures in Male mice Basal activity levels are compared between *Plaat1^{-/-}* and *Wt* mice. Representative plot of sums of infrared beam breaks per 28 min interval caused by locomotion movements (A), ambulation movements (B), and rearing movements (C), over a period of 24 h. Dark (denoted by shaded background) and light (denoted by unshaded background) cycles are shown. The corresponding bar graphs of the total sum, in addition to sums per photoperiod, of beam breaks caused by locomotor activity (D), ambulatory activity (E), and rearing activity (F) are also shown. Data are means \pm SEM ($n = 5-6$). * $p < 0.05$.

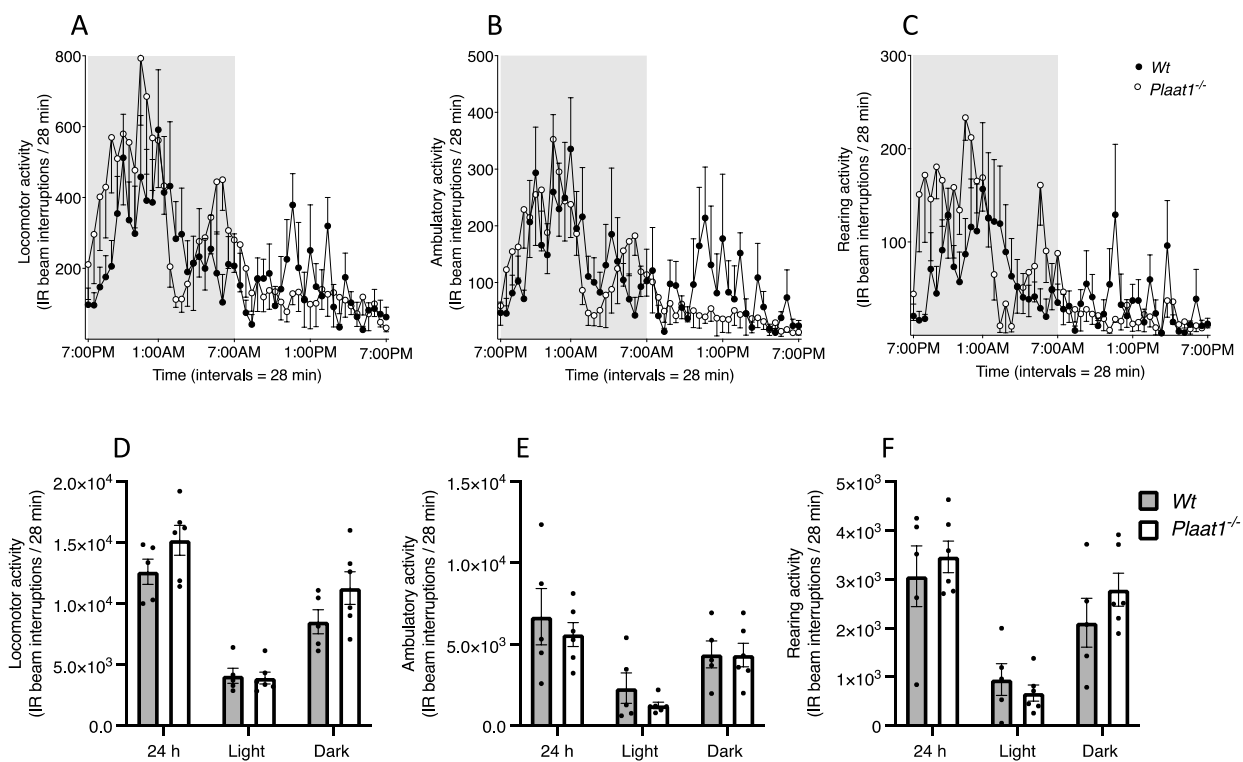


Figure 29: Voluntary activity measures in female mice. Basal activity levels are compared between *Plaat1*^{-/-} and *Wt* mice. Representative plot of sums of infrared beam breaks per 28 min interval caused by locomotion movements (A), ambulation movements (B), and rearing movements (C), over a period of 24 h. Dark (denoted by shaded background) and light (denoted by unshaded background) cycles are shown. The corresponding bar graphs of the total sum, in addition to sums per photoperiod, of beam breaks caused by locomotor activity (D), ambulatory activity (E), and rearing activity (F) are also shown. Data are means \pm SEM ($n = 6$).

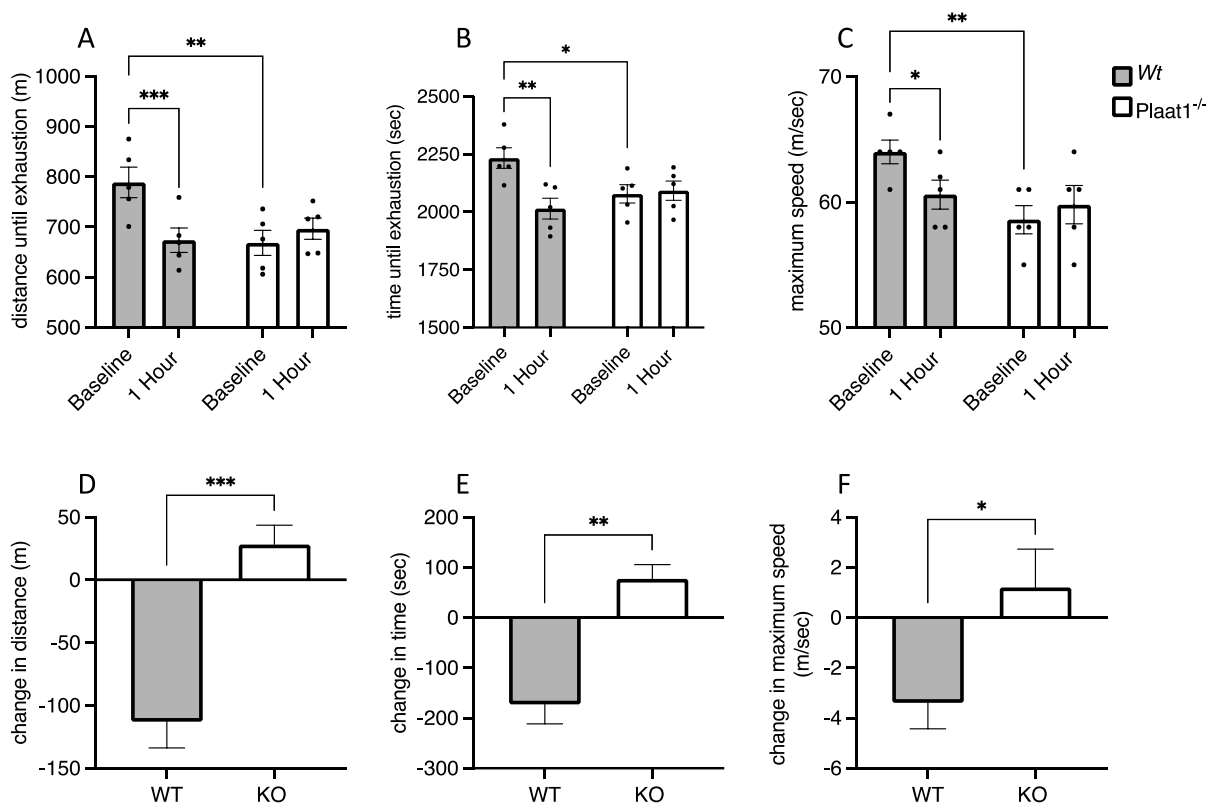


Figure 30: Treadmill exercise capacity and recovery testing of male mice. Distance ran until exhaustion (A), time ran until exhaustion (B), and maximum speed reached at exhaustion (C), during both the first and second treadmill tests. The difference in distance ran (D), time ran (E), and maximum speed achieved (F), for *Wt* mice and *Plaatl1*^{-/-} mice between trial 1 and trial 2 (after 1 h of rest) are also shown. Data are means ± SEM, n=5. *P<0.05, **P<0.01, ***P<0.001.

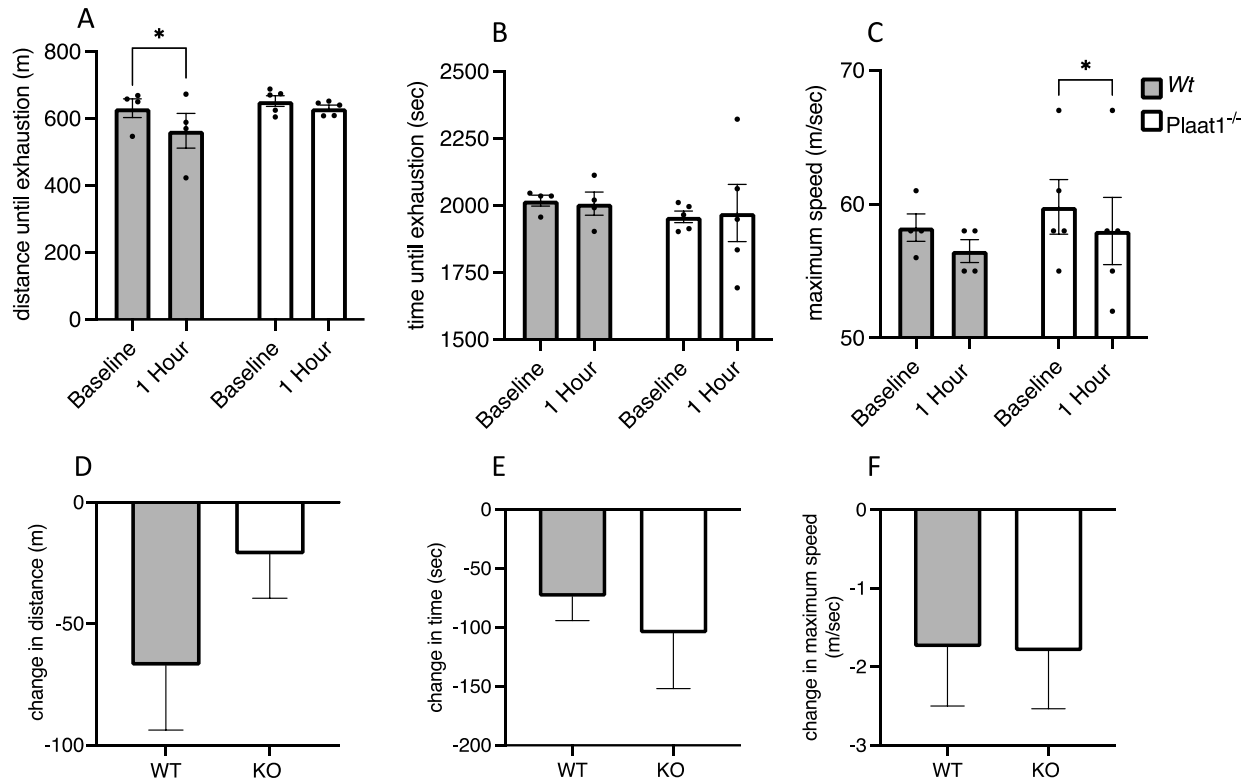


Figure 31: Treadmill exercise capacity and recovery testing of female mice. Distance ran until exhaustion (A), time ran until exhaustion (B), and maximum speed reached at exhaustion (C), during both the first and second treadmill tests. The difference in distance ran (D), time ran (E), and maximum speed achieved (F), for *Wt* mice and *Plaat1^{-/-}* mice between trial 1 and trial 2 (after 1 h of rest) are also shown. Data are means \pm SEM, n=4-5. *P<0.05.

Discussion

The objectives of this study were to observe major phenotypic differences resulting from *Plaat1*^{-/-} gene ablation, in the contexts of metabolic measures, altered behaviour, and exercise capacity. Metabolic and behavioural measures were quantified through CLAMS analysis, and exercise capacity and recovery were tested using a treadmill time-to-exhaustion test. This study indicated that substantial phenotypic changes result from *Plaat1*^{-/-} deficiency, with greater differences apparent within the male *Plaat1*^{-/-} mice.

Our findings indicate a pronounced phenotype associated with PLAAT1 deficiency, especially for male *Plaat1*^{-/-} mice in some instances. When considering a 24-hour metabolic assessment, the CLAMS analysis demonstrated that female and male *Plaat1*^{-/-} mice had lower oxygen intake levels and carbon dioxide production levels, accompanied by diminished energy usage compared to *Wt* controls. For male mice, these variations were mostly found in the dark phase, which is the active period for mice, which are nocturnal. An exception to this was seen in CO₂ production, which was reduced in both light and dark phases for male *Plaat1*^{-/-} mice. However, for the female mice these variations were derived from both the light and dark phase for all three aforementioned measures. This observed metabolic shift may be attributed, at least in part, to the behavioral alterations identified. The male *Plaat1*^{-/-} mice displayed fewer rearing actions, pointing towards a likely reduction in explorative behaviour and heightened apathy (190, 191).

When assessing the exercise capacity test, the male *Plaat1*^{-/-} mice performed poorly when compared to *Wt* controls, achieving a lower total distance, time spent running, as well as maximum speed achieved. These results initially seemed straightforward, suggesting a possible decline in metabolic capability leading to earlier fatigue due to the absence of PLAAT1, which

could explain the reduced exploratory behavior as well. However, the repeated exercise test offered a contrasting narrative, since the male *Plaat1*^{-/-} mice maintained their performance during the subsequent exhaustion test, and even managed to run further than they had during the first trial. These observations were surprising, and two possible mechanisms seem most likely.

The first is that the absence of PLAAT1 mirrors the effect of other CL remodeling enzymes, and leads to compromised metabolic function, consequently affecting energy metabolism, and thus manifesting in the observed behavioral and exercise variations that were evident in our *Plaat1*^{-/-} mice. The second, based on the recognized N-transacylase functions of PLAAT1, suggests that disruption in NAE production by loss of PLAAT1 activity may have contributed to the observed changes. For example, the deficiency in PLAAT1 might have reduced levels of AEA and OEA, affecting variables like pain perception or anxiety, which could influence motivation to explore the cage, and exertional limits in a forced exercise test. If PLAAT1 deficiency reduced PEA levels, this could potentially influence the recovery period post-exercise in a beneficial manner by reducing perceptions of muscle soreness after running, since PEA modulates inflammatory reactions through PPAR- α (137, 138).

The individual NAEs that could be altered in *Plaat1*^{-/-} mice would likely differ by cell type and tissue. Moreover, the various mechanisms that would be affected by dysfunctional NAE production are complex, and beyond the scope of investigation in the current work. Thus, no conclusions can be drawn regarding the potential role of altered NAE production in the metabolic and behaviour changes observed in *Plaat1*^{-/-} mice at present. However, the alignment of these changes with known roles for certain NAE in metabolism and behaviour regulation offers an intriguing avenue for examination that could be a component of future efforts to better

understand the overall phenotype of the mice, and in particular, the unexpected recovery patterns in male *Plaat1*^{-/-} mice.

Another interesting aspect of our findings lies in the distinct sex-specific impacts. Significant variations that were noted between male *Wt* and *Plaat1*^{-/-} mice were smaller or absent in female mice with similar sample sizes. For rearing behaviour and exercise capacity, differences were apparent in male mice that were not apparent in female mice, highlighting the smaller relative effects of PLAAT1 deficiency in female mice. Future work should delve deeper into these sex-specific disparities, both by increasing the sample sizes for comparisons in female mice, and by investigating additional physiological measures.

Chapter 7: Thesis Summary, Integrated Discussion, and Future Perspectives

Summary of key findings

Thesis Study I: Investigation and characterization of transacylase activity of PLAAT1 in cardiolipin remodeling using affinity-purified protein

- Affinity purified PLAAT1 demonstrates in vitro PC:MLCL O-transacylase activity, catalyzing the dose-dependent transacylation of MLCL using distearoyl-PC and dioleoyl-PC.

Thesis Study II: Characterization of Cardiolipin Content and Composition in PLAAT1-Deficient Heart, Brain, and Skeletal Muscle

- PLAAT1 deficiency results in higher total CL content in the female mouse brain and in both sexes changes the CL fatty acyl content to a less saturated composition, predominated by N-6 PUFA.
- PLAAT1 deficiency in mouse heart tissue results in lower total CL contents and a shift in CL fatty acyl content to a more saturated composition with a lowered relative abundance of linoleoyl CL species.
- PLAAT1 deficiency results in greater CL concentrations in the gastrocnemius muscle of both male and female mice, including higher relative composition by MUFA species and lower relative composition by N-6 PUFA species.

Thesis Study III: Gross Morphology and Survival Analysis of *Plaat1*^{-/-} Mice

- PLAAT1 deficiency results in reduced food intake in male mice.
- PLAAT1 deficiency results lower organ weights of the heart, liver, kidney and soleus muscle in male mice.
- *Plaat1*^{-/-} mice experienced premature mortality

Thesis Study IV: Phenotypic Characterization of *Plaat1*^{-/-} Mice

- *Plaat1*^{-/-} mice display lower oxygen consumption, carbon dioxide production, and energy expenditure.
- Male *Plaat1*^{-/-} mice display decreased rearing activity.
- Male *Plaat1*^{-/-} mice have lower exercise endurance during an initial exercise bout, but an increased capacity for recurrent exercise.

Integrated discussion and future perspectives

Prior to our findings published in (37) and presented in Study 1 of this thesis, four enzymes had been identified in CL remodelling as functional in the re-acylation of MLCL or DLCL to CL. These enzymes are Tafazzin, ALCAT1, MLCL-AT1, and α TFP (21). In the first study of this thesis, I determined that affinity purified PLAAT1 has O-transacylase activity *in vitro* using PC as an acyl donor and MLCL as an acyl acceptor. This work identified PLAAT1 as the only other CL remodelling enzyme, alongside Tafazzin, to act as a PC:MLCL transacylase. However, it also identified a substrate specificity for PLAAT1 as an O-transacylase that is distinct from Tafazzin, with PLAAT1 preferring 18:0 and 18:1 fatty acyl chains from PC species, in contrast to the preference by Tafazzin for 18:2n-6 (21).

While the findings from Study 1 demonstrate that PLAAT1 acts as a PC:MLCL O-transacylase *in vitro*, the contributions of this enzyme to CL content and composition *in vivo* are likely to be multi-faceted, and should be considered also in the context of its additional known enzymatic functions. Prior research has shown that PLAAT1 also displays N-transacylase activity, demonstrating an ability to increase the *in vivo* synthesis of NAPE when over-expressed in cells (39). NAPE are the immediate precursors for the generation of NAE signaling molecules that can elicit a host of effects in various biological systems (118), and the rise in PLAAT1-mediated NAPE that occurs in cells overexpressing this enzyme is, indeed, also associated with an increase in the cellular content of NAE (192).

NAE are bioactive and are known to affect myriad systems including mitochondrial processes. However, few studies have examined the effect of NAE directly on CL synthesis or levels. Work in our laboratory examined whether OEA treatment of lymphoblasts deficient in

tafazzin can improve some aspects of mitochondrial biology, and found beneficial effects, but these were not associated with increasing cellular CL content in this cell line (193). In 2015, a study on rat decidual cells found that treatment with arachidonylethanolamide (AEA, anandamide) decreased cellular CL levels (194). Regardless, NAE are potent bioactive signaling molecules in cells, with regulatory functions in lipid metabolism and mitochondrial biogenesis, and therefore modulation of these compounds is expected to indirectly influence CL synthesis and levels.

NAE are agonists of several receptor proteins (195). Of particular relevance to the current work, OEA is a high-affinity ligand for PPAR α , which has been shown to signal in phospholipid synthesis in murine tissues (196). For example, PPAR α activation can induce the expression of LPAAT/AGPAT enzymes that catalyze the synthesis of PA in the Kennedy Pathway from which all complex lipids, including nascent CL, is produced (172). PPAR α activation has also been shown to stimulate de novo CL biosynthesis via an increase in PGP synthase activity (173), catalyzing the conversion of CDP- DAG to PGP – the penultimate step for the synthesis of nascent CL (64).

In addition to O- and N-transacylase activities, PLAAT1 has also been found to have PLA1/2 phospholipase activity, catalyzing the calcium-independent cleavage of fatty acids from the sn-1 or sn-2 position of phospholipids (19). It is notable that phospholipase-mediated hydrolysis of fatty acyl chains from CL, resulting in the production of MLCL or DLCL, is the first step in Land's CL remodeling pathway (19). However, to the best of my knowledge, whether PLAAT1 has phospholipase activity with CL has not yet been studied. Thus, it is plausible that one or all of the catalytic functions of PLAAT1 may be involved in directly or indirectly regulating CL metabolism. When this complexity of activity is coupled with

differences in *Plaat1* expression in tissues (37), as well as differences in PLAAT1 subcellular localization (*i.e.* to the E.R. and MAM (37)), it is likely that PLAAT1 may play different roles in CL metabolism that could vary between different tissues and cell types, and potentially even between different subcellular compartments within the same cell. It is expected that studies to elucidate these distinct roles and interactions will require extensive effort.

To begin to examine the physiological role of PLAAT1, our research group generated *Plaat1*^{-/-} mice. Using this model, I was able to characterize some phenotypic characteristics arising from PLAAT1 deficiency. In Study 2, my first aim with the *Plaat1*^{-/-} mice was to analyze CL content and composition from the three tissues where PLAAT1 is most prevalent - the brain, heart, and skeletal muscle (37), making this the first study to quantify the CL content and composition of a PLAAT1 deficient organism. When compared to *Wt* controls, the content and composition of CL derived from *Plaat1*^{-/-} tissues showed profound differences. For male *Plaat1*^{-/-} mice, total CL concentrations were 95% lower in the heart, but almost 3-fold higher in the gastrocnemius muscle. In the case of female *Plaat1*^{-/-} mice, total CL concentrations were 154% higher in the brain, 82% lower in the heart, and almost 5-fold higher in the gastrocnemius muscle.

The nature of the differences in CL composition also varied widely between these tissues. In Study 1, I discovered that PLAAT1 has substrate specificity for the 18:0 and 18:1 species *in vitro*. Thus, loss of PLAAT1 would be expected to reduce the content of these fatty acyl species in CL, if the primary CL-related function of this enzyme in a tissue is the direct O-transacylase-mediated remodeling of this lipid. In PLAAT1-deficient cardiac tissue, the relative percentage of 18:0 in CL was, however, 12-fold higher, strongly suggesting that changes in this lipid were related not to loss of the direct O-transacylase activity of PLAAT1 with CL, *per se*, but rather to

the loss of another aspect of its function. On the other hand, the relative percentage of 18:1n-9 was 37% and 48% lower in cardiac tissues of *Plaat1*^{-/-} males and females, respectively. This latter finding does align with the *in vitro* results of Study 1, which indicate significant use of PC enriched with 18:1n-9 as a substrate.

The compositional changes in the brain did better coincide with our Study 1 findings, where the relative percentage of 18:0 species in brain tissues of *Plaat1*^{-/-} mice was found to be approximately 66% lower in both sexes, and 18:1n-9 was 36% and 22% lower in male and female mice, respectively, suggesting that this enzyme may contribute directly to CL compositional remodeling in this organ system. In contrast to the profiles observed in either cardiac or brain tissue, CL isolated from gastrocnemius tissue deficient in PLAAT1 activity had 92% and 81% higher levels of 18:1n-9 in males and females respectively, but 60% lower 18:0 content in both sexes.

It is clear from the substantial differences in CL content and composition observed between heart, brain and a skeletal muscle depot that the function of this enzyme is tissue-dependant. As noted in the discussion in Chapter 4, the effect of PLAAT1 deficiency in cardiac tissue is highly reminiscent of the effects resulting from increased CL remodeling by the ALCAT1 enzyme, but the relationship between ALCAT1 and CL composition in the brain and skeletal muscle are not well understood, making this proposition only relevant to comparisons of CL changes in the heart.

An intriguing aspect of these findings is the apparent gradation of change in total CL concentration between these tissues. PLAAT1 deficiency correlates with significantly lower total CL concentrations in the heart, moderately higher concentrations in the brain, and significantly higher concentrations in the gastrocnemius muscle. Coincidentally, the mRNA expression of

ALCAT1 is inversely correlated with this pattern, where within these tissues, it is most highly expressed in the heart, followed by the brain, and lowest in skeletal muscle (16). Whether the expression of *Alcat1* or other CL remodeling enzymes are altered in *Plaat1*-deficient tissues was not tested directly in this thesis, and will be a part of future studies planned to begin to elucidate mechanisms underlying differences observed.

The significant differences in CL levels that were observed in multiple tissues suggested that *Plaat1*^{-/-} mice would likely have phenotypic changes related to mitochondrial function. During preparation of this thesis, a paper was published reporting that PLAAT1 deficient mice are resistant to high fat diet (HFD)-induced weight gain, and have reduced liver weights and less hepatic lipid accumulation when subjected to this dietary challenge (155). This study however generated *Plaat1*^{-/-} mice by deleting exon 2 of the *Plaat1* gene in C57Bl/6N zygotes (155), while the mice I used were generated through deletion of exon 3 of the *Plaat1* gene in C57Bl/6J zygotes. This study made some measures in skeletal muscle from male mice, but did not explore the consequences of PLAAT1 deficiency on brain or heart tissues, report effects of PLAAT1 on survival, examine female mice, or make any measures of CL (155). I examined growth patterns and food intake patterns, organ weights, and birth rates and survival rates post-sexing. Male *Plaat1*^{-/-} mice had smaller liver, kidney, heart, and soleus muscle masses. Our findings regarding lower soleus mass were in line with that recent work by Rahman *et al.*, where they also demonstrated that skeletal muscle masses were lower in *Plaat1*^{-/-} mice, but our results regarding liver masses contrast theirs, as they did not observe a difference in *Plaat1*^{-/-} mice when fed a standard diet, despite also weighing tissues at 20-weeks of age (155). These differences are possibly due to the different approaches we used to generate *Plaat1*^{-/-} mice, though the reason behind this isn't immediately apparent.

In Study 3 we also reported that male and female *Plaat1*^{-/-} mice had 6- and 5-month shorter median lifespans when compared to *Wt* controls. Notably, the most frequently observed diseases that gave cause for euthanasia in *Plaat1*^{-/-} mice, were dermatitis in male mice, and eye ulcers in female mice. This finding may have fascinating implications for understanding the relationship between PLAAT1 and autophagy. A recent study utilizing zebra fish found that PLAAT1 would translocate to damaged organelles in the lens of the eye immediately before organelle degradation, suggesting that it functions in autophagy (154). From the perspective of an impaired autophagy process, PLAAT1 deficiency could be causal to both the development of dermatitis and eye ulcers. The most common cause for eye ulcers are infections, and despite the role of macular autophagy in infection control not being well documented (197), it's role in immunity is well documented. Autophagy affects the secretion of antimicrobial mediators, as wells as a host of other immune functions, such as enhancing phagosome formation, antigen presentation, and influencing T-cell homeostasis (198). In the case of dermatitis, it has been found during inflammatory skin diseases that a common function of inflammatory cytokines is the impairment of autophagy in keratinocytes, suggesting that impairment of this process is a contributing factor to the development of psoriasis and dermatitis (199). Furthermore, CL's role in the autophagic process was previously explained, where externalized CL on the OMM has been shown to bind directly to LC3, a protein critical to autophagosome formation (10). A disruption in these processes due to PLAAT1 deficiency, whether directly involved in the autophagic process or being functionally prudent for CL's appropriate functioning and subsequent contribution to autophagy, could culminate in a higher prevalence of eye ulcers and potentially also dermatitis.

In Study 3 we determined that male *Plaat1*^{-/-} mice have lower food intakes, despite not differing from *Wt* mice in terms of growth or body weight. Altered N-transacylase activity,

resulting in reduced AEA, an NAE that's been shown to stimulate appetite, could potentially play a role (132). The effects of diminished AEA could also potentially help to explain results in Study 4, where male *Plaat1*^{-/-} mice maintained their performance during a subsequent treadmill exhaustion test, and even managed to run further than in their first trial. Since AEA can modulate nociception, and has been suggested as an endogenous pain suppressor (133), it's plausible that *Plaat1*^{-/-} mice exhibited lower exercise capacity in test 1 due to decreased pain sensation rather than decreased cardiovascular capacity, although it is unclear why this would lead to a lack of decrease in performance at the second run.

Male *Plaat1*^{-/-} mice displayed fewer rearing actions, suggesting reduced explorative behaviour and heightened apathy (190, 191). FAAH is an important regulator of NAE since it has the capability to hydrolyse NAEs into their basic components (123, 124). FAAH^{-/-} mice have higher exploratory rearing in the open field testing paradigm, and more rearing behavior in general when compared to WT controls, strongly suggesting that NAE levels are correlated with rearing behaviour in that model (200). Thus the decreased rearing observed in male *Plaat1*^{-/-} mice could be connected to the loss of PLAAT1-mediated N-transacylase activity. This reduction in voluntary activity could also be a factor in metabolic shifts observed in both male and female *Plaat1*^{-/-} mice, where O² consumption, CO² production, and energy expenditure are all lower than in *Wt* controls. It should be noted, however, that the lower carbon dioxide production exhibited by *Plaat1*^{-/-} mice contrasts with the higher production exhibited by *Taz*-KO mice (163).

Results from this thesis, including findings that CL levels were increased in two tissues but decreased in a third, indicates a complex role for PLAAT1 in cellular, tissue and whole body CL, mitochondrial and energy metabolism, as well as bioactive lipid signaling, that will be difficult to unravel. In many regards, however, this story is not unlike that of ALCAT1. Like PLAAT1,

ALCAT1 is located in the ER and MAM (82). ALCAT1 has been identified as an enzyme that is active in remodelling CL to a highly unsaturated form, rendering CL more sensitive to oxidation by ROS (14, 51). However, this enzyme is also responsible for the acylation of other glycerophospholipids, including PG, a precursor for CL synthesis, and bis(monoacylglycero)phosphate, a structural isomer of lyso-PG and a metabolic intermediate of CL (201). Furthermore, ALCAT1 is also active in remodeling phosphatidylinositol, and therefore is a regulator of the acyl profile of phosphoinositides that are potent signaling molecules in cells (202). While there will be challenges in unravelling the various biological functions of PLAAT1 *in vivo* given the interrelated nature of these effects on metabolic and bioenergetic outcomes, as studies on ALCAT1 have provided, there is much that will be learned from these efforts.

The findings of this thesis sometimes demonstrated different findings between male and female *Plaat1*^{-/-} mice. Most notable were behavioural changes with PLAAT1 enzyme deficiency that were not manifest in the female mice. These included changes in rearing activity, as well as profound differences observed in our exercise capacity testing. Despite this, most of our tissue analyses, as well as our metabolic measures, were aligned between the sexes. In some instances, a lack of statistically significant differences in female compared to male mouse measures may have been the result of underpowering, but other findings simply did not trend in the same way that the differences in the male mice did. Given the novelty of this mouse model, there currently isn't enough information to unravel these observed sex differences, but these differences are a finding in their own right, giving reason for further research along these lines.

Prior to my research on this enzyme, PLAAT1 had already been identified as an O-transacylase, as well as a N-transacylase (39). Previous work by our research group identified a possible role for PLAAT1 in CL metabolism, and I aimed to further characterize this function. I

succeeded in demonstrating the ability of PLAAT1 to directly remodel CL *in vitro* and conducted studies using *Plaat1*^{-/-} mice to help elucidate this enzyme's physiological functions. I discovered novel characteristics derived from PLAAT1 deficiency through this model. However, the breadth of findings here did not determine whether PLAAT1 is directly or indirectly involved in CL synthesis and remodelling in this model, nor did it determine which enzymatic function is most likely to be involved in altering CL levels. Plausible avenues to explain PLAAT1's role in modulating CL levels include indirect effects on the production of NAPE and subsequently NAEs, direct effects through its function as an O-transacylase on MLCL, and potentially also direct effects on CL through PLA1/2 activity.

This thesis has limitations that also pose opportunities for future research. The experimental approach used in study 1 could not distinguish positional preference between the *sn-1* or *sn-2* position for substrate selectivity. The PLAAT enzyme family has previously shown preference for using fatty acids at the *sn-1* position on the glycerol backbone of PC (89, 105), thus leaving the possibility that reactions containing 1-palmitoyl-2-[¹⁴C]-linoleoyl phosphatidylcholine as an acyl-donor substrate failed to generate increased CL synthesis because of the stereochemical position of the radiolabeled linoleoyl residue in the *sn-2* position, rather than because of the chemical nature of the fatty acyl chain, *per se*. Despite this, given that PLAAT1 does exhibit activity with other PC substrates with fatty acyl moieties esterified at the *sn-2* position, the complete absence of transacylase activity recorded by PLAAT1 with 18:2n-6 in PC likely implies a lack of activity with this substrate. Further work will be needed to determine if either fatty acyl preference, positional preference, or both factors together result in the null activity observed.

Along these same lines, the GC analysis used in Study 2 cannot determine the degree of CL acylation. A future direction that can compensate for this to quantify the total content of MLCL

and DLCL in these tissues. This would also shed light on where our observed changes are stemming from. An increase in total MLCL content would suggest dysfunctional CL remodelling, or another change within the Lands pathway following PLA1/2 activity (19). Alternately, a lack of changes in total MLCL content suggest disruptions in the Kennedy pathway, suggesting alterations in the *de novo* synthesis of CL. If the latter scenario is confirmed, further quantification of NAPE and NAE in these tissues would be invaluable, as this could suggest changes incurred by altered activation of PPAR α and other regulators of lipid enzyme transcription (64). Furthermore, given the extent of altered CL content and composition that we observed in *Plaat1*^{-/-} mice, it is pertinent to elucidate how these changes impact mitochondrial function. This could be approached through the use of high-resolution respirometry, for the purpose of characterizing mitochondrial quality, as well as the function of the electron transport chain (203).

Another important limitation to the results of Study 2 that should be mentioned is the lack of a 2-step lipid separation process. This would first resolve neutral lipids away from phospholipids including CL, which remain at the origin, and then allow for those phospholipids to be scraped, recovered, and resolved on a second plate. In the work shown in this thesis, we opted to perform a single separation process, wherein total lipid extracts were spotted on a TLC plate, and the plate was resolved using a solvent mixture designed for phospholipid separation. In this process, phospholipid classes migrate according to polarity, while the neutral lipids, including free fatty acids and triacylglycerols, migrate with the solvent front. We used a cardiolipin standard to identify the appropriate band for scraping and analysis, and as expected CL ran near the top of the plate. It should be noted that this was close to the solvent front, which may have allowed for contamination by neutral lipids, which are quantitatively more abundant than CL in most, but not all tissues. The choice of a single-step separation was made in order to minimize losses of CL

during the 1st plate recovery and 2nd plate re-application and separation steps. However, given the risk for neutral lipid contamination in the scraped CL samples, it is important that this work is repeated, and confirmed with a 2-step lipid separation.

When characterizing gross morphology, total weight of fat-depot and fat-free mass was not measured. Differences in these measures between *Wt* and *Plaat1*^{-/-} mice would give further insight into to changes derived from differences in feeding and activity levels, as well as differences in organ weights, despite the lack of observed differences in total growth patterns.

Finally, due to the novelty of *Plaat1*^{-/-} mice, experiments and findings of studies 3 and 4 are overarching for many physiological pathways, and lack the specificity required to appropriately define mechanisms for PLAAT1's enzymatic functions. These studies were aimed to create direction for future phenotype analysis. For instance, the reduction in rearing activity through CLAMS analysis may give way for further experimentation using an elevated plus maze for assessing anxiety-like behaviour (204), and future studies should be directed towards these investigations.

References

1. Acehan D, Vaz F, Houtkooper RH, James J, Moore V, Tokunaga C, et al. Cardiac and skeletal muscle defects in a mouse model of human Barth syndrome. *Journal of biological chemistry*. 2011;286(2):899-908.
2. Landriscina C, Megli F, Quagliariello E. Turnover of fatty acids in rat liver cardiolipin: comparison with other mitochondrial phospholipids. *Lipids*. 1976;11(1):61-6.
3. Gomez B, Robinson NC. Phospholipase digestion of bound cardiolipin reversibly inactivates bovine cytochrome bc 1. *Biochemistry*. 1999;38(28):9031-8.
4. Schwall CT, Greenwood VL, Alder NN. The stability and activity of respiratory Complex II is cardiolipin-dependent. *Biochimica et Biophysica Acta (BBA)-Bioenergetics*. 2012;1817(9):1588-96.
5. Acehan D, Malhotra A, Xu Y, Ren M, Stokes DL, Schlame M. Cardiolipin affects the supramolecular organization of ATP synthase in mitochondria. *Biophysical journal*. 2011;100(9):2184-92.
6. DeVay RM, Dominguez-Ramirez L, Lackner LL, Hoppins S, Stahlberg H, Nunnari J. Coassembly of Mgm1 isoforms requires cardiolipin and mediates mitochondrial inner membrane fusion. *The Journal of cell biology*. 2009;186(6):793-803.
7. Chen S, Tarsio M, Kane PM, Greenberg ML. Cardiolipin mediates cross-talk between mitochondria and the vacuole. *Molecular biology of the cell*. 2008;19(12):5047-58.
8. Jiang F, Ryan MT, Schlame M, Zhao M, Gu Z, Klingenberg M, et al. Absence of cardiolipin in the *crd1* null mutant results in decreased mitochondrial membrane potential and reduced mitochondrial function. *Journal of Biological Chemistry*. 2000;275(29):22387-94.
9. Acehan D, Khuchua Z, Houtkooper RH, Malhotra A, Kaufman J, Vaz FM, et al. Distinct effects of tafazzin deletion in differentiated and undifferentiated mitochondria. *Mitochondrion*. 2009;9(2):86-95.
10. Chu CT, Ji J, Dagda RK, Jiang JF, Tyurina YY, Kapralov AA, et al. Cardiolipin externalization to the outer mitochondrial membrane acts as an elimination signal for mitophagy in neuronal cells. *Nature cell biology*. 2013;15(10):1197.
11. Gonzalez F, Schug ZT, Houtkooper RH, MacKenzie ED, Brooks DG, Wanders RJ, et al. Cardiolipin provides an essential activating platform for caspase-8 on mitochondria. *The Journal of cell biology*. 2008;183(4):681-96.
12. Lin MT, Beal MF. Mitochondrial dysfunction and oxidative stress in neurodegenerative diseases. *Nature*. 2006;443(7113):787.
13. Li J, Romestaing C, Han X, Li Y, Hao X, Wu Y, et al. Cardiolipin remodeling by ALCAT1 links oxidative stress and mitochondrial dysfunction to obesity. *Cell metabolism*. 2010;12(2):154-65.
14. Wang L, Liu X, Nie J, Zhang J, Kimball SR, Zhang H, et al. ALCAT1 controls mitochondrial etiology of fatty liver diseases, linking defective mitophagy to steatosis. *Hepatology*. 2015;61(2):486-96.
15. Uyama T, Jin X-H, Tsuboi K, Tonai T, Ueda N. Characterization of the human tumor suppressors TIG3 and HRASLS2 as phospholipid-metabolizing enzymes. *Biochimica et Biophysica Acta (BBA)-Molecular and Cell Biology of Lipids*. 2009;1791(12):1114-24.

16. Cao J, Liu Y, Lockwood J, Burn P, Shi Y. A novel cardiolipin-remodeling pathway revealed by a gene encoding an endoplasmic reticulum-associated acyl-CoA: lysocardiolipin acyltransferase (ALCAT1) in mouse. *Journal of Biological Chemistry*. 2004;279(30):31727-34.
17. Taylor WA, Hatch GM. Identification of the human mitochondrial linoleoyl-coenzyme A monolysocardiolipin acyltransferase (MLCL AT-1). *Journal of Biological Chemistry*. 2009;284(44):30360-71.
18. Xu Y, Kelley RI, Blanck TJ, Schlame M. Remodeling of cardiolipin by phospholipid transacylation. *Journal of Biological Chemistry*. 2003;278(51):51380-5.
19. Schlame M. Thematic Review Series: Glycerolipids. Cardiolipin synthesis for the assembly of bacterial and mitochondrial membranes. *Journal of lipid research*. 2008;49(8):1607-20.
20. Golczak M, Kiser PD, Sears AE, Lodowski DT, Blaner WS, Palczewski K. Structural basis for the acyltransferase activity of lecithin: retinol acyltransferase-like proteins. *Journal of Biological Chemistry*. 2012;287(28):23790-807.
21. Bradley RM, Stark KD, Duncan RE. Influence of tissue, diet, and enzymatic remodeling on cardiolipin fatty acyl profile. *Molecular nutrition & food research*. 2016;60(8):1804-18.
22. Guan Z, Söderberg M, Sindelar P, Edlund C. Content and fatty acid composition of cardiolipin in the brain of patients with Alzheimer's disease. *Neurochemistry international*. 1994;25(3):295-300.
23. Ghio S, Kamp F, Cauchi R, Giese A, Vassallo N. Interaction of α -synuclein with biomembranes in Parkinson's disease—role of cardiolipin. *Progress in lipid research*. 2016;61:73-82.
24. Dolinsky VW, Cole LK, Sparagna GC, Hatch GM. Cardiac mitochondrial energy metabolism in heart failure: Role of cardiolipin and sirtuins. *Biochimica et Biophysica Acta (BBA)-Molecular and Cell Biology of Lipids*. 2016;1861(10):1544-54.
25. Ma ZA, Zhao Z, Turk J. Mitochondrial dysfunction and β -cell failure in type 2 diabetes mellitus. *Experimental diabetes research*. 2011;2012.
26. Xiao M, Zhong H, Xia L, Tao Y, Yin H. Pathophysiology of mitochondrial lipid oxidation: role of 4-hydroxynonenal (4-HNE) and other bioactive lipids in mitochondria. *Free Radical Biology and Medicine*. 2017;111:316-27.
27. Colquhoun A. Lipids, mitochondria and cell death: implications in neuro-oncology. *Molecular neurobiology*. 2010;42(1):76-88.
28. Kiebish MA, Han X, Cheng H, Chuang JH, Seyfried TN. Brain mitochondrial lipid abnormalities in mice susceptible to spontaneous gliomas. *Lipids*. 2008;43(10):951-9.
29. Sandra F, Degli Esposti M, Ndebele K, Gona P, Knight D, Rosenquist M, et al. Tumor Necrosis Factor–Related Apoptosis-Inducing Ligand Alters Mitochondrial Membrane Lipids. *Cancer research*. 2005;65(18):8286-97.
30. Lesnefsky EJ, Hoppel CL. Cardiolipin as an oxidative target in cardiac mitochondria in the aged rat. *Biochimica et Biophysica Acta (BBA)-Bioenergetics*. 2008;1777(7-8):1020-7.
31. Lee H-J, Mayette J, Rapoport SI, Bazinet RP. Selective remodeling of cardiolipin fatty acids in the aged rat heart. *Lipids in health and disease*. 2006;5(1):2.
32. Lesnefsky EJ, Chen Q, Slabe TJ, Stoll MS, Minkler PE, Hassan MO, et al. Ischemia, rather than reperfusion, inhibits respiration through cytochrome oxidase in the isolated, perfused

- rabbit heart: role of cardiolipin. *American Journal of Physiology-Heart and Circulatory Physiology*. 2004;287(1):H258-H67.
33. Lesnefsky EJ, Minkler P, Hoppel CL. Enhanced modification of cardiolipin during ischemia in the aged heart. *Journal of molecular and cellular cardiology*. 2009;46(6):1008-15.
 34. Sparagna GC, Johnson CA, McCune SA, Moore RL, Murphy RC. Quantitation of cardiolipin molecular species in spontaneously hypertensive heart failure rats using electrospray ionization mass spectrometry. *Journal of lipid research*. 2005;46(6):1196-204.
 35. Zachman DK, Chicco AJ, McCune SA, Murphy RC, Moore RL, Sparagna GC. The role of calcium-independent phospholipase A2 in cardiolipin remodeling in the spontaneously hypertensive heart failure rat heart. *Journal of lipid research*. 2010;51(3):525-34.
 36. Sparagna GC, Chicco AJ, Murphy RC, Bristow MR, Johnson CA, Rees ML, et al. Loss of cardiac tetralinoleoyl cardiolipin in human and experimental heart failure. *Journal of lipid research*. 2007;48(7):1559-70.
 37. Bradley RM, Hashemi A, Aristizabal-Henao JJ, Stark KD, Duncan RE. PLAAT1 Exhibits Phosphatidylcholine: Monolysocardiolipin Transacylase Activity. *International Journal of Molecular Sciences*. 2022;23(12):6714.
 38. Bradley RM. Identification and characterization of a novel microsomal enzyme involved in cardiolipin synthesis and remodeling. Waterloo Ontario: University of Waterloo; 2018.
 39. Shinohara N, Uyama T, Jin X-H, Tsuboi K, Tonai T, Houchi H, et al. Enzymological analysis of the tumor suppressor A-C1 reveals a novel group of phospholipid-metabolizing enzymes. *Journal of lipid research*. 2011;52(11):1927-35.
 40. Berdyshev EV, Schmid PC, Krebsbach RJ, Kuwae T, Huang C, Ma W-Y, et al. Role of N-Acylethanolamines in Cell Signaling. In: Hamazaki T, Okuyama H, editors. *Fatty Acids and Lipids - New Findings: International Society for the Study of Fatty Acids and Lipids (ISSFAL), 4th Congress, Tsukuba, Japan, June 2000*. 88: S.Karger AG; 2000. p. 0.
 41. Paradies G, Paradies V, Ruggiero FM, Petrosillo G. Cardiolipin and mitochondrial function in health and disease. *Antioxidants & redox signaling*. 2014;20(12):1925-53.
 42. Schlame M, Ren M. Barth syndrome, a human disorder of cardiolipin metabolism. *FEBS letters*. 2006;580(23):5450-5.
 43. Youle RJ, Van Der Bliek AM. Mitochondrial fission, fusion, and stress. *Science*. 2012;337(6098):1062-5.
 44. De Brito OM, Scorrano L. Mitofusin 2 tethers endoplasmic reticulum to mitochondria. *Nature*. 2008;456(7222):605-10.
 45. Bustillo-Zabalbeitia I, Montessuit S, Raemy E, Basañez G, Terrones O, Martinou J-C. Specific interaction with cardiolipin triggers functional activation of dynamin-related protein 1. *PloS one*. 2014;9(7):e102738.
 46. Elmore S. Apoptosis: a review of programmed cell death. *Toxicologic pathology*. 2007;35(4):495-516.
 47. Kagan VE, Tyurin VA, Jiang J, Tyurina YY, Ritov VB, Amoscato AA, et al. Cytochrome c acts as a cardiolipin oxygenase required for release of proapoptotic factors. *Nature chemical biology*. 2005;1(4):223-32.
 48. Ott M, Robertson JD, Gogvadze V, Zhivotovsky B, Orrenius S. Cytochrome c release from mitochondria proceeds by a two-step process. *Proceedings of the national academy of sciences*. 2002;99(3):1259-63.

49. Kagan VE, Bayır HA, Belikova NA, Kapralov O, Tyurina YY, Tyurin VA, et al. Cytochrome c/cardiolipin relations in mitochondria: a kiss of death. *Free Radical Biology and Medicine*. 2009;46(11):1439-53.
50. Pizzuto M, Pelegrin P. Cardiolipin in immune signaling and cell death. *Trends in cell biology*. 2020;30(11):892-903.
51. Dudek J. Role of cardiolipin in mitochondrial signaling pathways. *Frontiers in cell and developmental biology*. 2017;5:90.
52. Rogov VV, Suzuki H, Marinković M, Lang V, Kato R, Kawasaki M, et al. Phosphorylation of the mitochondrial autophagy receptor Nix enhances its interaction with LC3 proteins. *Scientific reports*. 2017;7(1):1-12.
53. Iriundo MN, Etxaniz A, Varela YR, Ballesteros U, Hervás JH, Montes LR, et al. LC3 subfamily in cardiolipin-mediated mitophagy: a comparison of the LC3A, LC3B and LC3C homologs. *Autophagy*. 2022;18(12):2985-3003.
54. Iyer SS, He Q, Janczy JR, Elliott EI, Zhong Z, Olivier AK, et al. Mitochondrial cardiolipin is required for Nlrp3 inflammasome activation. *Immunity*. 2013;39(2):311-23.
55. Jin MS, Kim SE, Heo JY, Lee ME, Kim HM, Paik S-G, et al. Crystal structure of the TLR1-TLR2 heterodimer induced by binding of a tri-acylated lipopeptide. *Cell*. 2007;130(6):1071-82.
56. Kennedy EP, Weiss SB. The function of cytidine coenzymes in the biosynthesis of phospholipides. *Journal of Biological Chemistry*. 1956;222(1):193-214.
57. Vance JE. Phospholipid synthesis and transport in mammalian cells. *Traffic*. 2015;16(1):1-18.
58. Cases S, Smith SJ, Zheng Y-W, Myers HM, Lear SR, Sande E, et al. Identification of a gene encoding an acyl CoA: diacylglycerol acyltransferase, a key enzyme in triacylglycerol synthesis. *Proceedings of the National Academy of Sciences*. 1998;95(22):13018-23.
59. Stone SJ, Cui Z, Vance JE. Cloning and Expression of Mouse Liver Phosphatidylserine Synthase-1 cDNA Overexpression in Rat Hepatoma Cells Inhibits the CDP-ethanolamine Pathway for Phosphatidylethanolamine Biosynthesis. *Journal of Biological Chemistry*. 1998;273(13):7293-302.
60. STONE SJ, VANCE JE. Cloning and expression of murine liver phosphatidylserine synthase (PSS)-2: differential regulation of phospholipid metabolism by PSS1 and PSS2. *Biochemical Journal*. 1999;342(1):57-64.
61. Lykidis A, Jackson PD, Rock CO, Jackowski S. The role of CDP-diacylglycerol synthetase and phosphatidylinositol synthase activity levels in the regulation of cellular phosphatidylinositol content. *Journal of Biological Chemistry*. 1997;272(52):33402-9.
62. Diagne A, Fauvel J, Record M, Chap H, Douste-Blazy L. Studies on ether phospholipids: II. Comparative composition of various tissues from human, rat and guinea pig. *Biochimica et Biophysica Acta (BBA)-Lipids and Lipid Metabolism*. 1984;793(2):221-31.
63. Modi HR, Katyare SS, Patel MA. Ageing-induced alterations in lipid/phospholipid profiles of rat brain and liver mitochondria: implications for mitochondrial energy-linked functions. *Journal of Membrane Biology*. 2008;221(1):51-60.
64. Saunders RM, Schwarz HP. Synthesis of phosphatidylglycerol and diphosphatidylglycerol1, 2. *Journal of the American Chemical Society*. 1966;88(16):3844-7.

65. Hostetler K, Bosch H, Van Deenen L. The mechanism of cardiolipin biosynthesis in liver mitochondria. *Biochimica et Biophysica Acta (BBA)-Lipids and Lipid Metabolism*. 1972;260(3):507-13.
66. Schlame M, Hostetler KY. Cardiolipin synthase from mammalian mitochondria. *Biochimica et Biophysica Acta (BBA)-Lipids and Lipid Metabolism*. 1997;1348(1-2):207-13.
67. Schlame M, Ren M, Xu Y, Greenberg ML, Haller I. Molecular symmetry in mitochondrial cardiolipins. *Chemistry and physics of lipids*. 2005;138(1-2):38-49.
68. SCHLAME M, BRODY S, HOSTETLER KY. Mitochondrial cardiolipin in diverse eukaryotes: comparison of biosynthetic reactions and molecular acyl species. *European journal of biochemistry*. 1993;212(3):727-33.
69. Cheng H, Mancuso DJ, Jiang X, Guan S, Yang J, Yang K, et al. Shotgun lipidomics reveals the temporally dependent, highly diversified cardiolipin profile in the mammalian brain: temporally coordinated postnatal diversification of cardiolipin molecular species with neuronal remodeling. *Biochemistry*. 2008;47(21):5869-80.
70. Bione S, D'Adamo P, Maestrini E, Gedeon AK, Bolhuis PA, Toniolo D. A novel X-linked gene, G4. 5. is responsible for Barth syndrome. *Nature genetics*. 1996;12(4):385.
71. Xu Y, Malhotra A, Ren M, Schlame M. The enzymatic function of tafazzin. *Journal of Biological Chemistry*. 2006;281(51):39217-24.
72. Pizzuto M, Lonez C, Baroja-Mazo A, Martínez-Banaclocha H, Tourlomousis P, Gangloff M, et al. Saturation of acyl chains converts cardiolipin from an antagonist to an activator of Toll-like receptor-4. *Cellular and Molecular Life Sciences*. 2019;76(18):3667-78.
73. Vreken P, Valianpour F, Nijtmans LG, Grivell LA, Plecko B, Wanders RJ, et al. Defective remodeling of cardiolipin and phosphatidylglycerol in Barth syndrome. *Biochemical and biophysical research communications*. 2000;279(2):378-82.
74. Houtkooper RH, Rodenburg RJ, Thiels C, van Lenthe H, Stet F, Poll-The BT, et al. Cardiolipin and monolysocardiolipin analysis in fibroblasts, lymphocytes, and tissues using high-performance liquid chromatography–mass spectrometry as a diagnostic test for Barth syndrome. *Analytical biochemistry*. 2009;387(2):230-7.
75. Ferreira C, Pierre G, Thompson R, Vernon H. Barth syndrome. 2020.
76. Kelley RI, Cheatham JP, Clark BJ, Nigro MA, Powell BR, Sherwood GW, et al. X-linked dilated cardiomyopathy with neutropenia, growth retardation, and 3-methylglutaconic aciduria. *The Journal of pediatrics*. 1991;119(5):738-47.
77. Wang G, McCain ML, Yang L, He A, Pasqualini FS, Agarwal A, et al. Modeling the mitochondrial cardiomyopathy of Barth syndrome with induced pluripotent stem cell and heart-on-chip technologies. *Nature medicine*. 2014;20(6):616-23.
78. McKenzie M, Lazarou M, Thorburn DR, Ryan MT. Mitochondrial respiratory chain supercomplexes are destabilized in Barth Syndrome patients. *Journal of molecular biology*. 2006;361(3):462-9.
79. Schlame M, Rüstow B. Lysocardiolipin formation and reacylation in isolated rat liver mitochondria. *Biochemical journal*. 1990;272(3):589-95.
80. Acehan D, Xu Y, Stokes DL, Schlame M. Comparison of lymphoblast mitochondria from normal subjects and patients with Barth syndrome using electron microscopic tomography. *Laboratory investigation*. 2007;87(1):40-8.

81. Chicco AJ, Sparagna GC. Role of cardiolipin alterations in mitochondrial dysfunction and disease. *American Journal of Physiology-Cell Physiology*. 2007;292(1):C33-C44.
82. Zou C, Synan MJ, Li J, Xiong S, Manni ML, Liu Y, et al. LPS impairs oxygen utilization in epithelia by triggering degradation of the mitochondrial enzyme Alcat1. *Journal of cell science*. 2016;129(1):51-64.
83. Hamasaki M, Furuta N, Matsuda A, Nezu A, Yamamoto A, Fujita N, et al. Autophagosomes form at ER-mitochondria contact sites. *Nature*. 2013;495(7441):389.
84. Taylor WA, Mejia EM, Mitchell RW, Choy PC, Sparagna GC, Hatch GM. Human trifunctional protein alpha links cardiolipin remodeling to beta-oxidation. *PloS one*. 2012;7(11):e48628.
85. Matern D, Strauss AW, Hillman SL, Mayatepek E, Millington DS, Trefz F-K. Diagnosis of mitochondrial trifunctional protein deficiency in a blood spot from the newborn screening card by tandem mass spectrometry and DNA analysis. *Pediatric research*. 1999;46(1):45-9.
86. Zhang J, Guan Z, Murphy AN, Wiley SE, Perkins GA, Worby CA, et al. Mitochondrial phosphatase PTPMT1 is essential for cardiolipin biosynthesis. *Cell metabolism*. 2011;13(6):690-700.
87. Mejia EM, Zegallai H, Bouchard ED, Banerji V, Ravandi A, Hatch GM. Expression of human monolysocardiolipin acyltransferase-1 improves mitochondrial function in Barth syndrome lymphoblasts. *Journal of Biological Chemistry*. 2018;293(20):7564-77.
88. Taylor WA, Hatch GM. Purification and characterization of monolysocardiolipin acyltransferase from pig liver mitochondria. *Journal of Biological Chemistry*. 2003;278(15):12716-21.
89. Mardian EB, Bradley RM, Duncan RE. The HRASLS (PLA/AT) subfamily of enzymes. *Journal of biomedical science*. 2015;22(1):1-11.
90. Sers C, Emmenegger U, Husmann K, Bucher K, Andres A-C, Schäfer R. Growth-inhibitory activity and downregulation of the class II tumor-suppressor gene H-rev107 in tumor cell lines and experimental tumors. *The Journal of cell biology*. 1997;136(4):935-44.
91. Sers C, Husmann K, Nazarenko I, Reich S, Wiechen K, Zhumabayeva B, et al. The class II tumour suppressor gene H-REV107-1 is a target of interferon-regulatory factor-1 and is involved in IFN γ -induced cell death in human ovarian carcinoma cells. *Oncogene*. 2002;21(18):2829-39.
92. Akiyama H, Hiraki Y, Noda M, Shigeno C, Ito H, Nakamura T. Molecular cloning and biological activity of a novel Ha-Ras suppressor gene predominantly expressed in skeletal muscle, heart, brain, and bone marrow by differential display using clonal mouse EC cells, ATDC5. *Journal of Biological Chemistry*. 1999;274(45):32192-7.
93. Shyu R-Y, Hsieh Y-C, Tsai F-M, Wu C-C, Jiang S-Y. Cloning and functional characterization of the HRASLS2 gene. *Amino acids*. 2008;35(1):129-37.
94. Hajnal A, Klemenz R, Schäfer R. Subtraction cloning of H-rev107, a gene specifically expressed in H-ras resistant fibroblasts. *Oncogene*. 1994;9(2):479.
95. Wang C-H, Shyu R-Y, Wu C-C, Tsai T-C, Wang L-K, Chen M-L, et al. Phospholipase A/Acyltransferase enzyme activity of H-rev107 inhibits the H-RAS signaling pathway. *Journal of biomedical science*. 2014;21(1):1-9.
96. Tsai F-M, Shyu R-Y, Jiang S-Y. RIG1 suppresses Ras activation and induces cellular apoptosis at the Golgi apparatus. *Cellular signalling*. 2007;19(5):989-99.

97. Morales M, Arenas EJ, Urosevic J, Guiu M, Fernández E, Planet E, et al. RARRES 3 suppresses breast cancer lung metastasis by regulating adhesion and differentiation. *EMBO molecular medicine*. 2014;6(7):865-81.
98. Jin X-H, Uyama T, Wang J, Okamoto Y, Tonai T, Ueda N. cDNA cloning and characterization of human and mouse Ca²⁺-independent phosphatidylethanolamine N-acyltransferases. *Biochimica et Biophysica Acta (BBA)-Molecular and Cell Biology of Lipids*. 2009;1791(1):32-8.
99. Golczak M, Palczewski K. An acyl-covalent enzyme intermediate of lecithin: retinol acyltransferase. *Journal of Biological Chemistry*. 2010;285(38):29217-22.
100. Ren X, Lin J, Jin C, Xia B. Solution structure of the N-terminal catalytic domain of human H-REV107—a novel circularly permuted NlpC/P60 domain. *FEBS letters*. 2010;584(19):4222-6.
101. Jin X-H, Okamoto Y, Morishita J, Tsuboi K, Tonai T, Ueda N. Discovery and characterization of a Ca²⁺-independent phosphatidylethanolamine N-acyltransferase generating the anandamide precursor and its congeners. *Journal of Biological Chemistry*. 2007;282(6):3614-23.
102. Amidon B, Brown A, Waite M. Transacylase and phospholipases in the synthesis of bis (monoacylglycero) phosphate. *Biochemistry*. 1996;35(44):13995-4002.
103. Duncan RE, Sarkadi-Nagy E, Jaworski K, Ahmadian M, Sul HS. Identification and functional characterization of adipose-specific phospholipase A2 (AdPLA). *Journal of biological chemistry*. 2008;283(37):25428-36.
104. Uyama T, Ikematsu N, Inoue M, Shinohara N, Jin X-H, Tsuboi K, et al. Generation of N-acylphosphatidylethanolamine by members of the phospholipase A/acyltransferase (PLA/AT) family. *Journal of Biological Chemistry*. 2012;287(38):31905-19.
105. Uyama T, Morishita J, Jin X-H, Okamoto Y, Tsuboi K, Ueda N. The tumor suppressor gene H-Rev107 functions as a novel Ca²⁺-independent cytosolic phospholipase A1/2 of the thiol hydrolase type. *Journal of lipid research*. 2009;50(4):685-93.
106. Uyama T, Inoue M, Okamoto Y, Shinohara N, Tai T, Tsuboi K, et al. Involvement of phospholipase A/acyltransferase-1 in N-acylphosphatidylethanolamine generation. *Biochimica et Biophysica Acta (BBA)-Molecular and Cell Biology of Lipids*. 2013;1831(12):1690-701.
107. Ueda N, Tsuboi K, Uyama T. Enzymological studies on the biosynthesis of N-acylethanolamines. *Biochimica et Biophysica Acta (BBA)-Molecular and Cell Biology of Lipids*. 2010;1801(12):1274-85.
108. Hussain Z, Uyama T, Tsuboi K, Ueda N. Mammalian enzymes responsible for the biosynthesis of N-acylethanolamines. *Biochimica et Biophysica Acta (BBA)-Molecular and Cell Biology of Lipids*. 2017;1862(12):1546-61.
109. Coulon D, Faure L, Salmon M, Wattalet V, Bessoule J-J. Occurrence, biosynthesis and functions of N-acylphosphatidylethanolamines (NAPE): not just precursors of N-acylethanolamines (NAE). *Biochimie*. 2012;94(1):75-85.
110. Jaworski K, Ahmadian M, Duncan RE, Sarkadi-Nagy E, Varady KA, Hellerstein MK, et al. AdPLA ablation increases lipolysis and prevents obesity induced by high-fat feeding or leptin deficiency. *Nature medicine*. 2009;15(2):159-68.
111. DiSepio D, Ghosn C, Eckert RL, Deucher A, Robinson N, Duvic M, et al. Identification and characterization of a retinoid-induced class II tumor suppressor/growth regulatory gene. *Proceedings of the National Academy of Sciences*. 1998;95(25):14811-5.

112. Huang S-L, Shyu R-Y, Yeh M-Y, Jiang S-Y. Cloning and characterization of a novel retinoid-inducible gene 1 (RIG1) deriving from human gastric cancer cells. *Molecular and cellular endocrinology*. 2000;159(1-2):15-24.
113. Casanova B, De la Fuente M, Garcia-Gila M, Sanz L, Silva A, Garcia-Marco J, et al. The class II tumor-suppressor gene RARRES3 is expressed in B cell lymphocytic leukemias and down-regulated with disease progression. *Leukemia*. 2001;15(10):1521-6.
114. Jans R, Sturniolo MT, Eckert RL. Localization of the TIG3 transglutaminase interaction domain and demonstration that the amino-terminal region is required for TIG3 function as a keratinocyte differentiation regulator. *Journal of investigative dermatology*. 2008;128(3):517-29.
115. Yamano Y, Asano A, Ohyama K, Ohta M, Nishio R, Morishima I. Expression of the Ha-ras suppressor family member 5 gene in the maturing rat testis. *Bioscience, biotechnology, and biochemistry*. 2008;72(5):1360-3.
116. Hansen HS, Kleberg K, Hassing HA. Non-endocannabinoid N-acylethanolamines and monoacylglycerols: old molecules new targets. *The endocannabinoidome: Elsevier*; 2015. p. 1-13.
117. Simon GM, Cravatt BF. Anandamide biosynthesis catalyzed by the phosphodiesterase GDE1 and detection of glycerophospho-N-acyl ethanolamine precursors in mouse brain. *Journal of Biological Chemistry*. 2008;283(14):9341-9.
118. Okamoto Y, Morishita J, Tsuboi K, Tonai T, Ueda N. Molecular characterization of a phospholipase D generating anandamide and its congeners. *Journal of Biological Chemistry*. 2004;279(7):5298-305.
119. Ueda N, Tsuboi K, Uyama T. N-acylethanolamine metabolism with special reference to N-acylethanolamine-hydrolyzing acid amidase (NAAA). *Progress in lipid research*. 2010;49(4):299-315.
120. Kaczocha M, Glaser ST, Maher T, Clavin B, Hamilton J, Rourke JO, et al. Fatty acid binding protein deletion suppresses inflammatory pain through endocannabinoid/N-acylethanolamine-dependent mechanisms. *Molecular Pain*. 2015;11:s12990-015-0056-8.
121. Tsuboi K, Uyama T, Okamoto Y, Ueda N. Endocannabinoids and related N-acylethanolamines: biological activities and metabolism. *Inflammation and Regeneration*. 2018;38:1-10.
122. Fu J, Gaetani S, Oveisi F, Lo Verme J, Serrano A, Rodríguez de Fonseca F, et al. Oleylethanolamide regulates feeding and body weight through activation of the nuclear receptor PPAR- α . *Nature*. 2003;425(6953):90-3.
123. Cravatt BF, Giang DK, Mayfield SP, Boger DL, Lerner RA, Gilula NB. Molecular characterization of an enzyme that degrades neuromodulatory fatty-acid amides. *Nature*. 1996;384(6604):83-7.
124. Scherma M, Masia P, Satta V, Fratta W, Fadda P, Tanda G. Brain activity of anandamide: a rewarding bliss? *Acta Pharmacologica Sinica*. 2019;40(3):309-23.
125. Di Marzo V, Fontana A, Cadas H, Schinelli S, Cimino G, Schwartz J-C, et al. Formation and inactivation of endogenous cannabinoid anandamide in central neurons. *Nature*. 1994;372(6507):686-91.
126. Hansen HS, Diep TA. N-acylethanolamines, anandamide and food intake. *Biochemical pharmacology*. 2009;78(6):553-60.

127. Pertwee RG. The pharmacology of cannabinoid receptors and their ligands: an overview. *International journal of obesity*. 2006;30(1):S13-S8.
128. Di Marzo V, Bisogno T, De Petrocellis L. Anandamide: some like it hot. *Trends in pharmacological sciences*. 2001;22(7):346-9.
129. Mallet P, Beninger R. The endogenous cannabinoid receptor agonist anandamide impairs memory in rats. *Behavioural pharmacology*. 1996;7(3):276-84.
130. Goonawardena AV, Sesay J, Sexton CA, Riedel G, Hampson RE. Pharmacological elevation of anandamide impairs short-term memory by altering the neurophysiology in the hippocampus. *Neuropharmacology*. 2011;61(5-6):1016-25.
131. Garani R, Watts JJ, Mizrahi R. Endocannabinoid system in psychotic and mood disorders, a review of human studies. *Progress in Neuro-Psychopharmacology and Biological Psychiatry*. 2021;106:110096.
132. Jamshidi N, Taylor DA. Anandamide administration into the ventromedial hypothalamus stimulates appetite in rats. *British journal of pharmacology*. 2001;134(6):1151-4.
133. Piomelli D, Giuffrida A, Calignano A, de Fonseca FRG. The endocannabinoid system as a target for therapeutic drugs. *Trends in pharmacological sciences*. 2000;21(6):218-24.
134. Leweke FM, Giuffrida A, Wurster U, Emrich HM, Piomelli D. Elevated endogenous cannabinoids in schizophrenia. *Neuroreport*. 1999;10(8):1665-9.
135. Hill MN, Gorzalka BB. Is there a role for the endocannabinoid system in the etiology and treatment of melancholic depression? *Behavioural pharmacology*. 2005;16(5-6):333-52.
136. Pacher P, Kunos G. Modulating the endocannabinoid system in human health and disease—successes and failures. *The FEBS journal*. 2013;280(9):1918-43.
137. LoVerme J, Russo R, La Rana G, Fu J, Farthing J, Mattace-Raso G, et al. Rapid broad-spectrum analgesia through activation of peroxisome proliferator-activated receptor- α . *Journal of Pharmacology and Experimental Therapeutics*. 2006;319(3):1051-61.
138. LoVerme J, La Rana G, Russo R, Calignano A, Piomelli D. The search for the palmitoylethanolamide receptor. *Life sciences*. 2005;77(14):1685-98.
139. Lambert DM, Vandevoorde S, Jonsson K-O, Fowler CJ. The palmitoylethanolamide family: a new class of anti-inflammatory agents? *Current medicinal chemistry*. 2002;9(6):663-74.
140. Calignano A, La Rana G, Piomelli D. Antinociceptive activity of the endogenous fatty acid amide, palmitoylethanolamide. *European journal of pharmacology*. 2001;419(2-3):191-8.
141. Calignano A, Rana GL, Giuffrida A, Piomelli D. Control of pain initiation by endogenous cannabinoids. *Nature*. 1998;394(6690):277-81.
142. Lambert DM, Vandevoorde S, Diependaele G, Govaerts SJ, Robert AR. Anticonvulsant activity of N-palmitoylethanolamide, a putative endocannabinoid, in mice. *Epilepsia*. 2001;42(3):321-7.
143. Sheerin AH, Zhang X, Saucier DM, Corcoran ME. Selective antiepileptic effects of N-palmitoylethanolamide, a putative endocannabinoid. *Epilepsia*. 2004;45(10):1184-8.
144. Di MARZO V, MELCK D, ORLANDO P, BISOGNO T, ZAGOORY O, BIFULCO M, et al. Palmitoylethanolamide inhibits the expression of fatty acid amide hydrolase and enhances the anti-proliferative effect of anandamide in human breast cancer cells. *Biochemical Journal*. 2001;358(1):249-55.

145. Romano A, Coccorello R, Giacobuzzo G, Bedse G, Moles A, Gaetani S. Oleoylethanolamide: a novel potential pharmacological alternative to cannabinoid antagonists for the control of appetite. *BioMed research international*. 2014;2014.
146. Tutunchi H, Saghafi-Asl M, Ostadrahimi A. A systematic review of the effects of oleoylethanolamide, a high-affinity endogenous ligand of PPAR- α , on the management and prevention of obesity. *Clinical and Experimental Pharmacology and Physiology*. 2020;47(4):543-52.
147. Yu Y, Park SJ, Beyak MJ. Inducible nitric oxide synthase-derived nitric oxide reduces vagal satiety signalling in obese mice. *The Journal of Physiology*. 2019;597(6):1487-502.
148. Artmann A, Petersen G, Hellgren LI, Boberg J, Skonberg C, Nellesmann C, et al. Influence of dietary fatty acids on endocannabinoid and N-acylolethanolamine levels in rat brain, liver and small intestine. *Biochimica et Biophysica Acta (BBA)-Molecular and Cell Biology of Lipids*. 2008;1781(4):200-12.
149. Ishida T, Nishiumi S, Tanahashi T, Yamasaki A, Yamazaki A, Akashi T, et al. Linoleoyl ethanolamide reduces lipopolysaccharide-induced inflammation in macrophages and ameliorates 2, 4-dinitrofluorobenzene-induced contact dermatitis in mice. *European journal of pharmacology*. 2013;699(1-3):6-13.
150. Maccarrone M, Cartoni A, Parolaro D, Margonelli A, Massi P, Bari M, et al. Cannabimimetic activity, binding, and degradation of stearoylethanolamide within the mouse central nervous system. *Molecular and Cellular Neuroscience*. 2002;21(1):126-40.
151. Kosiakova H, Berdyshev A, Dosenko V, Drevytska T, Herasymenko O, Hula N. The involvement of peroxisome proliferator-activated receptor gamma (PPAR γ) in anti-inflammatory activity of N-stearoylethanolamine. *Heliyon*. 2022;8(11).
152. Berdyshev AG, Kosiakova HV, Onopchenko OV, Panchuk RR, Stoika RS, Hula NM. N-Stearoylethanolamine suppresses the pro-inflammatory cytokines production by inhibition of NF- κ B translocation. *Prostaglandins & other lipid mediators*. 2015;121:91-6.
153. Terrazzino S, Berto F, Carbonare MD, Fabris M, Guiotto A, Bernardini D, et al. Stearoylethanolamide exerts anorexic effects in mice via downregulation of liver stearyl-coenzyme A desaturase-1 mRNA expression. *The FASEB Journal*. 2004;18(13):1580-2.
154. Morishita H, Eguchi T, Tsukamoto S, Sakamaki Y, Takahashi S, Saito C, et al. Organelle degradation in the lens by PLAAT phospholipases. *Nature*. 2021;592(7855):634-8.
155. Rahman SK, Sasaki S, Uyama T, Hussain Z, Sikder MM, Saiga H, et al. PLAAT1 deficiency alleviates high-fat diet-induced hepatic lipid accumulation in mice. *The FASEB Journal*. 2023;37(7):e23032.
156. Phoon CK, Acehan D, Schlame M, Stokes DL, Edelman-Novemsky I, Yu D, et al. Tafazzin knockdown in mice leads to a developmental cardiomyopathy with early diastolic dysfunction preceding myocardial noncompaction. *Journal of the American Heart Association*. 2012;1(2):e000455.
157. Kim J, Lee K, Fujioka H, Tandler B, Hoppel CL. Cardiac mitochondrial structure and function in tafazzin-knockdown mice. *Mitochondrion*. 2018;43:53-62.
158. Cole LK, Kim JH, Amoscato AA, Tyurina YY, Bayir H, Karimi B, et al. Aberrant cardiolipin metabolism is associated with cognitive deficiency and hippocampal alteration in tafazzin knockdown mice. *Biochimica et Biophysica Acta (BBA)-Molecular Basis of Disease*. 2018;1864(10):3353-67.

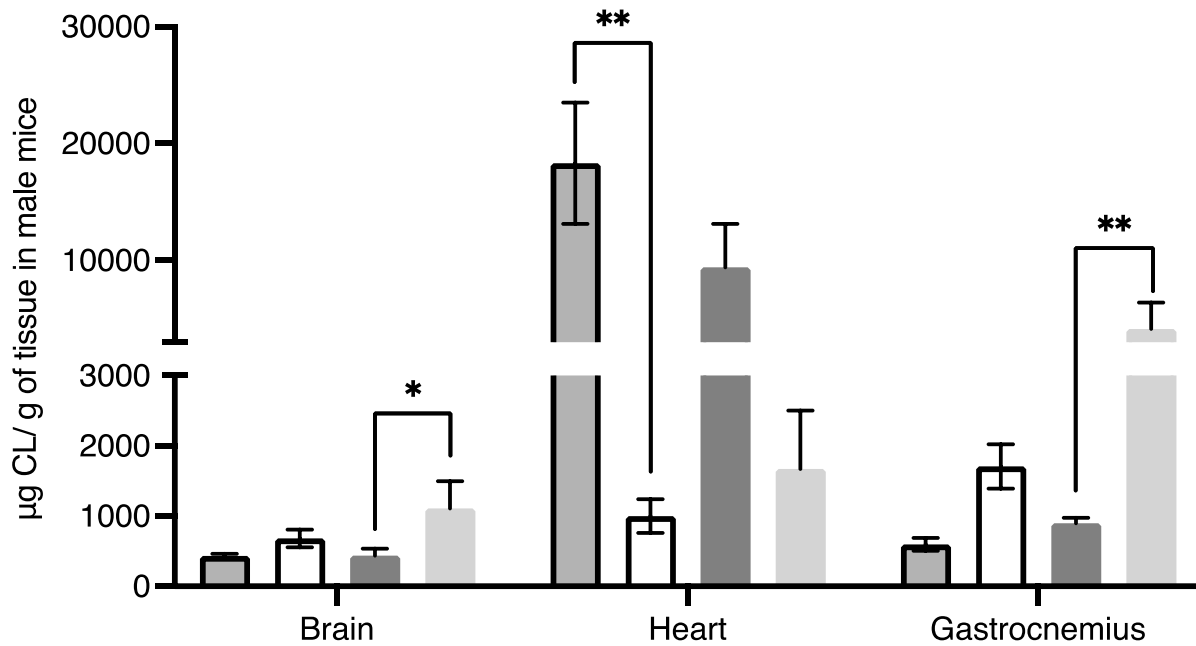
159. Soustek MS, Baligand C, Falk DJ, Walter GA, Lewin AS, Byrne BJ. Endurance training ameliorates complex 3 deficiency in a mouse model of Barth syndrome. *Journal of inherited metabolic disease*. 2015;38(5):915-22.
160. Powers C, Huang Y, Strauss AW, Khuchua Z. Diminished exercise capacity and mitochondrial bc1 complex deficiency in tafazzin-knockdown mice. *Frontiers in physiology*. 2013;4:74.
161. Huang Y, Powers C, Madala SK, Greis KD, Haffey WD, Towbin JA, et al. Cardiac metabolic pathways affected in the mouse model of Barth syndrome. *PloS one*. 2015;10(6):e0128561.
162. Wang S, Li Y, Xu Y, Ma Q, Lin Z, Schlame M, et al. AAV gene therapy prevents and reverses heart failure in a murine knockout model of Barth syndrome. *Circulation research*. 2020;126(8):1024-39.
163. Tomczewski MV, Chan JZ, Campbell ZE, Strathdee D, Duncan RE. Phenotypic Characterization of Male Tafazzin-Knockout Mice at 3, 6, and 12 Months of Age. *Biomedicines*. 2023;11(2):638.
164. Sohn J, Milosevic J, Brouse T, Aziz N, Elkhoury J, Wang S, et al. A new murine model of Barth syndrome neutropenia links TAFAZZIN deficiency to increased ER stress-induced apoptosis. *Blood advances*. 2022;6(8):2557-77.
165. Song C, Zhang J, Qi S, Liu Z, Zhang X, Zheng Y, et al. Cardiolipin remodeling by ALCAT1 links mitochondrial dysfunction to Parkinson's diseases. *Aging cell*. 2019;18(3):e12941.
166. Liu X, Ye B, Miller S, Yuan H, Zhang H, Tian L, et al. Ablation of ALCAT1 mitigates hypertrophic cardiomyopathy through effects on oxidative stress and mitophagy. *Molecular and cellular biology*. 2012;32(21):4493-504.
167. Mejia EM, Ibdah JA, Sparagna GC, Hatch GM. Differential reduction in cardiac and liver monolysocardiolipin acyltransferase-1 and reduction in cardiac and liver tetralinoleoyl-cardiolipin in the α -subunit of trifunctional protein heterozygous knockout mice. *Biochemical Journal*. 2015;471(1):123-9.
168. Sharma P, Martis PC, Excoffon KJ. Adenovirus transduction: More complicated than receptor expression. *Virology*. 2017;502:144-51.
169. Chatterjee SD, Zhou J, Dasgupta R, Cramer-Blok A, Timmer M, van der Stelt M, et al. Protein dynamics influence the enzymatic activity of phospholipase A/Acyltransferases 3 and 4. *Biochemistry*. 2021;60(15):1178-90.
170. Wang S, Yazawa E, Keating EM, Mazumdar N, Hauschild A, Ma Q, et al. Genetic modifiers modulate phenotypic expression of tafazzin deficiency in a mouse model of Barth syndrome. *Human Molecular Genetics*. 2023;32(12):2055-67.
171. Wasilewski M, Więckowski MR, Dymkowska D, Wojtczak L. Effects of N-acylethanolamines on mitochondrial energetics and permeability transition. *Biochimica et Biophysica Acta (BBA)-Bioenergetics*. 2004;1657(2-3):151-63.
172. Lu B, Jiang YJ, Zhou Y, Xu FY, Hatch GM, Choy PC. Cloning and characterization of murine 1-acyl-sn-glycerol 3-phosphate acyltransferases and their regulation by PPAR α in murine heart. *Biochemical Journal*. 2005;385(2):469-77.
173. Jiang YJ, Lu B, Xu FY, Gartshore J, Taylor WA, Halayko AJ, et al. Stimulation of cardiac cardiolipin biosynthesis by PPAR α activation. *Journal of lipid research*. 2004;45(2):244-52.

174. Heyman E, Gamelin FX, Aucouturier J, Di Marzo V. The role of the endocannabinoid system in skeletal muscle and metabolic adaptations to exercise: potential implications for the treatment of obesity. *obesity reviews*. 2012;13(12):1110-24.
175. Folch J, Lees M, Stanley GS. A simple method for the isolation and purification of total lipides from animal tissues. *Journal of biological chemistry*. 1957;226(1):497-509.
176. Pennington ER, Funai K, Brown DA, Shaikh SR. The role of cardiolipin concentration and acyl chain composition on mitochondrial inner membrane molecular organization and function. *Biochimica et Biophysica Acta (BBA)-Molecular and Cell Biology of Lipids*. 2019;1864(7):1039-52.
177. Courtade S, Marinetti G, Stotz E. The structure and abundance of rat tissue cardiolipins. *Biochimica et Biophysica Acta (BBA)-Lipids and Lipid Metabolism*. 1967;137(1):121-34.
178. Kakisaka K, Cazanave SC, Fingas CD, Guicciardi ME, Bronk SF, Werneburg NW, et al. LYSPHOSPHATIDYLCHOLINE IS A LIKELY MEDIATOR OF FREE FATTY ACID-INDUCED HEPATOCYTE LIPOAPOPTOSIS: 60. *Hepatology*. 2011;54(4):389A.
179. Lehmann R, Franken H, Dammeier S, Rosenbaum L, Kantartzis K, Peter A, et al. Circulating lysophosphatidylcholines are markers of a metabolically benign nonalcoholic fatty liver. *Diabetes care*. 2013;36(8):2331-8.
180. He Q, Wang M, Harris N, Han X. Tafazzin knockdown interrupts cell cycle progression in cultured neonatal ventricular fibroblasts. *American Journal of Physiology-Heart and Circulatory Physiology*. 2013;305(9):H1332-H43.
181. Mahler SV, Smith KS, Berridge KC. Endocannabinoid hedonic hotspot for sensory pleasure: anandamide in nucleus accumbens shell enhances 'liking' of a sweet reward. *Neuropsychopharmacology*. 2007;32(11):2267-78.
182. Mallick A, Gautam A. Mendelian Crosses. 2018.
183. Udalova L. Sex ratio in hybrid mice CBA X C57BL. *Biulleten'Eksperimental'noi Biologii i Meditsiny*. 1979;88(10):473-4.
184. Kathuria S, Gaetani S, Fegley D, Valiño F, Duranti A, Tontini A, et al. Modulation of anxiety through blockade of anandamide hydrolysis. *Nature medicine*. 2003;9(1):76-81.
185. Koltyn KF, Brellenthin AG, Cook DB, Sehgal N, Hillard C. Mechanisms of exercise-induced hypoalgesia. *The Journal of Pain*. 2014;15(12):1294-304.
186. Randall MD, Harris D, Kendall DA, Ralevic V. Cardiovascular effects of cannabinoids. *Pharmacology & therapeutics*. 2002;95(2):191-202.
187. Suardiaz M, Estivill-Torrús G, Goicoechea C, Bilbao A, de Fonseca FR. Analgesic properties of oleoylethanolamide (OEA) in visceral and inflammatory pain. *PAIN®*. 2007;133(1-3):99-110.
188. Bouter Y, Brzózka MM, Rygula R, Pahlisch F, Boost C, Leweke FM, et al. Chronic psychosocial stress causes increased anxiety-like behavior and alters endocannabinoid levels in the brain of C57Bl/6J Mice. *Cannabis and Cannabinoid Research*. 2020;5(1):51-61.
189. Verme JL, Fu J, Astarita G, La Rana G, Russo R, Calignano A, et al. The nuclear receptor peroxisome proliferator-activated receptor- α mediates the anti-inflammatory actions of palmitoylethanolamide. *Molecular pharmacology*. 2005;67(1):15-9.
190. Chen Y, Liu J, Yao Y, Yan H, Su R. Rearing behaviour in the mouse behavioural pattern monitor distinguishes the effects of psychedelics from those of lisuride and TBG. *Frontiers in Pharmacology*. 2023;14:1021729.

191. Lin Y-H, Liu A-H, Xu Y, Tie L, Yu H-M, Li X-J. Effect of chronic unpredictable mild stress on brain–pancreas relative protein in rat brain and pancreas. *Behavioural brain research*. 2005;165(1):63-71.
192. Hussain Z, Uyama T, Kawai K, Rahman IAS, Tsuboi K, Araki N, et al. Comparative analyses of isoforms of the calcium-independent phosphatidylethanolamine N-acyltransferase PLAAT-1 in humans and mice. *Journal of lipid research*. 2016;57(11):2051-60.
193. Chan JZ, Fernandes MF, Steckel KE, Bradley RM, Hashemi A, Groh MR, et al. N-oleoylethanolamide treatment of lymphoblasts deficient in Tafazzin improves cell growth and mitochondrial morphology and dynamics. *Scientific Reports*. 2022;12(1):9466.
194. Almada M, Domingues MR, Dória ML, Fonseca BM, Teixeira NA, Correia-da-Silva G. Lipidomic approach towards deciphering anandamide effects in rat decidual cell. *Journal of cellular physiology*. 2015;230(7):1549-57.
195. Ueda N, Tsuboi K, Uyama T. Metabolism of endocannabinoids and related N-acylethanolamines: Canonical and alternative pathways. *The FEBS journal*. 2013;280(9):1874-94.
196. Lee SS, Chan W-Y, Lo CK, Wan DC, Tsang DS, Cheung W-T. Requirement of PPAR α in maintaining phospholipid and triacylglycerol homeostasis during energy deprivation. *Journal of lipid research*. 2004;45(11):2025-37.
197. Martin LM, Jeyabalan N, Tripathi R, Panigrahi T, Johnson PJ, Ghosh A, et al. Autophagy in corneal health and disease: A concise review. *The ocular surface*. 2019;17(2):186-97.
198. Deretic V, Saitoh T, Akira S. Autophagy in infection, inflammation and immunity. *Nature Reviews Immunology*. 2013;13(10):722-37.
199. Hailfinger S, Schulze-Osthoff K. Impaired autophagy in psoriasis and atopic dermatitis: a new therapeutic target? *Journal of Investigative Dermatology*. 2021;141(12):2775-7.
200. Bambico FR, Cassano T, Dominguez-Lopez S, Katz N, Walker CD, Piomelli D, et al. Genetic deletion of fatty acid amide hydrolase alters emotional behavior and serotonergic transmission in the dorsal raphe, prefrontal cortex, and hippocampus. *Neuropsychopharmacology*. 2010;35(10):2083-100.
201. Cao J, Shen W, Chang Z, Shi Y. ALCAT1 is a polyglycerophospholipid acyltransferase potently regulated by adenine nucleotide and thyroid status. *American Journal of Physiology-Endocrinology and Metabolism*. 2009;296(4):E647-E53.
202. Zhang K, Chan V, Botelho RJ, Antonescu CN. A tail of their own: regulation of cardiolipin and phosphatidylinositol fatty acyl profile by the acyltransferase LCLAT1. *Biochemical Society Transactions*. 2023.
203. Djafarzadeh S, Jakob SM. High-resolution respirometry to assess mitochondrial function in permeabilized and intact cells. *JoVE (Journal of Visualized Experiments)*. 2017(120):e54985.
204. Rodgers R, Dalvi A. Anxiety, defence and the elevated plus-maze. *Neuroscience & Biobehavioral Reviews*. 1997;21(6):801-10.

Appendices

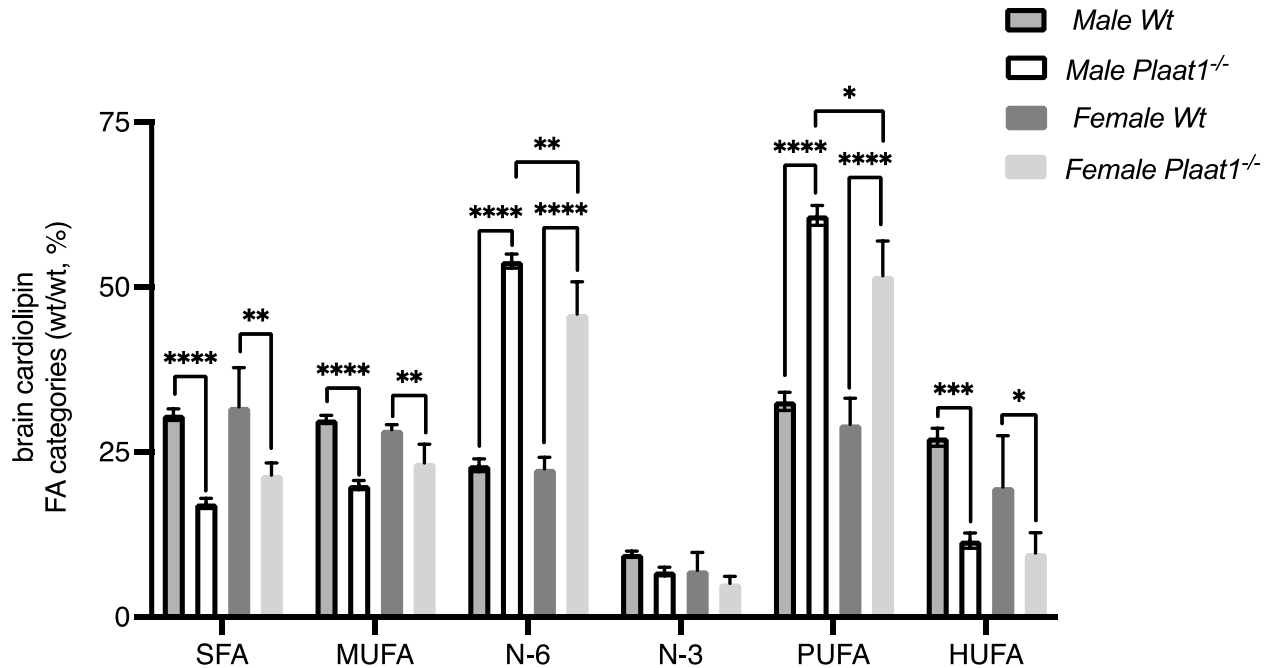
Appendix A: 2-way ANOVA analysis for determining sex differences in total cardiolipin content.



Appendix Figure 1: Total CL content is not different between male and female *Wt* and *Plaat1*^{-/-} Mice.

Total CL concentrations in brain, heart and gastrocnemius tissues of *Wt* and *Plaat1*^{-/-} male and female mice. Data are means \pm S.E.M; n = 4-5. *P < 0.05, **P < 0.01.

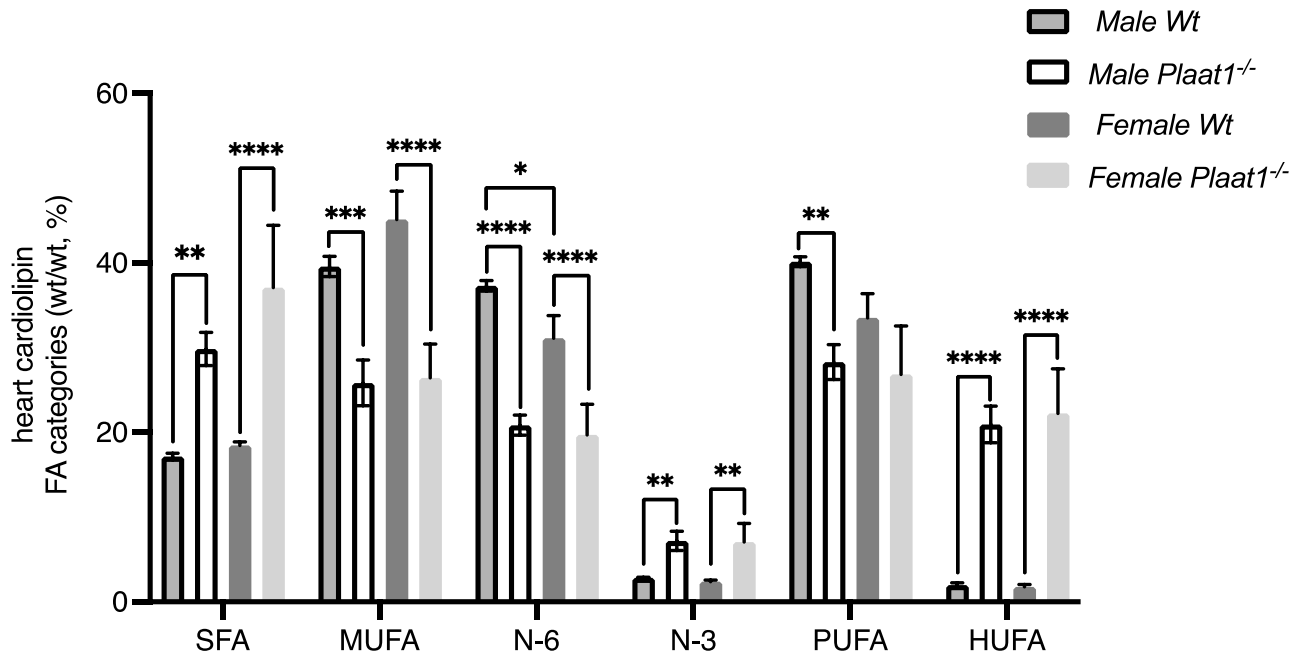
Appendix B: 2-way ANOVA analysis for determining sex differences in brain cardiolipin composition.



Appendix Figure 2: Male and female *Plaat1*^{-/-} mice display differences in total N-6 and PUFA composition.

CL was isolated from brain, and the fatty acyl content and composition were analyzed by gas chromatography in tissues taken from *Wt* and *Plaat1*^{-/-} mice. The relative proportional abundances of fatty acyl classes were analyzed as mass percentages for male and female mice. Data are means \pm S.E.M; n = 5. *P < 0.05, **P < 0.01, ***P < 0.001, ****P < 0.0001.

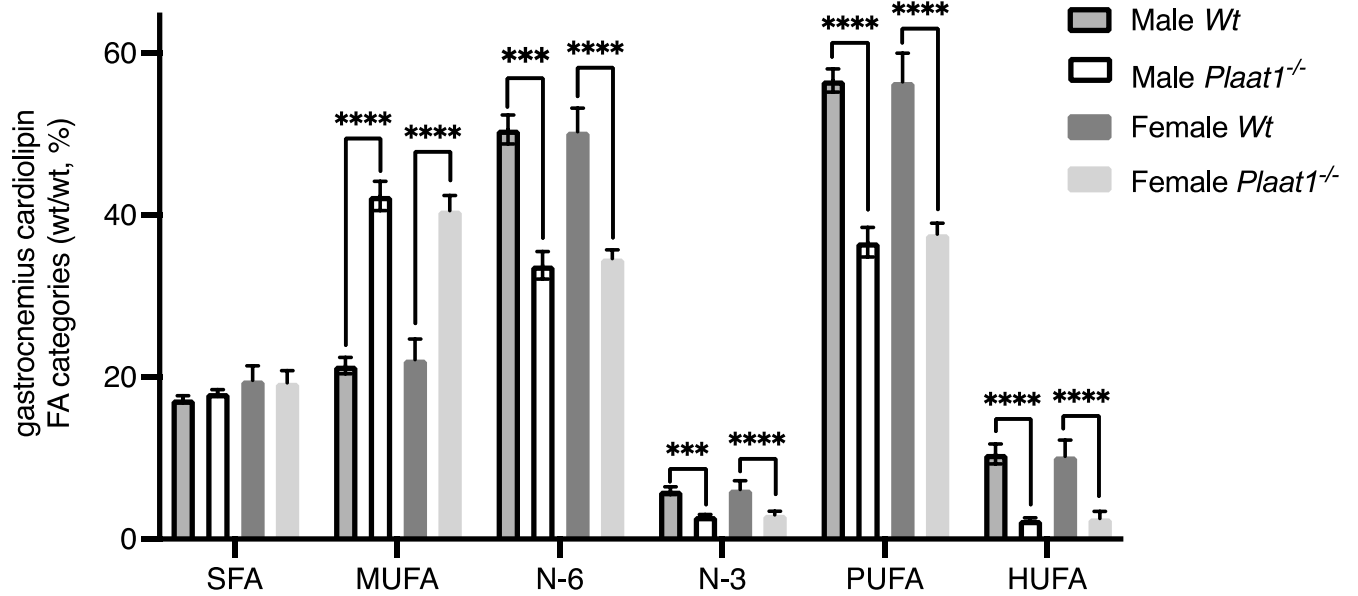
Appendix C: 2-way ANOVA analysis for determining sex differences in heart cardioliipin composition.



Appendix Figure 3: Male and female *Wt* mice display differences in total N-6 composition.

CL was isolated from the heart, and the fatty acyl content and composition were analyzed by gas chromatography in tissues taken from *Wt* and *Plaat1*^{-/-} mice. The relative proportional abundances of fatty acyl classes were analyzed as mass percentages for male and female mice. Data are means \pm S.E.M; n = 5. *P < 0.05, **P < 0.01, ***P < 0.001, ****P < 0.0001.

Appendix D: 2-way ANOVA analysis for determining sex differences in gastrocnemius cardiolipin composition.



Appendix Figure 4: Gastrocnemius CL composition is not different between male and female *Wt* and *Plaat1*^{-/-} Mice.

CL was isolated from the heart, and the fatty acyl content and composition were analyzed by gas chromatography in tissues taken from *Wt* and *Plaat1*^{-/-} mice. The relative proportional abundances of fatty acyl classes were analyzed as mass percentages for male and female mice. Data are means \pm S.E.M; n = 5. ***P < 0.001, ****P < 0.0001.

Appendix E: Fatty acyl composition of CL isolated from brain tissues of *Plaat1*^{-/-} and *Wt* mice.

Fatty Acid	Male <i>Wt</i>	Male <i>Plaat1</i> ^{-/-}	Female <i>Wt</i>	Female <i>Plaat1</i> ^{-/-}
Total SFA	30.67 ± 0.89	17.21 ± 0.76 ****	31.86 ± 2.30	21.51 ± 0.83 **
10:0	0.16 ± 0.08	0.03 ± 0.01	0.03 ± 0.02	0.03 ± 0.02
12:0	0.09 ± 0.04	0.02 ± 0.02	0.03 ± 0.02	0.05 ± 0.02
14:0	0.23 ± 0.05	0.35 ± 0.09	0.24 ± 0.10	0.62 ± 0.10 *
15:0	0.23 ± 0.06	0.06 ± 0.03 *	0.12 ± 0.07	0.13 ± 0.05
16:0	11.27 ± 0.65	10.60 ± 0.87	8.88 ± 2.89	13.51 ± 0.96
17:0	0.40 ± 0.10	0.17 ± 0.04	0.29 ± 0.10	0.18 ± 0.01
18:0	15.91 ± 0.65	5.45 ± 0.34 ****	18.05 ± 0.91	6.48 ± 0.60 ****
20:0	1.05 ± 0.12	0.37 ± 0.02 **	0.72 ± 0.12	0.26 ± 0.04
22:0	0.64 ± 0.15	0.17 ± 0.07 *	0.39 ± 0.08	0.20 ± 0.04
24:0	0.67 ± 0.19	0.07 ± 0.04 *	0.45 ± 0.10	0.07 ± 0.01 **
Total MUFA	29.94 ± 0.62	20.01 ± 0.68 ****	28.38 ± 0.34	23.35 ± 1.41**
12:1	0.18 ± 0.10	0.02 ± 0.01	0.06 ± 0.02	0.07 ± 0.03
14:1	0.13 ± 0.04	0.02 ± 0.01 *	0.09 ± 0.06	0.09 ± 0.01
18:1n-7	5.15 ± 0.16	3.84 ± 0.24 **	3.59 ± 0.46	3.65 ± 0.31
18:1n-9	19.58 ± 0.59	12.52 ± 0.57 ****	21.07 ± 0.71	16.38 ± 1.05
20:1n-9	1.53 ± 0.10	1.28 ± 0.19	1.37 ± 0.19	0.78 ± 0.09 *
22:1n-9	0.86 ± 0.11	0.39 ± 0.17	0.47 ± 0.08	0.29 ± 0.08
Total Omega-6	22.99 ± 0.97	53.93 ± 1.06 ****	22.43 ± 0.79	45.90 ± 2.19 ****
18:2n-6	4.31 ± 0.28	47.22 ± 0.98 ****	8.5 ± 1.73	40.09 ± 1.76 ****
18:3n-6	0.14 ± 0.06	0.18 ± 0.06	0.07 ± 0.04	0.09 ± 0.03
20:2n-6	0.23 ± 0.06	0.67 ± 0.17	0.21 ± 0.02	0.66 ± 0.07
20:3n-6	1.21 ± 0.07	2.17 ± 0.40 *	0.76 ± 0.13	0.91 ± 0.13
20:4n-6	15.13 ± 0.84	2.55 ± 0.58 ****	11.18 ± 2.14	2.95 0.43 **
22:2n-6	0.19 ± 0.11	0.09 ± 0.08	0.17 ± 0.03	0.20 ± 0.07
22:4n-6	1.55 ± 0.15	0.61 ± 0.18 **	1.31 ± 0.11	0.55 ± 0.13 **
22:5n-6	0.23 ± 0.06	0.43 ± 0.15	0.23 ± 0.02	0.45 ± 0.10
Total Omega-3	9.54 ± 0.44	6.87 ± 0.64	7.07 ± 1.35	5.09 ± 0.55
18:3n-3	0.38 ± 0.13	0.96 ± 0.04 **	0.30 ± 0.10	0.90 ± 0.07 **
18:4n-3	0.19 ± 0.06	0.15 ± 0.09	0.08 ± 0.09	0.09 ± 0.04
20:3n-3	0.22 ± 0.08	0.11 ± 0.06	0.04 ± 0.03	0.13 ± 0.06
20:4n-3	0.39 ± 0.24	0.05 ± 0.03	0.10 ± 0.09	0.06 ± 0.02
20:5n-3	0.26 ± 0.07	0.15 ± 0.12	0.08 ± 0.05	0.06 ± 0.02
22:5n-3	0.50 ± 0.13	1.02 ± 0.28	0.14 ± 0.05	0.60 ± 0.12 **
22:6n-3	7.61 ± 0.37	4.44 ± 0.72 **	6.6 ± 1.40	3.3 ± 0.36

Data are means (wt/wt, %) ± S.E.M calculated by Student's t-test within each sex; n = 5.

*P < 0.05, **P < 0.01, ***P < 0.001, ****P < 0.0001, versus.

Appendix F: Fatty acyl composition of CL isolated from heart tissues of *Plaat1^{-/-}* and *Wt* mice.

Fatty Acid	Male <i>Wt</i>	Male <i>Plaat1^{-/-}</i>	Female <i>Wt</i>	Female <i>Plaat1^{-/-}</i>
Total SFA	15.85 ± 0.40	25.08 ± 1.96 ****	17.94 ± 0.19	37.11 ± 3.23 ***
10:0	0.01 ± 0.00	0.02 ± 0.01	0.00 ± 0.00	0.10 ± 0.05
12:0	0.03 ± 0.01	0.02 ± 0.01	0.04 ± 0.00	0.05 ± 0.02
14:0	0.77 ± 0.02	0.31 ± 0.07 ***	0.77 ± 0.05	0.19 ± 0.03 ****
15:0	0.14 ± 0.01	0.13 ± 0.06	0.12 ± 0.01	0.12 ± 0.08
16:0	14.57 ± 0.48	10.19 ± 2.49	15.30 ± 0.13	11.68 ± 1.75
17:0	0.11 ± 0.01	0.21 ± 0.05	0.13 ± 0.00	0.24 ± 0.04 *
18:0	1.36 ± 0.19	16.99 ± 1.33 ****	1.90 ± 0.07	22.63 ± 2.57 ****
20:0	0.07 ± 0.01	0.86 ± 0.08 ****	0.11 ± 0.01	0.90 ± 0.13 ***
22:0	0.06 ± 0.02	0.49 ± 0.03 ****	0.04 ± 0.01	0.57 ± 0.13 **
24:0	0.04 ± 0.02	0.63 ± 0.10 ***	0.03 ± 0.01	0.62 ± 0.15 **
Total MUFA	39.58 ± 1.19	25.83 ± 2.71 **	45.14 ± 1.48	26.46 ± 1.78 ****
12:1	0.02 ± 0.01	0.08 ± 0.03	0.02 ± 0.01	0.03 ± 0.02
14:1	0.11 ± 0.01	0.12 ± 0.04	0.10 ± 0.01	0.06 ± 0.02
18:1n-7	2.7 ± 0.11	3.90 ± 0.56	2.81 ± 0.10	4.02 ± 0.62
18:1n-9	27.79 ± 0.90	17.64 ± 1.63 **	35.28 ± 1.34	18.22 ± 1.40 ****
20:1n-9	0.044 ± 0.03	1.42 ± 0.10 ****	0.45 ± 0.03	1.51 ± 0.21 ***
22:1n-9	0.08 ± 0.02	0.51 ± 0.06	0.05 ± 0.62	0.62 ± 0.10 ***
Total Omega-6	37.30 ± 0.62	20.86 ± 1.18 ****	31.11 ± 1.19	19.72 ± 1.62 ***
18:2n-6	35.59 ± 0.79	6.04 ± 0.77 ****	29.73 ± 1.19	3.95 ± 0.38 ****
18:3n-6	0.15 ± 0.03	0.13 ± 0.05	0.08 ± 0.00	0.07 ± 0.03
20:2n-6	0.20 ± 0.03	0.46 ± 0.14	0.24 ± 0.01	0.20 ± 0.04
20:3n-6	0.27 ± 0.02	0.96 ± 0.06 ****	0.20 ± 0.02	0.85 ± 0.12 ***
20:4n-6	0.63 ± 0.11	11.38 ± 1.36 ****	0.63 ± 0.03	12.86 ± 1.44 ****
22:2n-6	0.03 ± 0.1	0.37 ± 0.33	0.03 ± 0.01	0.17 ± 0.07
22:4n-6	0.13 ± 0.03	1.19 ± 0.12 ****	0.11 ± 0.01	1.44 ± 0.13 ****
22:5n-6	0.10 ± 0.02	0.32 ± 0.24	0.09 ± 0.01	0.17 ± 0.02 **
Total Omega-3	2.84 ± 0.07	7.19 ± 1.14 **	2.38 ± 0.08	7.06 ± 0.98 **
18:3n-3	1.95 ± 0.08	0.33 ± 0.11 ****	1.61 ± 0.09	0.14 ± 0.01 ****
18:4n-3	0.08 ± 0.03	0.02 ± 0.01	0.05 ± 0.02	0.07 ± 0.04
20:3n-3	0.04 ± 0.00	0.01 ± 0.01 *	0.03 ± 0.01	0.02 ± 0.01
20:4n-3	0.03 ± 0.01	0.03 ± 0.03	0.03 ± 0.00	0.06 ± 0.05
20:5n-3	0.06 ± 0.00	0.03 ± 0.01	0.05 ± 0.01	0.05 ± 0.03
22:5n-3	0.19 ± 0.03	0.07 ± 0.03 *	0.13 ± 0.01	0.08 ± 0.02
22:6n-3	0.49 ± 0.12	6.70 ± 1.16 ***	0.49 ± 0.05	6.63 ± 1.01 ***

Data are means (wt/wt, %) ± S.E.M calculated by Student's t-test within each sex; n = 5.

*P < 0.05, **P < 0.01, ***P < 0.001, ****P < 0.0001, versus.

Appendix G: Fatty acyl composition of CL isolated from gastrocnemius tissues of *Plaat1*^{-/-} and *Wt* mice.

Fatty Acid	Male <i>Wt</i>	Male <i>Plaat1</i> ^{-/-}	Female <i>Wt</i>	Female <i>Plaat1</i> ^{-/-}
Total SFA	17.26 ± 0.44	18.03 ± 0.41	19.61 ± 0.80	19.29 ± 0.67
10:0	0.01 ± 0.00	0.00 ± 0.00	0.01 ± 0.01	0.02 ± 0.00
12:0	0.01 ± 0.01	0.03 ± 0.02	0.01 ± 0.01	0.04 ± 0.01
14:0	0.20 ± 0.07	0.53 ± 0.14	0.61 ± 0.07	1.07 ± 0.04 ***
15:0	0.09 ± 0.04	0.16 ± 0.05	0.12 ± 0.01	0.18 ± 0.04
16:0	10.58 ± 0.61	15.37 ± 0.29 ****	12.44 ± 0.66	15.29 ± 0.76 *
17:0	0.19 ± 0.03	0.17 ± 0.04	0.18 ± 0.01	0.16 ± 0.04
18:0	5.55 ± 0.12	1.55 ± 0.34 ****	5.71 ± 0.31	2.26 ± 0.47 ***
20:0	0.29 ± 0.04	0.15 ± 0.06	0.27 ± 0.04	0.18 ± 0.06
22:0	0.26 ± 0.07	0.03 ± 0.01 **	0.17 ± 0.02	0.02 ± 0.01 ***
24:0	0.10 ± 0.05	0.02 ± 0.01	0.08 ± 0.02	0.07 ± 0.02
Total MUFA	21.42 ± 1.01	42.37 ± 1.81 ****	22.16 ± 1.13	40.55 ± 0.83 ****
12:1	0.01 ± 0.01	0.00 ± 0.00	0.01 ± 0.01	0.01 ± 0.03
14:1	0.03 ± 0.02	0.14 ± 0.05	0.04 ± 0.01	0.22 ± 0.07 *
18:1n-7	3.40 ± 0.18	2.99 ± 0.23	15.98 ± 0.98	28.95 ± 0.76 ****
18:1n-9	15.08 ± 1.04	29.01 ± 2.32 **	3.30 ± 0.12	2.82 ± 0.13 *
20:1n-9	1.09 ± 0.12	0.47 ± 0.03 ***	0.80 ± 0.04	0.38 ± 0.03 ****
22:1n-9	0.35 ± 0.07	0.12 ± 0.03	0.23 ± 0.02	0.18 ± 0.09
Total Omega-6	50.58 ± 1.78	33.80 ± 1.68 ***	50.31 ± 1.30	34.64 ± 0.47 ****
18:2n-6	44.34 ± 2.59	32.00 ± 1.67 **	44.38 ± 0.89	32.79 ± 0.35 ****
18:3n-6	0.03 ± 0.02	0.12 ± 0.01 **	0.03 ± 0.01	0.08 ± 0.03
20:2n-6	0.70 ± 0.02	0.26 ± 0.03 ****	0.77 ± 0.08	0.28 ± 0.06 **
20:3n-6	1.48 ± 0.11	0.30 ± 0.03 ****	1.05 ± 0.11	0.28 ± 0.07 ***
20:4n-6	2.81 ± 0.59	0.82 ± 0.09 **	2.95 ± 0.26	0.89 ± 0.09 ****
22:2n-6	0.09 ± 0.08	0.01 ± 0.01	0.06 ± 0.02	0.03 ± 0.01
22:4n-6	0.65 ± 0.09	0.16 ± 0.03 ***	0.62 ± 0.89	0.19 ± 0.05 **
22:5n-6	0.49 ± 0.10	0.14 ± 0.03	0.45 ± 0.09	0.11 ± 0.04
Total Omega-3	5.97 ± 0.47	2.86 ± 0.17 ***	6.11 ± 0.48	2.99 ± 0.20 ***
18:3n-3	0.94 ± 0.05	1.84 ± 0.16 **	1.00 ± 0.03	1.90 ± 0.08 ****
18:4n-3	0.02 ± 0.01	0.07 ± 0.06	0.02 ± 0.00	0.02 ± 0.01
20:3n-3	0.09 ± 0.05	0.01 ± 0.01	0.04 ± 0.01	0.02 ± 0.01
20:4n-3	0.04 ± 0.02	0.01 ± 0.01	0.03 ± 0.01	0.01 ± 0.00
20:5n-3	0.03 ± 0.02	0.05 ± 0.02	0.03 ± 0.01	0.04 ± 0.01
22:5n-3	0.96 ± 0.08	0.20 ± 0.02 ****	0.56 ± 0.07	0.20 ± 0.06 **
22:6n-3	3.89 ± 0.44	0.68 ± 0.09 ****	4.43 ± 0.47	0.80 ± 0.14 ****

Data are means (wt/wt, %) ± S.E.M calculated by Student's t-test within each sex; n = 5.

*P < 0.05, **P < 0.01, ***P < 0.001, ****P < 0.0001, versus.